Limb Position Estimation:

Neural Mechanisms and Consequences for Movement Production

by

Ying Shi

A Dissertation Presented in Partial Fulfillment
of the Requirements for the Degree
Doctor of Philosophy

Approved September 2011 by the
Graduate Supervisory Committee:

Christopher Buneo, Chair
Stephen Helms Tillery
Marco Santello
Jiping He
Veronica Santos

ARIZONA STATE UNIVERSITY

December 2011

ABSTRACT

An accurate sense of upper limb position is crucial to reaching movements where sensory information about upper limb position and target location is combined to specify critical features of the movement plan. This dissertation was dedicated to studying the mechanisms of how the brain estimates the limb position in space and the consequences of misestimation of limb position on movements. Two independent but related studies were performed. The first involved characterizing the neural mechanisms of limb position estimation in the non-human primate brain. Single unit recordings were obtained in area 5 of the posterior parietal cortex in order to examine the role of this area in estimating limb position based on visual and somatic signals (proprioceptive, efference copy). When examined individually, many area 5 neurons were tuned to the position of the limb in the workspace but very few neurons were modulated by visual feedback. At the population level however decoding of limb position was somewhat more accurate when visual feedback was provided. These findings support a role for area 5 in limb position estimation but also suggest that visual signals regarding limb position are only weakly represented in this area, and only at the population level.

The second part of this dissertation focused on the consequences of misestimation of limb position for movement production. It is well known that limb movements are inherently variable. This variability could be the result of noise arising at one or more stages of movement production. Here we used biomechanical modeling and simulation techniques to characterize movement variability resulting from noise in estimating limb position ('sensing noise') and in planning required movement vectors ('planning noise'), and compared that to the

variability expected due to noise in movement execution. We found that the effects of sensing and planning related noise on movement variability were dependent upon both the planned movement direction and the initial configuration of the arm and were different in many respects from the effects of execution noise.

DEDICATION

To Hongwei, my dear husband, for your endless love and support.

To dear Mom and Dad, for providing me with continuous encouragement.

ACKNOWLEDGMENTS

Deepest appreciation to Dr. Christopher Buneo. I always feel I'm the luckiest one to have you as my mentor. Thanks for choosing me as your first PhD student and continuously supporting me during my graduate study. I would not have completed this project without your guidance, encouragement, and confidence in me. Thanks for having patience with me and treating me like a family member.

Appreciation to Dr. Stephen Helms Tillery. Thanks for your guidance and encouragement throughout the process of this research. Your advice and input shed light and inspired additional insights into this research project.

Appreciation to Dr. Jiping He. Thanks for sharing with me your lab space and equipments during the first year of my graduate school. Thanks for the warm encouragements and suggestions. This helped me enormously to adapt to a new life in a new country.

Appreciation to Dr. Marco Santello and Dr. Veronica Santos. Thanks for serving as my dissertation committee and contributing time, effort and expertise in the development and evaluation of this work. In addition, a special thanks to Dr. Veronica Santos for constantly inviting me to your lab meetings.

Appreciation to coworkers in the visuomotor learning laboratory. Thanks to Rachele Valente, for managing the lab and providing tremendous help with monkey training. Thanks to Gregory Apker for providing assistance on data recording and data analysis in neurophysiological studies.

Thanks to colleagues in the SensoriMotor Research Group, Dr. David Meller, Dr. Remy Wahnoun, Flavio Da Silva, Cynthia Pierce, Stephanie Naufel, who shared research experiences as well as jokes with me, which cheered up my life.

Thanks to the Division of Animal Care and Technologies, especially Susan Neill-Eastwood, Francis Condit, Dr.Joanne Tetens-Woodring and Dr. Juan.Jordan. Your professional care of our research animals contributed immeasurably to the success of this work.

Finally, thanks especially to God, who made all things possible.

TABLE OF CONTENTS

CHAPTER Page

CHAPTER Page

CHAPTER Page

LIST OF TABLES

Table Page

LIST OF FIGURES

Figure Page

Figure Page

Chapter 1

INTRODUCTION

1.1. Overview and Significance

Movement production by a biological system is far more complex than we can currently understand. Often we perform activities of daily living with such ease that most of us are not consciously aware of the exquisite movement control that is required to achieve these goals. However, when we observe toddlers who make such a big effort when learning to walk, we may realize that it is not as simple as it looks on adults. In fact, from the simple movement of blinking the eyes to a more deliberate one such as putting a thread through a needle, a collaboration of sensory and motor systems in the body is required. In a process called sensorimotor transformation, sensory representations of the environment are transformed into muscle-control signals. For goal directed movements, movement production could be considered as involving three functional stages: sensing, planning and execution. However, due to the complexity of the process of movement production, we should keep in mind that it is very hard to physically differentiate these stages. For example, during movement production, there is often continuous information flow between stages and a neural structure involved in one stage could also contribute to another stage. Nevertheless, to aid our understanding, it is advantageous to examine these stages one by one in the beginning, while keeping in mind the influences from other stages.

This dissertation is focused on the sensing stage of movement production. More specifically, we are interested in the mechanisms of sensing limb positions for making visually guided reaching movements. An accurate sense of the upper

limb position is crucial to performance of reaching movements. In the beginning of a visually guided reaching movement, sensory information about target location and the position of the upper limb is processed to specify critical features of the upcoming limb movement. For example, the parameters for a reaching movement, notably its direction and extent, depend on the location of the target relative to the hand. All these critical features are considered when generating a proper initial movement plan. During the movement, the information about the spatial arrangement of upper limb is continuously monitored and updated in the brain where the information is processed to make necessary adjustments to the movement plan. This on-line control mechanism ensures reaching accuracy in this noisy internal/external environment. We would be unable to guide precise reaching movements without knowing the exact positions of the limb.

Both peripheral and central mechanisms contribute to the sensing processes of limb position. Compared with more easily accessed peripheral structures, it is relatively difficult to probe the mechanisms of limb position estimation in the brain. Moreover, estimates of where the limb is in space can be achieved by combining information from multiple sources which could be multisensory or both sensory and motor based. The presence of various sources regarding limb position makes the problem more complex.

While a great deal is known about the nature and corresponding neural substrate for each source, little is known about how those sources are combined in the brain to provide a single estimate of limb position. Although we probably can gain some insight by referring to concepts and theories proposed from studies of various other cue integration problems, there may be a difference between the cue integration problem for limb position estimation and the other

cue integration problems. The difference concerns the nature of the cues, which could be both sensory and motor based for limb position estimation. In visually guided reaching movements, estimation of limb position involves the integration of vision, proprioception and efference copy of previous motor command. Vision and proprioception are commonly regarded as sensory cues. Efference copy is regarded as a motor cue. Because of the aforementioned reasons, the mechanisms of how the brain integrates sensory and motor signals across space and time to form a coherent representation of the state of the limb during visually guided movement are still poorly understood, although the representation of the positions of body parts in the brain for perception and action has long been an object of research interest for many neuroscientists.

In this dissertation, we tried to probe this problem via both neurophysiological studies and simulation methods. In neurophysiological studies, we used somatic cues to represent a combination of proprioception and efference copy since vision can be relatively easily isolated from these other cues. **The ultimate goal of this study is to characterize the mechanisms of integration of somatic and visual cues for limb position estimation in the brain and the consequences of misestimation of limb position on movement production.**

1.2. Specific Aims and Hypotheses

This section presents the specific aims, hypotheses, a brief description of method and the contributions of each specific aim.

1.2.1 Specific Aim 1

Specific Aim 1: To characterize the mechanisms of integration of somatic and visually-based limb position signals in area 5 of the posterior parietal cortex.

Hypothesis: Neurons in area 5 of the posterior parietal cortex are involved in integrating somatic and visual signals for limb position estimation and this integration strategy may manifest in individual neurons or population of neurons.

Rationale: Several brain areas are likely to be suited for probing the neural mechanisms of limb position estimation. Among these areas, area 5 appears to be a particularly good candidate. Anatomical evidence shows that area 5 receives both visual and somatic inputs from other brain areas. Lesion studies support a role of area 5 in integrating sensory and motor information for limb position estimation (Wolpert, Goodbody, and Husain 1998). Neurophysiological studies of non-human primates also suggest a role for area 5 in the integration of somatic and visual limb position cues (Graziano, Cooke, and Taylor 2000). However, there are also limitations to these studies in that visual and somatic signals may not have been perceptually equivalent during the studied tasks. In addition, in the study by Graziano and colleagues (2000), it is uncertain if cells were modulated by visually sensed arm positions or just responded to arm-like visual stimulus. As a result we sought to examine the integration of visual and somatic signals in area 5 under conditions where visual information should be more critical to task performance, i.e. during the maintenance of static limb positions in free (3D) space.

Method: The hypothesis was tested by mapping the positional discharge of area 5 neurons in the presence and absence of concurrent visual input and comparing the results on a single cell basis, as well as with a population decoding of arm position under the two visual conditions.

An experimental setup was constructed to build a 3D virtual reality (VR) working environment. In this environment, the real arm position was viewed as a

spherical cursor and the target was presented as a 3D virtual target ball. This design is ideal for complete control over the degree and timing of visual feedback and provided no tactile or force feedback of the target. The VR working environment is similar to the one employed by Schwartz and colleagues (Taylor, et al., 2002). The VR environment was built using custom C++ code and displayed via a 3D monitor. The image from the 3D monitor was then provided to the subject by the reflection of a mirror. Arm movements were monitored using an active LED based motion tracking system. Eye movements were monitored using a remote optical eye tracking system.

Two rhesus monkeys (Macaca mulatta) were trained to do center-out reach movements to one of the eight virtual targets in a vertical plane. Upon the completion of each reaching movement, the animal had to stabilize his arm position on the target while maintaining the gaze at the center of the display. This hold state could last from 800 ms to 1200 ms. During the hold period, the visual feedback of hand position was alternately allowed ('vision' condition) or disallowed ('no-vision' condition) for different trials on a pseudorandom basis. Under the 'no-vision' condition, the information of arm position was solely based on somatic input. Under the 'vision' condition, the arm position was estimated from both somatic and visual input.

While the animals were performing these tasks, cell responses were recorded from the brain of the head-fixed animals. Single cell activity in dorsal area 5 of superior parietal lobule (SPL) of PPC was recorded extracellularly using standard neurophysiological techniques. Tungsten or Platinum-iridium microelectrodes were inserted into the brain to record neural signals. Unconditioned signals were amplified and filtered (600-6000 Hz) first and then

sampled at 2.5 kHz. Single action potentials (spikes) were isolated from the signal via a time-amplitude window discriminator. Approximately 200 neurons were recorded from animal X and 120 from animal B.

Data analysis focused on the neural activity during the hold period on the target. The positional response fields of each area 5 neuron were mapped with or without concurrent visual input ('vision' or 'no-vision' condition). The mean firing rate of each neuron during the hold period was analyzed for positional dependence and visual modulation using a 2-way ANOVA (factors: position in the workspace, visual condition). Cells showing significant main effects for both factors or a significant effect for interaction between these two factors were considered to be involved in the integration of somatic and visual cues and were subjected to further analyses. Neuronal population responses under the two visual conditions were analyzed as well to examine whether the integration of visual and somatic signals was encoded by the population of neurons and to identify potential integration strategies adopted by the neuronal population.

Innovation: We designed an 'active' experimental paradigm for investigating the involvement of area 5 neurons involved in static limb position estimation. In a previous study (Graziano, Cooke, and Taylor 2000), each monkey's arm was passively varied between two positions. There was no visual input about the real arm. Instead, a fake monkey arm that was either congruent or incongruent with the position of the real monkey arm was presented in view. The cells responding to both the position of the fake arm and the position of the real arm were considered possibly involved in integrating somatic cues with visual cues of arm position. However, it is unclear if the fake arm was perceived by the animals as a visual input regarding the real arm position since the animals

were not required to make a perceptual judgment nor were they required to actively control the position of their limbs to perform a particular motor task.

In our experimental paradigm, the animals were required to make an active reach movement before maintaining the arm position on the target. During the static hold period, the arm either could be seen under the 'vision' condition or could not be seen under the 'no-vision' condition. The static arm position could be estimated either from somatic information under the 'no-vision' condition or from both somatic and visual information under the 'vision' condition. By making concurrent neurophysiological recordings, we could determine if the cell was involved in integrating somatic and visual signals by testing whether cell responses were modulated by positional and visual input during the hold period.

The other innovation lies in the application of a virtual reality environment. This design is ideal for complete control over the degree and timing of visual feedback. And since a 3D virtual target ball was presented instead of a real tangible target, no tactile or force feedback was experienced during the hold period. The dependence of vision for position estimation was enhanced to some extent as well.

1.2.2 Specific Aim 2

Specific Aim 2: To characterize, via biomechanical modeling and simulation techniques, movement variability resulting from various noise sources.

Hypothesis: Movement variability is the result of noise arising from different stages of movement production and manifests differently for different noise sources.

Rationale: Limb movements are inherently variable and become even more variable in disorders affecting the nervous system. This variability is the

result of noise arising from one or more neural processes. For example, noise arising during the process of limb/target localization is called "sensing noise"; noise arising during the process of movement planning is called "planning noise"; noise arising during the process of movement execution is called "execution noise". The relative contributions of these noise sources to movement variability are not well understood. Naturally noise at each level of neural processes has an effect on movement variability. It is possible that for some experimental conditions, particular noise sources can be minimized. However, no noise source can be fully eliminated or isolated from other noise sources. As a preliminary study of the contributions of various noise sources to movement variability, simulation methods can provide a relatively convenient and effective way to characterize the corresponding effects of various noise sources on movement variability.

Method: Two joint (shoulder and elbow) arm movements in the horizontal plane were simulated using custom Matlab® code (The Mathworks Inc., Natick, MA). Simulations were entirely feedforward and employed a combination of inverse and forward kinematics and dynamics. We first produced an idealized trajectory in Cartesian endpoint coordinates, under the standard assumptions that handpaths are rectilinear and tangential velocity profiles are bell-shaped (Morasso 1981; Soechting and Lacquaniti 1981). Hand positions along the planned trajectory were then converted to time-varying angular positions at the shoulder and elbow using standard trigonometric equations. After numerical differentiation of the angular positions, shoulder and elbow torques were calculated using inverse dynamics equations (Hollerbach and Flash 1982) and motor commands were calculated from the joint torques using a simple inverse

muscle model (van Beers, Haggard, and Wolpert 2004). To simulate movements in different directions, the procedure described above was inverted (forward model). Motor commands were used to calculate joint torques via the forward muscle model and joint torques were used to derive movements in joint coordinates by simultaneously solving for the shoulder and elbow angular positions and velocities using a fourth order Runge-Kutta method. Finally, trajectories in endpoint coordinates were obtained by transforming the angular motions into hand paths.

Movements were simulated in 24 directions with respect to the endpoint of the arm. In addition, movements were simulated using four different initial arm configurations. Effects of noise were evaluated for three different stages of arm movement production. Simulation I (SI) evaluated the effects of sensing noise alone, Simulation II (SII) evaluated the joint effects of sensing noise and planning noise, and Simulation III (SIII) evaluated the effects of execution noise. Sensing noise refers to the situation where the sensing of initial arm position is imprecise. It was simulated by introducing random perturbations into the initial hand position/arm configuration and assuming that the motor system was unaware of these perturbations and thus failed to compensate for them. For these simulations, movement directions were defined with respect to the initial hand position only and were not directed to particular locations in the workspace, thus this simulation evaluated the motor system's response to errors in sensing the initial conditions only. In contrast, when movements are planned to a fixed spatial location rather than simply along a particular direction, errors in sensing initial conditions are compounded by errors in planning the required movement vector. These joint effects were evaluated in SII. Execution noise occurs during

the movement execution stage and was simulated by introducing noise directly into the motor commands (SIII). For SIII, the overall noise level was determined from parameters derived in previous studies involving neurologically-intact human subjects (van Beers, Haggard, and Wolpert 2004). For all three simulations, the effect of noise was assessed by analyzing the variability of directional errors during the initial phase of the movement (1/3rd of total movement time). Directional errors were quantified as the deviation of the actual trajectory from the idealized, straight-line trajectory connecting the starting position to the target. The variability of these directional errors was quantified by calculating the circular standard deviation (CSD) (Fisher 1993).

Innovation: The innovation of Specific Aim #2 lies first in emphasizing the effect of imprecise sensing of hand position (sensing noise) on movement variability. Most of studies have focused on the effects of noise in planning or execution while few studies have specifically examined the effects of sensing noise. Although the effects of sensing noise on movement may not be noticed in normal subjects, the larger sensing noise exhibited by patients with neurological deficiencies could affect the movement dramatically. Meanwhile, in some circumstances where movements are planned to a fixed spatial location, the misestimation of hand positions (sensing errors) are compounded by errors in planning the appropriate movement vectors (planning errors). The joint effects of sensing errors and planning errors may affect movements even more than the effects of sensing errors only.

Secondly, various initial arm configurations were examined respectively for all simulations. Rather than using one initial arm configuration, we used four

initial arm configurations across the workspace to assess the generality of the results for different arm configurations.

1.3. Organization of Work

This dissertation has been organized into six chapters. Chapter 1 provides an introduction to the work, including overview, significance, ultimate goal, and brief description of two proposed specific aims. Under each specific aim, the corresponding hypothesis, rationale, method and innovation are presented in a concise manner. Chapter 2 provides some important concepts and theories about some aspects of neural and peripheral mechanisms of movement production. Having those concepts and theories in mind would greatly help to understand other chapters. This chapter is recommended to go through for those who are new to this research area or who want to refresh the memory. However, it is also beneficial to refer to this chapter from time to time while reading other chapters. Chapter 3 presents general methods for fulfilling the two specific aims. For Specific Aim 1 which is related to the neurophysiological studies, about half of this chapter describes in detail a novel experimental setup developed for conducting the neurophysiological and behavioral experiments. For Specific Aim 2 which is about modeling and simulation studies, the other half of the chapter details the biomechanical arm model employed and presents all equations and parameters necessary for the simulations. Each of Chapter 4 and 5 focuses on one specific aim. Details of the work for Specific Aim 1 can be found in Chapter 4 and those for Specific Aim 2 can be found in Chapter 5. In an equivalent manner, Chapter 4 and 5 both provide a separate abstract, introduction, methods, results and discussion. The introduction part of each chapter provides background information of the specific

aim including a review of similar studies and their limitations. The methods part of Chapter 4 contains details about behavioral experimental design, surgical procedure and data analysis. In the methods part of Chapter 5, methods are detailed regarding simulating arm movements affected by three types of noise. Chapter 6 concludes the dissertation by summarizing findings in previous chapters and providing insight on possible improvements and future directions of the work.

Chapter 2

BACKGROUND

2.1. Motor System for Reaching

Before we discuss the problem of how limb position is estimated in the brain in order to reach to a target, let us first take a look at the motor system underlying reaching movements. It is known that original vertebrate motor system evolved to produce swimming and eating. Later, it adapted into the one that is capable of producing reaching movements. This study focuses on the more advanced and complex motor system in primates which can reach and point with a two-joint arm. In the terminology of robotics, the motor system could be thought of mainly including four components: actuators (muscles), multi-joint levers (bones), communication lines (nerves) and a central controller (CNS). The CNS (central nervous system) generates patterns of muscle activation (motor commands) which travel down the nerves (axons) to the corresponding muscles. The muscles contract and cause forces to act on the bones in the arm. Sensory system also plays an important role in movement production. In order to generate desired motor commands which move the hand swiftly and accurately to a target, the CNS needs to estimate hand location and target location at the beginning and throughout the movement. If the target location is fixed, the hand location is continuously updated by the CNS. This estimation is essentially a computation process in which sensory feedback is required.

In many ways of reaching movement, the upper limb can be compared to a robotic arm. However, there are a couple of essential differences (Shadmehr and Wise 2005). First, unlike rigid actuators used in robots, muscles are springy and generate force slowly where force varies as a function of muscle length and

depending upon recent usage, growth and other factors. Second, the two-joint skeletal architecture for reaching provides limited five degrees of freedom (two at the elbow and three at the shoulder) while a commercial robotic arm can be easily made to achieve full six degrees of freedom. Nonetheless, five is more than enough since we only need four degrees of freedom to navigate the limb through three-dimensional space. The redundancy in degrees of freedom allows more flexibility in achieving the goals of a movement. The disadvantage is that it creates additional computational burdens for the controlling system. Third, neural transmission is sluggish. In contrast to metal wires in robots, nerves (axons) are really slow communication lines along which information travels at approximately the speed of sound rather than at the speed of light. The CNS must analyze inputs from sensory transducers that provide feedback after a relatively long delay and send neural signals to the actuators with equally slow conduction.

The physiology puts the biological arm at a disadvantage in regard to robotic arm. CNS must overcome these fundamental physical and physiological limitations. As the central controller, CNS has the advantage in terms of computation. CNS has evolved neural structures that learn to predict the relationship between state changes in the limb and motor commands to the muscles. The computations underlying those estimates are called internal models (Shadmehr and Wise 2005). A kind of internal model that reflects the causal nature of the relationship is called forward model. For example, forward dynamics involves predicting the limb states (the change of limb's configuration and the rate at which the configuration changes, etc.) that will result from a given set of forces produced by the limb's muscles. Forward kinematics computes

hand location from corresponding limb configuration or joint angles. The reverse computation to forward model is called inverse model. Inverse model allows the motor system to transform the desired movement into a pattern of muscle activation that produces the required forces. Either forward model or inverse model involves a surprising amount of computations. However, CNS has acquired the ability to learn internal models. The internal models could be envisioned as a sort of memory of what has worked in a particular situation. For example, when controlling hand movements, the CNS needs to estimate hand location at the beginning and throughout the movement. In order to deal with much slower sensory feedback pathways, CNS learns to estimate what sensory feedback might result from a copy of the planned motor command. The copy of the planned motor command is called efference copy (Shadmehr and Wise 2005). During hand movements, CNS predicts hand location in the near future based on lagging sensory feedback (proprioception and vision) and prediction from current efference copy using a forward model. By knowing the hand location, CNS can make adjustments to ongoing movements if they go off track. Another situation where internal model is necessary is during movement planning. In planning a reaching movement, CNS relies on an inverse model that predicts the forces/motor commands needed to reach the target. This inverse model maps the desired limb states to forces/motor commands. Although biological limitations put us at a disadvantage in regard to robots, the great computational power possessed by the CNS allows something a robot can not do: we can effortlessly adapt movements to rapidly changing and partially predictable surroundings of the environment.

2.2. Production of Reaching Movement

To probe the problem of integration of somatic and visual cues for hand position estimation, it would be helpful to first look into the overall scheme of visually guided reaching and how hand position estimation fits into this scheme. The biological process of producing a reaching movement is far more complex than what we have currently known. But as an initial attempt to understand the general mechanism, for simplicity we could regard the reaching movement as consisted of three stages (Figure 1): sensing, planning and execution. In the sensing stage, the positions of the target and the hand are estimated by a state estimator in the CNS based on information coming from sensory and motor cues. In the planning stage, the output of the sensing stage, or the estimated positions of the target and the hand, is used by a planner in the CNS which gives out the correct motor commands that can control the movement of hand to the target. In the stage of movement execution, the planned motor commands are sent to the corresponding muscles which contract and produce torques to initiate or facilitate the movement of associated appendages. Note that there is no clear boundary between different stages. Part of stages could be overlapped. For example, muscles not only generate force needed for movement during the execution stage but also give rise to the proprioceptive feedback signals that convey information about the state of the arm and its movement to the sensing stage. For movements requiring reaching accuracy, sensing, planning and execution could be carried out throughout the movement where the hand position is continuously updated to prevent it from going off track. This type of movement control mechanism is called feedback control. In feedback movement control, the position of the hand is continuously monitored and fed back into the control

system. If there is a difference between the monitored and the desired reference hand positions, the system is able to make adjustments to the movement plan so that a new set of motor commands can be formed to create a movement of the hand to the reference location. The other type of movement control mechanism is called feedforward control. In feedforward control mechanism, only initial positions of the hand and the target are fed into the control system as the input and positional errors cannot be corrected on line. A fast, uncorrected movement is often thought to be mainly under feedforward control since feedback control requires relatively long loop delays (Zucker, Iverson, and Hummel 1990; Gordon, Ghilardi, and Ghez 1994). This type of movement is often investigated under experimental conditions for scientific purposes.

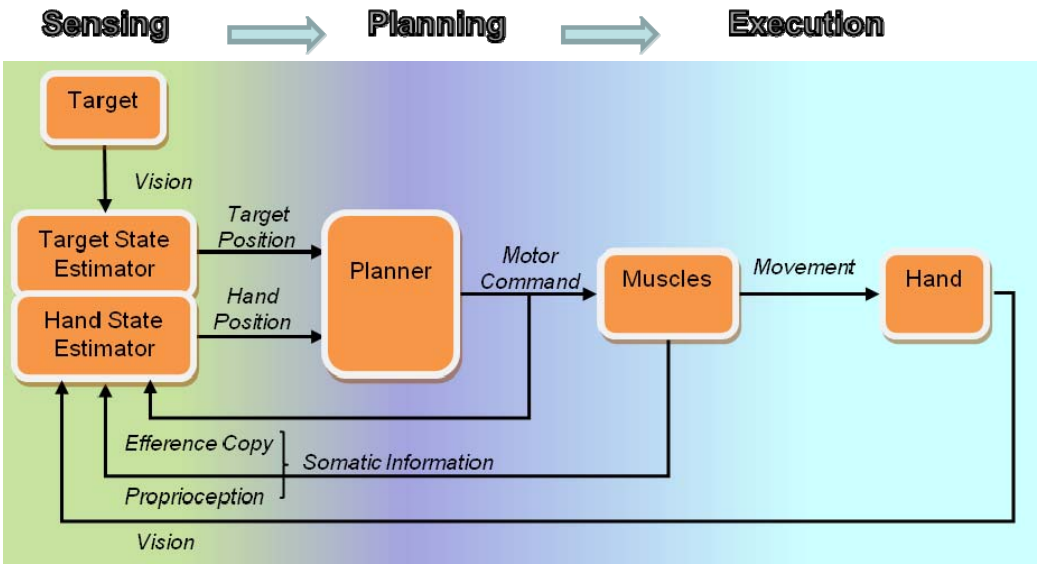

Figure 1. Schematic representation of visually-guided reaching.

2.2.1 Planning to Reach

Sensing of hand location and target location is closely related to planning of reaching movements. Before we start to discuss the mechanism by which

hand locations are estimated, it would be helpful if we have some knowledge of the planning processes. In planning a reaching movement, the CNS first needs to compute the difference between current hand location and desired hand location (the target location). This difference can be quantified as a vector, called difference vector, which has particular amplitude and direction. In order to compute the difference vector, the CNS needs to transform the location of hand and target into a common coordinate frame (Flanders, Helms-Tillery, and Soechting 1992). Early ideas focused on body/shoulder centered coordinates. More recent research in neurophysiology, suggests that in parts of PPC, neural networks transform hand location in joint-centered coordinates into a fixation centered coordinates (Buneo et al. 2002). These data accord with psychophysical findings, which indicate that the CNS plans reaching movements in an extrinsic, vision-based coordinate frame (Vindras and Viviani 1998; Bock 1986). Thus, it seems that at least in the presence of vision, this common coordinate would likely be vision based coordinates, though in other contexts a body-centered frame could be used (McIntyre, Stratta, and Lacquaniti 1997, 1998). If both target and hand locations are represented as vectors in the same coordinate frame, the CNS can compute the difference vector by subtracting the vector that represents current hand location from the vector that represents target location.

The difference vector represents a high level movement plan for reaching the target. After the difference vector is computed, next thing the CNS needs to do is to transform this desired difference vector into a trajectory that specifies the speed of the movement and its path. Although the CNS can select any one of an infinite number of paths from hand's starting location to a target, under most

unconstrained circumstances, the CNS plans the movement so that the hand moves along an approximately straight trajectory with a smooth, unimodal velocity profile (or bell-shaped profile). The trajectory may have a gentle curvature for some movement directions. Very likely the CNS tries to generate a trajectory that is perceived as straight in visual coordinates but may not be actually straight in Cartesian coordinates (Wolpert, Ghahramani, and Jordan 1995). Nevertheless, the smoothness of trajectory has been studied for many years. Various schemes have been proposed trying to account for this movement property. These schemes regarded trajectory planning as solving an optimization problem. Different cost functions were employed, including minimization of jerk (Hogan and Flash 1987), minimization of torque-change (Uno, Kawato, and Suzuki 1989), and minimization of energy (Soechting et al. 1995). These theories propose that movement trajectories are planned in terms of optimizing features of motion (Flanagan and Rao 1995). More recently it has been proposed that many known characteristics of reaching movements can be explained by an optimization process that seeks to minimize the variance in movement end points (Harris and Wolpert 1998). In this context, movement trajectory planning is influenced more by perceptual factors and the state estimator works to provide information of hand and target locations to minimize hand positional variability in the end of the movement.

The final step in the planning process is to decide the forces and motor commands needed to transform this trajectory from a plan into action. In planning forces and motor commands, the CNS does not have to perform a lot of calculations to specify how much to contract each muscle in order to move the hand at the desired states. Instead, the CNS has learned to establish an inverse

model that maps the desired limb states to forces and motor commands. In computing this map, the CNS has to represent limb states in intrinsic coordinates such as joint angles or muscle lengths.

2.2.2 Estimating Hand location

According to the previous section, in order to make motor plans, the CNS needs to compute a difference vector based on the current location of hand and target encoded in fixation-centered coordinates. Potentially two problems are involved in calculating this difference vector: determining target location and determining hand location. According to the model presented in Shadmehr's book (Shadmehr and Wise 2005), the CNS employs a series of neural networks to compute the difference vector based on inputs from various information sources about hand and target location. One neural network estimates hand locations in fixation-centered coordinates given inputs about hand location. A second neural network estimates target locations in fixation-centered coordinates given inputs about target location. A third neural network computes the difference vector by subtracting the vector representing hand location from the vector representing target location. Estimation of either target or hand location could be regarded as solving a cue integration problem. Information about target location typically is provided by vision alone although other sensory cues may also be involved if the target is attached to part of the body or auditory cue of the target location is provided, as in estimating the location of a buzzing fly. Estimation of hand location differs from estimation of target location in that it involves the integration of sensory cues with motor cues. The sensory cues primarily refer to vision and proprioception (via tactile and muscle spindle afferents). The motor

cues refer to the motor prediction of hand location from the efference copy of previous motor command.

As mentioned in previous section, in the presence of vision, the hand location is most likely to be represented as a vector in fixation-centered coordinates. However, hand locations are initially encoded in the brain in the natural reference frames of the sensors. For example, proprioception encodes hand location as joint angles and muscle lengths in intrinsic frame of reference. Vision encodes hand location in fixation-centered coordinates. Efference copy doesn't explicitly indicate where the hand is in space but provide some information about future hand location via current motor commands. The CNS has to align/match the mappings of hand location in different coordinates to visual coordinates. For hand locations estimated from proprioceptive inputs, the CNS needs to solve the problem of forward kinematics which maps the estimated hand location in proprioceptive coordinates to visual coordinates. The mathematical solution to the forward kinematics problem involves doing a series of coordinate transformations. First, limb configuration in joint coordinates (intrinsic frame of reference) is transformed into hand location in extrinsic Cartesian coordinates centered on the shoulder. Second, the origin of the Cartesian coordinates is moved to the head. Third, head centered Cartesian coordinates is moved to fixation centered Cartesian coordinates. Regarding efference copy, knowledge of motor commands alone cannot specify the future hand location since you also have to know the arm's configuration before the motor commands are generated. A forward model could be employed to predict hand location at some future time using sensory feedback and efference copy. There are good reasons to believe that efference copy works in closer concert

with proprioception. First, motor commands acting on muscles cause muscles to contract and change their lengths which are directly sensed by proprioception. Second, occasionally, vision is not available as in the darkness or when image of hand falls outside field of view. But you could still reach by predicting both target location, based on memory, and the current hand location, based on inputs from proprioception and efference copy. In this dissertation, we use somatic cues/inputs to represent information from both proprioception and efference copy.

Experiments suggest that you do not have independent measures of hand location, as estimated from different inputs; but instead, the CNS aligns information available from various cues to produce a single estimate of hand location (Shadmehr and Wise 2005). This alignment reflects contribution from each of these input signals. The estimate changes when any of these inputs indicates a change in hand location. A neural network might be used to find the best alignment between various information sources. Such network can computes whichever estimate is lacking given some initial estimate of hand location using either somatic or visual inputs. It seems that CNS relies on somatic inputs, at least in large part, to estimate the current location of the hand. Under normal conditions, even if you can see your hand, when you reach to a target, you usually look at the target, not the hand. The image of your hand usually falls outside fovea, but falls on a part of retina where lower-resolution distance receptors locate, and sometimes outside the visual field entirely. In that case, high-quality somatic information is weighted more than low-quality visual information. Visual information, however, is still very important to reaching. Prism adaptation experiments confirm that reaching movements should adapt more rapidly if the hand can be seen (Sekiyama, Miyauchi, and Imaruoka 2000;

Norris et al. 2001). Since hand location is estimated in fixation-centered coordinates, it would make sense that the actual sight of the hand has influence on reaching. In fact, visual information might be used to calibrate the mapping of hand location from proprioceptive to fixation-centered coordinates (Shadmehr and Wise 2005).

The integration of various cues for hand location estimation must address either implicitly or explicitly the reference frame problem. Should hand locations encoded in different coordinates be transformed into the same reference frame before cue integration takes place? Recent modeling and neurophysiological studies have demonstrated that explicit coordinate transformations are not necessary for optimal cue integration to occur (Gu, Angelaki, and DeAngelis 2008; Pouget, Deneve, and Duhamel 2002), though such computations might still be beneficial in certain contexts. Thus, it is unclear whether the "state estimator" shown in Figure 1 is involved in both coordinate transformations and cue integration and, if so, whether these computations involve the same or different neural structures/networks.

2.3. Cue integration in Hand Location Estimation

2.3.1 Optimal Cue Integration Theory

The CNS computes an estimate of hand location through an alignment of information from various cues, including vision, proprioception and efference copy. Proprioception and efference copy together can be regarded as somatic cues. How are various cues integrated to provide a single estimate of hand location? The mechanism of cue integration for limb state estimation has been studied in humans using a variety of motor tasks. These studies give us a picture generally showing that the relative weighting of visual and somatic cues

to the final estimate is highly context dependent, varying as a function of movement time, sensorimotor context, stage of motor planning, and also on whether the hand is static or moving (Wolpert, Ghahramani, and Jordan 1995; Vetter and Wolpert 2000; Sober and Sabes 2003; Kording and Wolpert 2004; Scheidt et al. 2005). Several recent studies suggest this weighting is not arbitrary decided but appears to reflect an integration strategy that is statistically optimal (van Beers et al., 1998, 1999; Ernst and Banks, 2002; van Beers et al., 2002). In other words, the weighting relates to the relative precision of individual input and is selected in order to reduce uncertainty in the estimate of limb position and velocity. For example, if noise in one input exceeds that in the other inputs, the CNS tends to weight the noisy input less than the others and the estimate of hand location should depend more on the more reliable input.

What's the relative precision of hand location sense decided by somatic cues or visual cues? For arm movements, the precision of somatic and visual information about hand location varies as a function of arm configuration. For example, localization on the basis of somatic signals alone is more precise when the hand is closer to the body and is more precise in depth (radial direction with respect to the shoulder) than in azimuth (van Beers, Baraduc, and Wolpert 2002; van Beers, Sittig, and van der Gon 1998). In contrast, vision is more precise in azimuth than in depth. These findings are summarized in Figure 2 which shows precision ellipses associated with somatic and visual sense. Differences in precision as a function of arm configuration can be gleaned from the relative sizes of the 'near' and 'far' somatic ellipses; direction dependence can be appreciated from the elongated shapes of the 'far' somatic and visual ellipses. According to the optimal cue integration theory, cues are weighted according to

their relative precision. The differences in precision ellipse between visual and somatic sense lead to a weighting of somatic and visual signals during the estimation of hand location that is both position and direction dependent. This finding also suggests the joint probability distribution describing the static position of the hand in the horizontal plane can appear to be more isotropic or anisotropic depending on the arm configuration in the workspace ('near' or 'far') and is generally smaller for the 'near' positions (van Beers, Sittig, and van der Gon 1998; van Beers, Wolpert, and Haggard 2002).

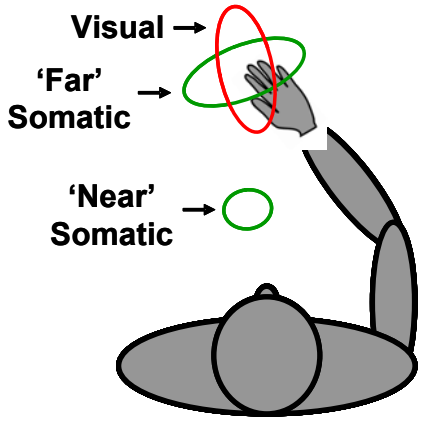

Figure 2. Direction and position-dependent precision of somatic and visual sense of arm endpoint localization. Adapted from van Beers et al. (van Beers, Wolpert, and Haggard 2002).

2.3.2 Neural Correlates of Cue Integration

It seems that the CNS combines visual and somatic information optimally to produce an estimate of hand location. This means the computation that produces this estimate takes into account the relative precision of different inputs. However, the neural mechanisms/correlates for this computation remain an open question. Before probing this problem in any more detail, it would be helpful to know a little about the organization of the vertebrate CNS. It is known that the

CNS of vertebrates is composed of the spinal cord and the brain. The brain has three major components: brain stem, diencephalon and telencephalon. Brain stem includes medulla, pons, midbrain and cerebellum. Diencephalon includes thalamus and hypothalamus. Telencephalon includes cerebral cortex and basal ganglia. All components of the CNS are not working on the same level. The brain stem and spinal cord are in the lowest level of the hierarchy. Generally speaking, all levels of the CNS participate in motor control. No parts of the CNS works in isolation. But higher level components of the CNS are more likely to play a role in solving computation problems for reaching.

Cerebral cortex which makes up most of the CNS in advanced mammals is on the highest level in the system. In humans and non-human primates, two large parts of cerebral cortex, frontal cortex and parietal cortex make important contributions to reaching movements. Everything rostral/anterior to the central sulcus (CS) is frontal cortex. From caudal to rostral, the frontal cortex has primary motor cortex (M1) and premotor cortex and prefrontal cortex. M1 lies in the rostral bank of CS. It contains the arm and hand representations and has direct projections to the spinal cord which are responsible for execution of movements. In non-human primates, premotor cortex lies in the caudal bank of the arcuate sulcus (AS) and is rostral to M1. It mainly comprises dorsal premotor cortex (PMd), ventral premotor cortex (PMv) and the supplementary motor area (SMA). All these premotor areas play a role in reaching movements and have direct projections to the spinal cord. The prefrontal cortex (PFC) is the anterior part of the frontal cortex, lying in front of M1 and premotor areas. This cortical area has been implicated in planning complex cognitive behaviors, decision making and moderating correct social behavior. Instead of being involved in

actual movement production, this region seems to focus on solving the problem of whether or not the movement should be made. Everything caudal/posterior to the CS and rostral/anterior to the occipital cortex is parietal cortex. The parietal cortex can be further divided into primary somatosensory cortex (S1) and posterior parietal cortex (PPC). S1 lies in the caudal bank of CS and comprises Brodmann areas 3, 1 and 2. It receives and processes sensory inputs transmitted from the body via thalamus. PPC lies caudal / posterior to S1. In non-human primates, it is separated into superior posterior lobule (SPL) and inferior posterior lobule (IPL) by the intraparietal sulcus (IPS). The surface of SPL contains Brodmann area 5. The surface of IPL contains Brodmann area 7. Some other SPL or IPL areas folded inside the IPS include medial intraparietal area (MIP), ventral intraparietal area (VIP), lateral intraparietal area (LIP) and anterior intraparietal area (AIP). Generally, PPC is regarded as an association area which receives multimodal sensory inputs and motor inputs from various cortices. Based on various inputs received, it plays roles in the localization of the body and external objects in space.

It is been suggested that areas in PPC, working in close concert with premotor areas, participate in computing the difference vector between hand's location and target's location in fixation centered coordinates. Premotor cortex and M1 cortex may convert this difference vector into a joint-rotation vector; and M1, the cerebellum, and maybe SMA further transform this information into a force vector, which manifests as spike trains sent through various routes to the spinal cord (Shadmehr and Wise 2005). But before the difference vector could be computed, the location of hand need to be determined in fixation centered

coordinates. Solid evidences are still lacking in regard to whether PPC or premotor cortex play the most direct role in computing this hand location.

Which arm movement related cortical areas in PPC or premotor cortex are best suited for probing the neural mechanisms of limb position estimation? Since limb position can be estimated based on the integration of visual information and somatic information, it is reasonable to focus on areas presenting neurons that respond to both visual and somatic signals of limb position. In non-human primates, several areas have been implicated in the integration of somatic information with visual information of limb position. These areas include ventral/dorsal premotor cortex (PMv/d), and the following parietal areas: 5, 7, the medial intraparietal area (MIP) and the ventral intraparietal area (VIP) (Duhamel, Colby, and Goldberg 1998; Graziano, Cooke, and Taylor 2000; Graziano and Gross 1993; Graziano, Cooke, et al. 2004; Graziano, Gross, et al. 2004; Graziano, Yap, and Gross 1994). Figure 3 illustrates the relative locations of some of these cortical areas in non-human primates. Of these areas, PMv and PMd are located in the premotor cortex. But most of the areas are located in the PPC.

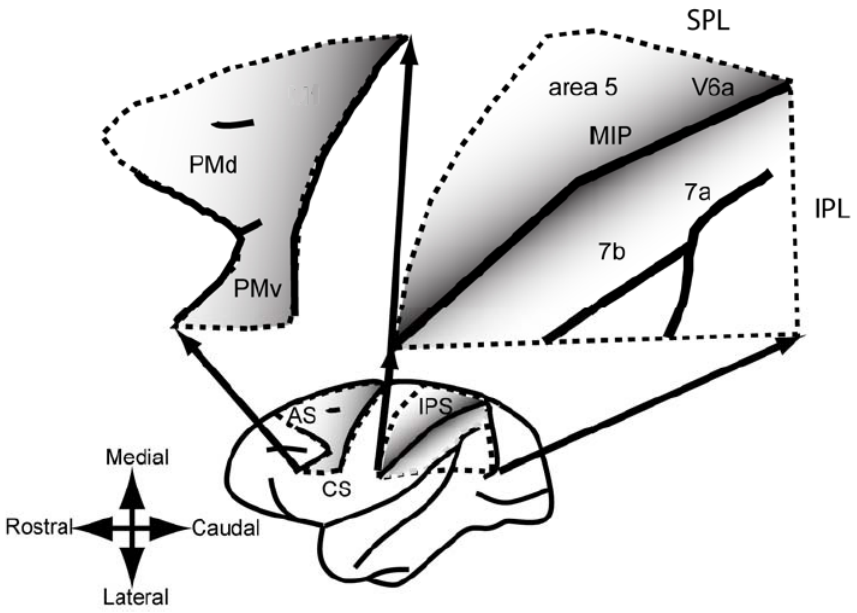

Figure 3. Lateral view of the rhesus monkey brain illustrating cortical areas potentially involved in limb position estimation. Parts of the frontal and parietal lobes are highlighted and expanded. Shaded regions indicate the banks of sulci. AS: arcuate sulcus. CS: central sulcus. IPS: intraparietal sulcus. SPL: superior parietal lobule. IPL: inferior parietal lobule.

What types of responses would one expect of neurons modulated by both visual and somatic signals of limb position? We could be hinted by the responses of cells that are involved in integrating some other multimodal inputs. For example, early work evaluating the responses of cat SC neurons to visual, somatosensory, and auditory stimuli indicated an effect of “superadditivity” in regard to responses of multimodal cell (Stein and Stanford 2008). This effect states that multimodal responses are generally greater than corresponding unimodal responses. However, some researchers found, as stimulus strength moved to threshold levels and beyond, multimodal responses were no longer superadditive but were more consistent with a linear summation of unimodal

responses (Stanford, Quessy, and Stein 2005). Another study in non-human primates examined responses of neurons in the dorsal medial superior temporal area (MSTd) in a heading detection task (Gu, Angelaki, and DeAngelis 2008). The researchers found neurons with congruent, or nearly congruent, preferred directions for vestibular and visual heading in general demonstrated a subadditive combination of unimodal responses as opposed to summation or superadditive combination of unimodal activity levels. All these observations, along with other recent evidence from single-unit studies suggests that superadditivity may not be the sole mechanism underlying cue integration (Stanford and Stein 2007). Recently, more and more interests are aroused in the prediction of optimal cue integration theory. According to this theory, multimodal population/single unit activity would approximate a weighted sum of the population / single unit response to unimodal inputs (Ma and Pouget 2008). This theory could easily explain varying degrees of additivity demonstrated by the firing rates of multimodal cells. In addition to the observations of subadditivity made by Gu et al., a similar study of bimodal MSTd neurons in which coherence of visual feedback was varied further strengthened the prediction of the theory (Morgan, DeAngelis, and Angelaki 2008). Observations of optimal integration also appear to extend beyond the combination of one more unimodal signals to the integration of single modalities over time. For example, it has recently been shown that during information accumulation, neurons in LIP encode probability distributions that can accurately predict an animal's behavior (Beck et al. 2008). The neural correlates of cue integration for limb position estimation may also employ this Bayesian optimal integration strategy. Though manifestations at the single unit level may be different from cell to cell and depending on which brain

area is examined. This is because somatic and visual information about arm position could be encoded in the same or different reference frame for different brain areas.

Chapter 3

METHODOLOGY

3.1. Introduction

In this chapter we present general methods for fulfilling the two specific aims proposed in Chapter 1: 1) to characterize the mechanisms of integration of somatic and visually-based limb position signals in area 5 of posterior parietal cortex; 2.) to characterize, via biomechanical modeling and simulation techniques, movement variability resulting from misestimation of limb position. Specific Aim #1 required being able to record brain activity with under controlled behavioral conditions. For fulfilling this aim, we developed a neurophysiological recording system together with behavior training and a motion tracking apparatus which enabled correlation of brain activity with behavioral events. Specific Aim #2 required programming an arm model and movement simulations with which biomechanical and movement parameters could be easily adjusted and manipulated. For Specific Aim #2, we used custom Matlab® code (The Mathworks Inc., Natick, MA) to build a two joint (shoulder and elbow) arm model and a combination of inverse and forward kinematics and dynamics to simulate arm movements in the horizontal plane. The detailed descriptions of the methods associated with these two specific aims are organized into two separate sections below.

3.2. Experimental Methods for Neurophysiological Studies

3.2.1 Overview of General Methods

Two head-fixed rhesus monkeys (Macaca mulatta) have been trained to make arm movements within a computer-generated, 3D virtual reality (VR) environment, similar to the one employed by Schwartz and colleagues (Taylor,

Tillery, and Schwartz 2002)). This paradigm is ideal for studying the responses of neurons in the presence and absence of visual input, as it allows complete control over the degree and timing of visual feedback. As illustrated in Figure 4, in the virtual reality setup, the monkey's arm movements were monitored using an active LED based motion tracking system. Vision of the animal's arm was blocked by a mirror, but the position of the endpoint of the arm (the wrist) was viewed by the animal as a spherical cursor displayed on a 3D monitor and projected onto the mirror. Eye movements were monitored using a remote optical eye tracking system (not shown).

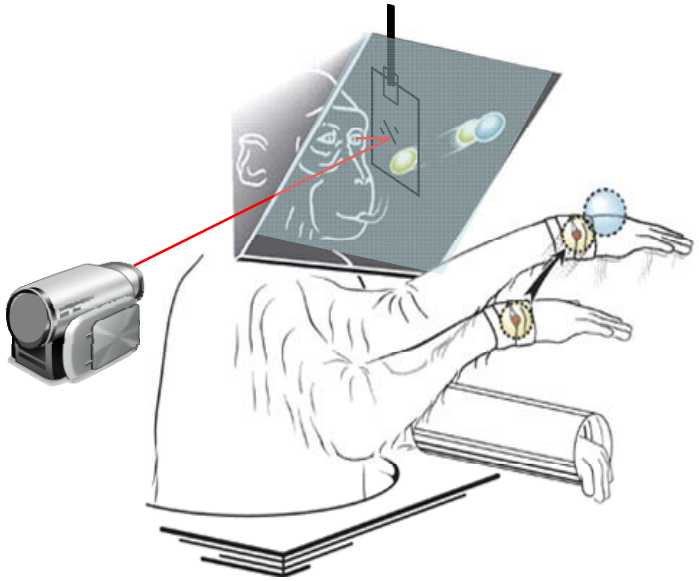

Figure 4. Monkey working in VR environment. Courtesy of Stephen Helms-TIllery.

While animals were making arm movements in the VR environment, neurophysiological recordings were made in dorsal area 5 of the superior parietal lobule (SPL). Single cell recordings were obtained from both animals using standard neurophysiological techniques. Activity was recorded extracellularly with varnish-coated tungsten microelectrodes (~1-2MΩ impedance at 1 kHz).

Single action potentials (spikes) were isolated from the amplified and filtered (600-6000 Hz) signal via a time-amplitude window discriminator (Plexon Inc.). Spike times were sampled at 2.5 kHz.

3.2.2 Experimental Apparatus

The experimental apparatus for neurophysiological studies consisted of a dark room with a mechanical construct for primate behavioral training, a motion capture system for tracking eye and arm movements, a 3D visualization system for creating and displaying the virtual reality environment, a reward system for allowing a specified amount of water/juice for each successful trial, and a neurophysiological recording system for acquiring and recording neural activity. A simple schematic of lab architecture integrating all the sub-systems is shown in Figure 5. A real-time computer (PXI-6259, National Instruments Corporation) was used to run the master control program (MCP). Three standard personal computers were employed to further distribute the computational load: a behavioral PC for acquiring eye and arm position signals, a data PC for behavioral data and neural data storage, and a display PC for creating and displaying the virtual reality environment. The behavioral PC also served as a control PC which communicated with the real-time computer. The MCP was developed and stored on the control PC (host). At run time, the MCP code was uploaded to the real-time computer (target) on which it was compiled and executed.

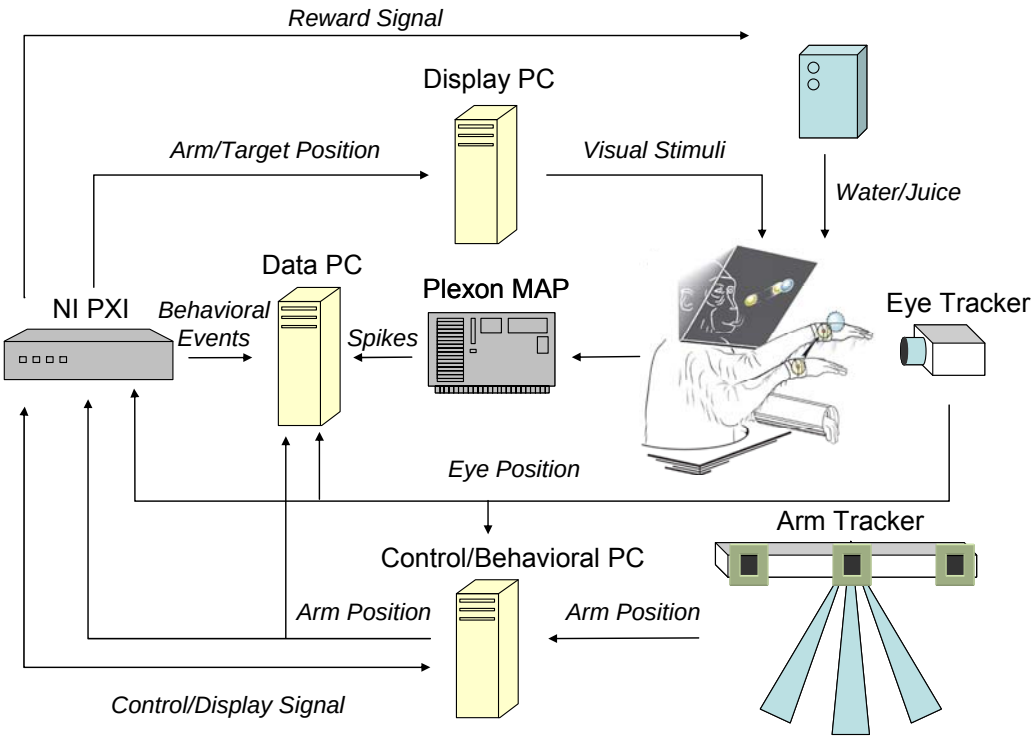

Figure 5. A simple schematic of lab architecture.

The master control program (MCP) was the heart and soul of this complicated system. It integrated the various subsystems into a coordinated whole by monitoring and guiding data flow of various forms among these subsystems. The MCP was developed and implemented in the LabVIEW® graphical programming environment. It ran a continuous loop that read eye and arm position data from the behavioral PC during each cycle. The arm position data were transmitted to the display PC as visual feedback. The eye position data were used to control eye movement. According to the specified behavioral task, target positions were generated by MCP and transmitted to the display PC as well. MCP did all the essential calculations and determined performance of successful trials. Upon each successful trial, MCP sent out a reward signal specifying the length of reward duration to the reward controller box. The MCP

also generated digital events in response to behavioral events which were then temporally aligned with the neural data and saved in the same file in the data PC.

3.2.2.1 Precision Positioning System

The precision positioning system was employed for accommodating animals comfortably and stably in the working environment. It mainly involved a table construct (Thomas RECORDING GmbH, Germany) and a custom made monkey chair. As shown in Figure 6, the table construct consisted of a table with a steel table board, an aluminum frame assembly mounted on the table, a flat guide mounted on the frame and a monkey head holder mounted on the flat guide. The table was cut out on one side to hold and fit the monkey chair. The frame assembly could be moved a little forward and backward depending on the location of screw holes on the table. The flat guide could be moved easily upwards and downwards before being locked into place. Similarly, the head holder used to fix the head could move along the flat guide before being fastened. The frame and the flat guide usually were used for the installation of the head holder. Additional instruments could also be installed and positioned on the frame or on the flat guide. The monkey chair was designed in a way that could accommodate different sizes of monkeys. When the chair was mounted on the table with the animal sitting in it, the body part below the chest of the animal is underneath the table, but the animal was free to move both arms on the table.

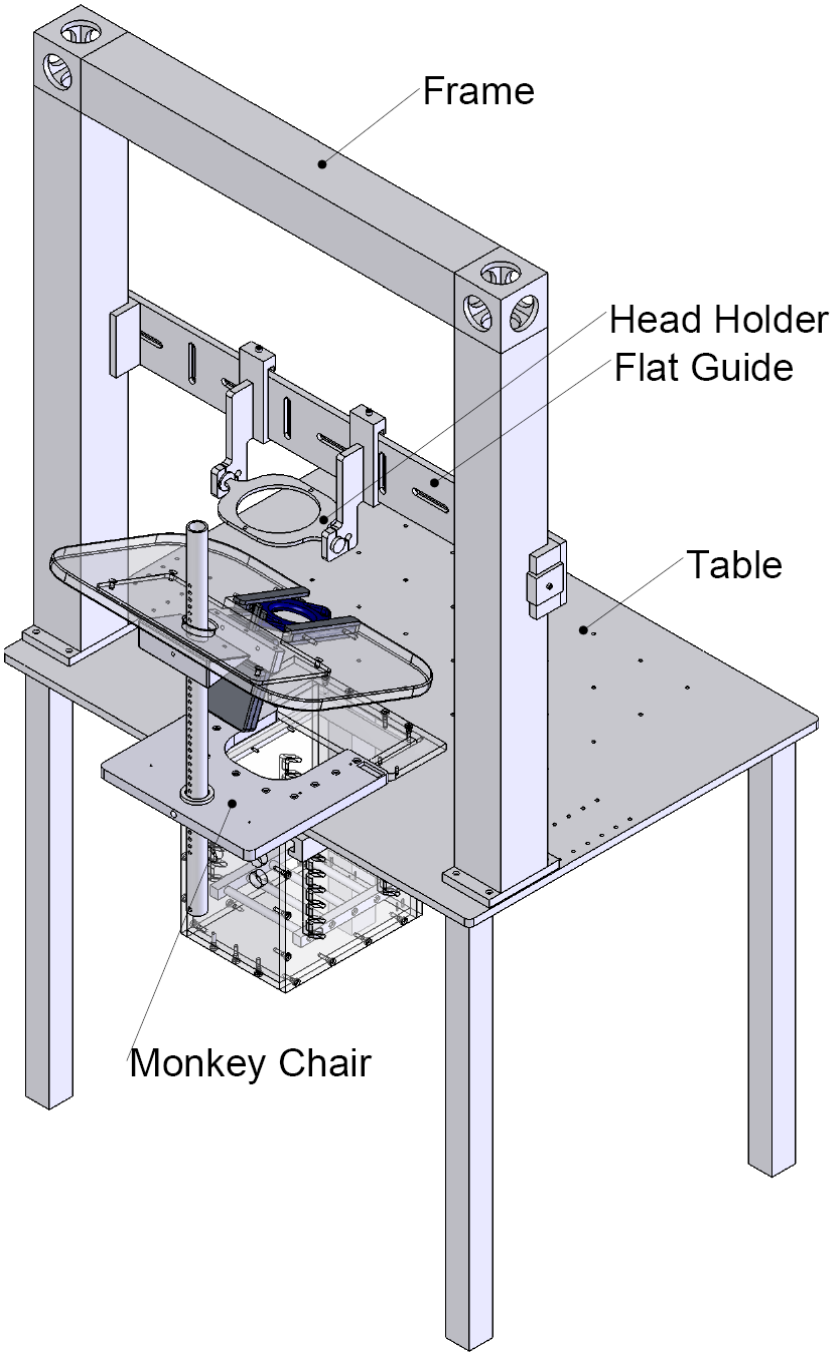

Figure 6. Precision positioning system: table construct with monkey chair in the construct. The illustration of table construct is used with the friendly allowance of Thomas RECORDING GmbH (Winchester Strasse 8, D-35394 Giessen, Germany)

3.2.2.2 VR Working Environment

The VR working environment provided all visual cues to the animals during the behavioral task. It incorporated both hardware and software to build a comfortable working platform.

3.2.2.2.1 Hardware

The mechanical setup of VR environment was based on establishment of a monitor-mirror assembly. A monitor with large screen 2D/3D switchable display (Dimension Technologies Inc., NY) was used to generate the 3D image. During the experiment, the monitor was working under “Side-by-Side” stereo mode which is compatible with a 3D source associated with left and right eye images. No glasses or visors were required for seeing the 3D image. As illustrated in Figure 7, the monitor was mounted horizontally on a frame assembly. A mirror was placed at a 45° angle against the monitor screen. The 3D image generated by the horizontal monitor was displayed through the mirror vertically and in an opposite direction. The height of the monitor and mirror could be adjusted independently so that the vertical image could be viewed closer to or farther away from the eyes. In addition, a position of the mirror could be found, with which only the head of the animal was above the mirror, allowing the animal to use the arms freely in the workspace without viewing anything else except from the image from the monitor. To start behavioral training, the whole assembly needed to be pushed against the table construct of the precision positioning system. The integration of these mechanical systems is illustrated in Figure 11.

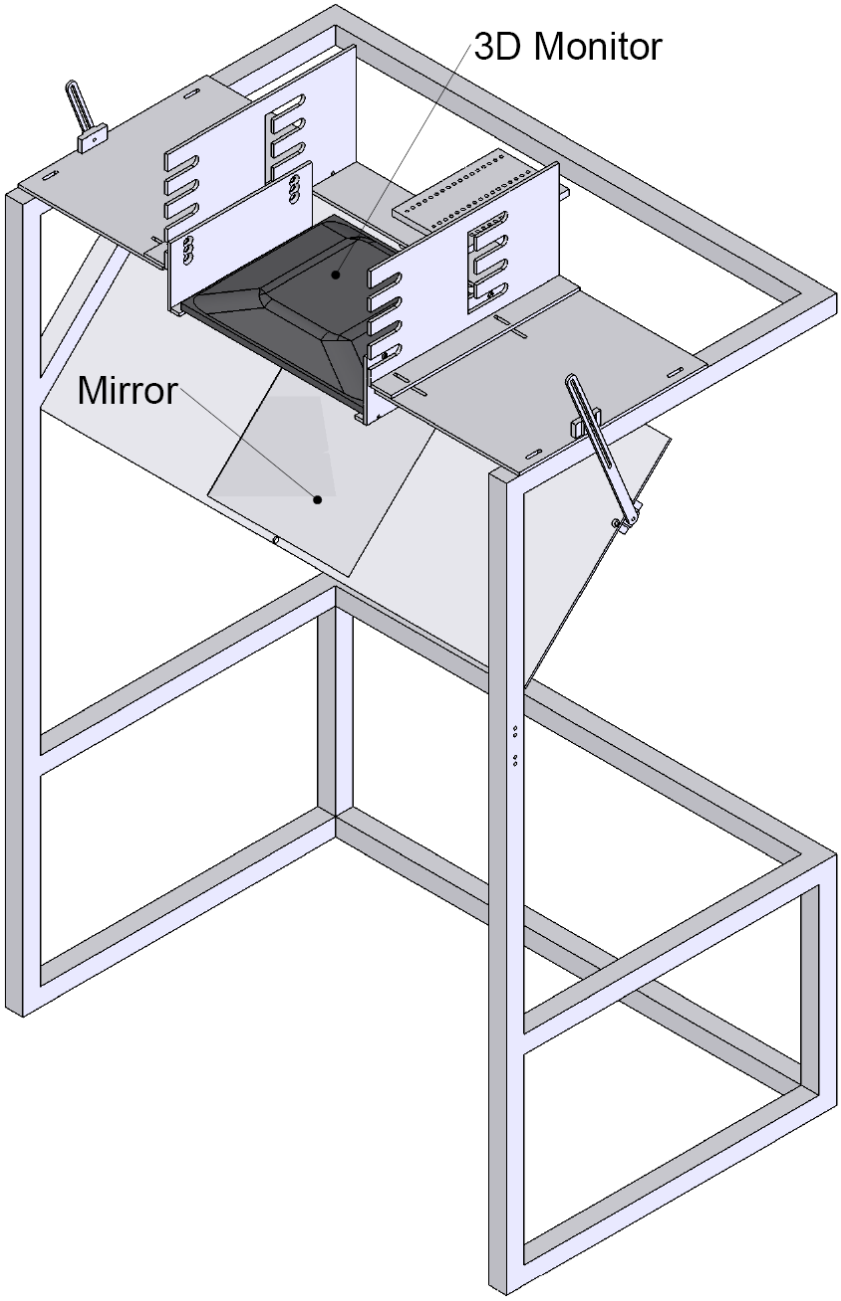

Figure 7. Mechanical setup for displaying virtual reality working environment.

3.2.2.2.2 Software

The VR environment was programmed in the display PC. The software implementation either used C++ programming or a software toolkit (Vizard, WorldViz LLC, Santa Barbara, CA, USA) based on the Python programming

language (Python Software Foundation Corporation, DE, USA). The VR displaying program generated 3D graphic objects including colored balls representing the non-tangible virtual target or the actual wrist position and a surrounding cube frame used to give additional depth cues (Figure 8). UDP network connections were established from the real-time computer to the display PC which received the 3D position data of the wrist and target. To produce a realistic representation of hand movement, the VR program continuously updated the position of the wrist ball based on the readout from the real wrist position. Meanwhile, the wrist ball and the target ball could be programmed as either visible or invisible in order to control the visual feedback of the wrist position.

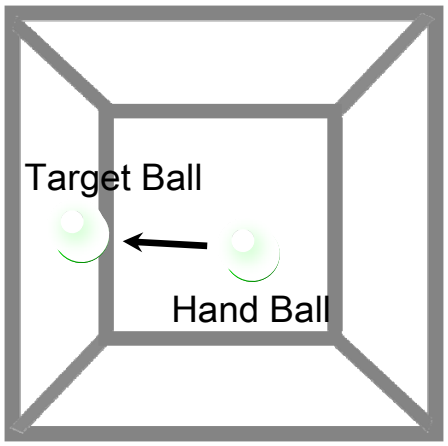

Figure 8. Front view of VR working environment.

3.2.2.3 Motion Capture System

Our experiments required both arm movements and eye movements to be monitored. The 3D position of wrist was captured at all times to provide the visual stimulus of the wrist ball in the VR environment. In addition, the position data of the wrist were correlated with simultaneously recorded neural activity and monitored to examine the behavioral performance of the animal. The 2D position of the point of gaze of the left eye was monitored to control eye movement.

3.2.2.3.1 Arm Tracker

We employed a Visualeyez Motion sensing system (Visualeyze VZ3000, Phoenix Technologies Inc.) for tracking arm movements in 3D free space. The system consisted of a few essential parts: a tracking unit with tripod, target control module (TCM), light emitting diode (LED) markers/targets, and a graphical user interface (VZSoft™). The tracking unit detects the lights from a LED marker, calculates its 3D position, and then transmits the computed position coordinates to the behavioral PC. The function of TCM is to turn on the connected LED markers according to the sampling rate pre-programmed in the VZSoft™ user interface. In our setup, the tracking unit was mounted horizontally on the tripod and was faced the side of the table construct. We attached four LED markers to the wrist of the monkey by placing them on a circular adhesive wrist band. The wrist position was determined based on the average of the four LED positions. The LED markers were about 1.2 m away from the tracking unit. Our motion tracking system had a sampling rate of 250 Hz with spatial resolution of 0.015mm at 1.2m distance.

3.2.2.3.2 Eye Tracker

During the experiments, eye movements were tracked using a remote optical eye tracking system (ASL Inc., sampling rate: 120 Hz, spatial resolution: 0.25 degrees of visual angle). Figure 9 shows the system configuration which includes an Eye-Trac 6000 Control Unit, an eye camera, two video monitors (one for the eye image and one for the scene image), a scan converter, a behavioral PC, and a display PC with subject display monitor. No head tracker was involved since the animal's head was fixed at all times. The eye camera illuminated the

eye with the beam from integrated near infrared LEDs and focused a telephoto image of the eye onto a solid state video sensor through a lens system in the optics. The Eye-Trac 6000 Control Unit received video from the eye camera and sent the eye images to the eye monitor for video display. Meanwhile, the processing board dwelling in the unit box recognized features in the video eye image and computed the point of gaze which was displayed on the behavioral PC and also exported as a real time serial data stream to the real-time machine. The behavioral PC served as the user interface device which ran the ASL supplied Eye-Trac Interface program. The Eye-Trac 6000 Control Unit also received video signals from a scan converter which converted the VGA computer screen image to a composite video signal. The VGA image was generated by the display PC and was the same as the image viewed by the subject (scene image). The scene video was then transmitted from the control unit to a scene monitor and was watched by the investigator.

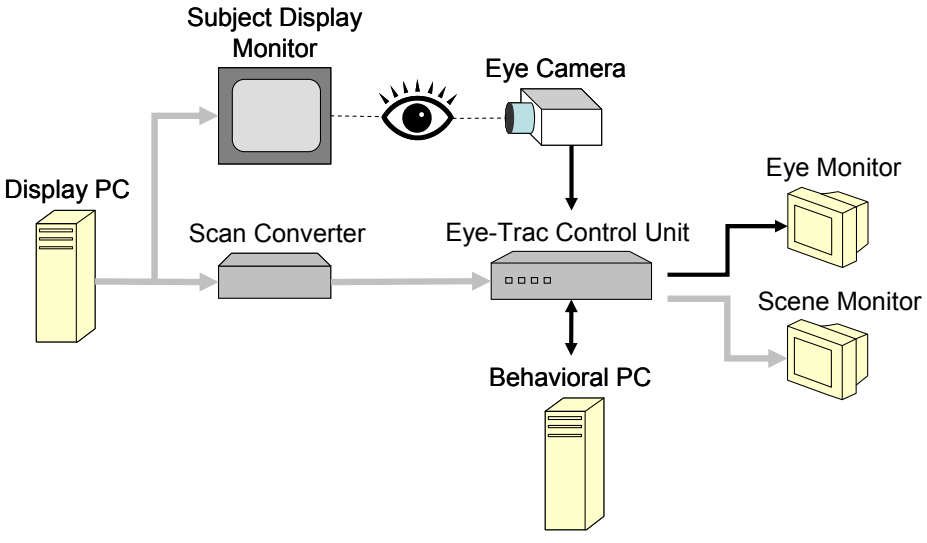

Figure 9. Schematic showing the configuration of remote eye tracking system. The black arrows represent data flow of eye image related information. The grey arrows represent data flow of scene related information.

Integrating eye tracking into the VR working environment is particularly difficult. It is mainly because the monitor-mirror assembly for the VR setup leaves minimum space for the camera while the recommended camera to eye distance is 20-25 inches. To solve this problem, we introduced a hot mirror which could reflect eye image back to the camera while still allowing visible light to pass. The camera was mounted on the frame (which was also used to hold the monitor) and could be moved along and tilted around all three axes if needed. The hot mirror was attached to the flat guide of PPS and fit into the optics system at an incidence angle of 45°. The hot mirror could be adjusted vertically and could rotate to adjust the incidence angle. The positions of the camera and hot mirror are illustrated in Figure 10. By integrating all mechanical parts of PPS, the VR display assembly, the eye tracking system and reward system, we eventually built up a mechanical ensemble system as illustrated in Figure 11.

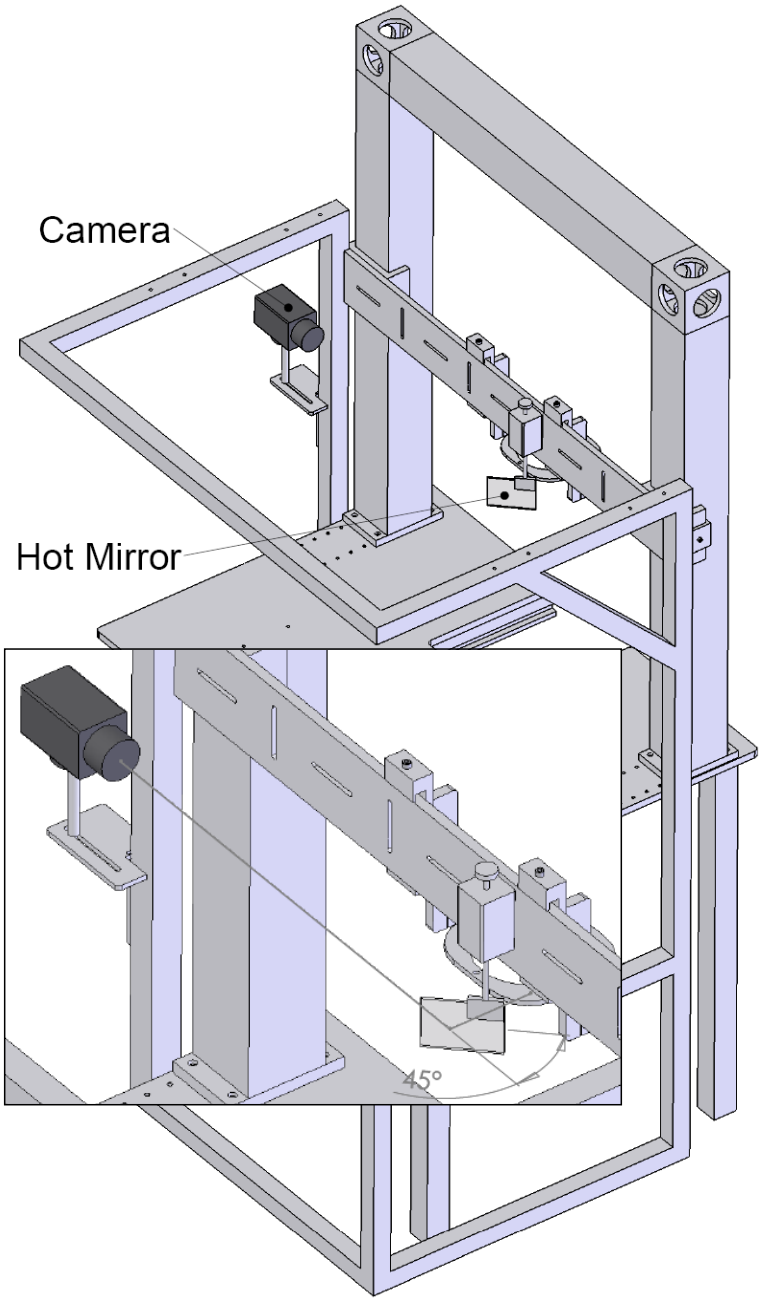

Figure 10. Relative positions of the eye camera and hot mirror. Inset illustrates the light path.

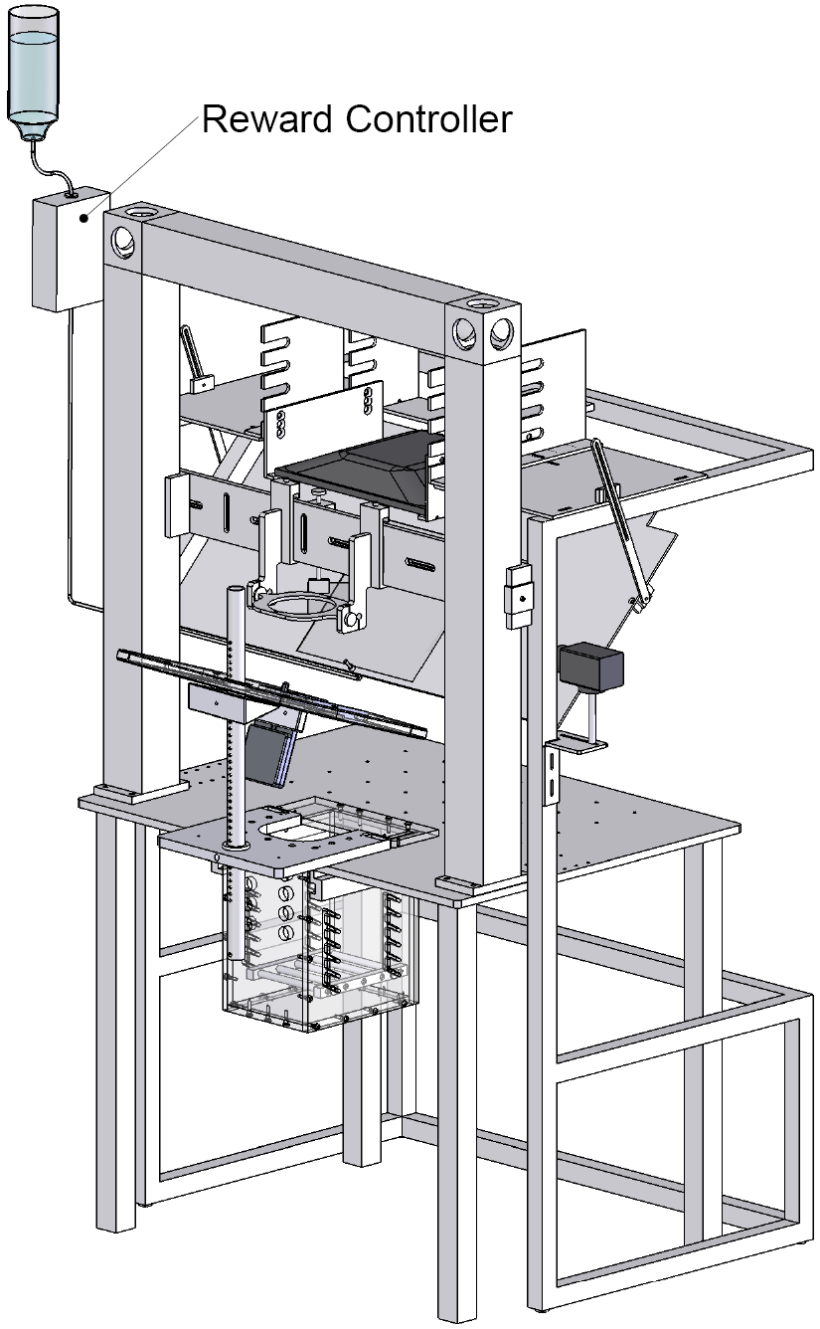

Figure 11. Mechanical ensemble of PPS, VR display assembly, eye tracking system, and reward system.

3.2.2.4 Neurophysiological Recording System

We investigated the activity of the brain by extracellularly recording the firing patterns of single neurons. Neural recordings were accomplished using a neurophysiological recording system which incorporated a microdrive and a multichannel data acquisition system.

3.2.2.4.1 Microdrive

The microdrive (NaN Instruments LTD.) worked as multiple microelectrode positioning system which was assembled of mechanical components and a DSP based controller. The mechanical components included a base and 4 towers which were assembled to position and hold the electrodes. The controller was used for running miniature motors coupled to the towers. A PC (the data PC) was also incorporated in the microdrive system to run user friendly software and communicate with the controller via RS232. The microdrive system could independently position multiple microelectrodes within a desired target structure. Each electrode could be independently manipulated in the Z direction (the vertical direction) with variable speed from 0.001 mm/sec to 0.2 mm/sec and a step resolution of 0.001 mm. The system also allowed independent adjustment of each electrode in the XY planes with a positioning precision of 0.1mm. In our experiments, we employed varnish-coated tungsten microelectrodes with ~1-2MΩ impedance at 1 kHz Neural.

3.2.2.4.2 Data Acquisition System

After the electrodes were positioned in the brain, a 16-channel data acquisition system (MAP System, Plexon Inc., 59 Dallas, TX, USA) was employed for amplification, filtering and recording raw neural signals captured by

the electrodes. The MAP system (Multichannel Acquisition Processor System) incorporated both advanced hardware and software and was capable of programmable amplification (1000-32000), filtering (600-6000 Hz) and real-time spike sorting of multi-electrode signals. Besides spikes, the MAP system could record other continuous analog signals, such as field potentials, eye position, or other behavioral signals using a National Instruments™ Data Acquisition (NI DAQ) device.

The hardware architecture of the MAP system consisted of a headstage, preamplifier, MAP main box, host PC, oscilloscope and loudspeaker. The headstage acquired neuronal signals from high impedance microelectrodes and sent signals to the preamplifiers. The MAP main box received neural signals from the preamplifier and communicated with the host PC (the data PC) after initial processing (including amplification, filtering and A/D conversion). It also received 8 digital inputs or 8-bit strobed word data encoding behavioral events from a 68-pin terminal block (SCC-68, National Instruments Corporation) for external synchronization. The digital-event data together with the spike and other analog signals were saved within a single data file in the host PC. Recorded signals from the MAP main box were also displayed on an oscilloscope and made audible via a loudspeaker, which helped the experimenter in providing additional feedback cues on spike occurrence.

The MAP system also provided a suite of software tools that works with the MAP hardware. This combination of software and hardware enables users to view waveforms, acquire action potential waveforms around a voltage-threshold crossing, sort them in real time according to their shape, record continuous

analog signals, and capture external digital-event data. All programs were run on the host PC under the Microsoft Windows™ operating system.

3.3. General Simulation Methods for Probing Consequences of Noises on Movement

We used a biomechanical modeling and simulation approach to probe the effects of noise at different stages of movement production. Two joint (shoulder and elbow) arm movements in the horizontal plane were simulated using custom Matlab® code (The Mathworks Inc., Natick, MA). As illustrated in Figure 12, simulations employed a combination of inverse and forward models and were entirely feedforward; feedback control was not simulated. An inverse model was used to determine joint angles (inverse kinematics), joint torques (inverse dynamics) and motor commands (inverse muscle model) based on the endpoint/hand trajectory. The procedure was then inverted and a forward model was used to determine the joint torques (forward muscle model), joint angles (forward dynamics) and the endpoint/hand trajectory (forward kinematics) based on the motor commands. The general approach taken was to introduce noise into different stages of these transformations and to quantify the resulting movement errors. Noise was introduced either into the sensing of initial hand position (Noise Simulation I and Noise Simulation II) or into the motor commands (Noise Simulation III). All equations and parameters used in the simulations are provided below. The specific details of each noise simulation are discussed in Chapter 5.

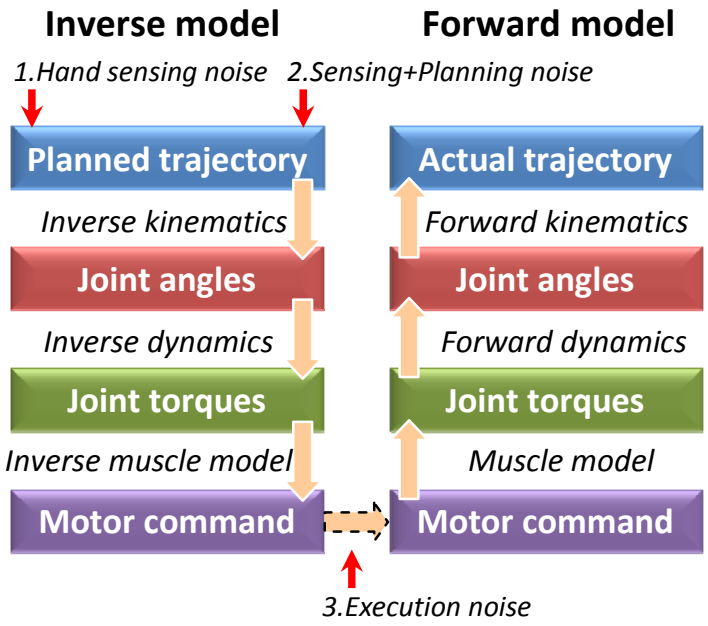

Figure 12. Schematic representation of inverse and forward models used to simulate movements.

3.3.1 Inverse and Forward Transformations

3.3.1.1 Trajectory Determination

We first produced an idealized trajectory in Cartesian endpoint coordinates, under the assumptions that handpaths are rectilinear and tangential velocity profiles are bell-shaped (Morasso 1981; Soechting and Lacquaniti 1981). Thus, the distance d(t) along the hand path as a function of time t was given by :

$$d(t) = d_f\left(\frac{t}{T} - \frac{\sin(2\pi \cdot t)}{2\pi}\right) \qquad [1]$$

where d_f denotes movement amplitude and T is the movement duration. This function analytically approximates a bell-shaped tangential velocity profile (Buneo et al. 1995).

Movement direction (α) was defined as increasing in the counterclockwise direction, with movements to the 3 o'clock position being defined as movements at 0°. For a movement directed at an angle α, the hand location $\vec{P}(t) = (x(t), y(t))^T$ in Cartesian coordinates with an origin at the shoulder was given by:

$$\vec{P}(t) = \vec{P}_0 + d(t)\begin{bmatrix}\cos\alpha \\ \sin\alpha\end{bmatrix} \qquad [2]$$

where $\vec{P}_0 = (x_0, y_0)^T$ denotes the location of the hand at the start of the movement. Accordingly, the hand velocity was given by:

$$\dot{\vec{P}}(t) = \dot{d}(t)\begin{bmatrix}\cos\alpha \\ \sin\alpha\end{bmatrix} \qquad [3]$$

3.3.1.2 Inverse Kinematics

Hand positions along the planned trajectory were then converted to time-varying angular positions at the shoulder and elbow using standard trigonometric equations. The angular position $\vec{\theta} = (\theta_s, \theta_e)^T$ at the shoulder (s) and the elbow (e) was determined from the hand position $\vec{P} = (x, y)^T$ via inverse kinematics (Hollerbach and Flash 1982):

$$\vec{\theta} = f^{-1}(\vec{P}) = \begin{bmatrix} \tan^{-1}\left(\frac{y}{x}\right) - \tan^{-1}\left(\frac{l_e \sin\theta_e}{l_s + l_e\cos\theta_e}\right) \\ \cos^{-1}\left(\frac{x^2 + y^2 - l_s^2 - l_e^2}{2 l_s l_e}\right) \end{bmatrix} \qquad [4]$$

where l_s = the length of the upper arm, and l_e = the length of the forearm.

3.3.1.3 Inverse Dynamics

After numerical differentiation of the angular positions ($\vec{\theta}, \dot{\vec{\theta}}, \ddot{\vec{\theta}}$), shoulder and elbow torques $\vec{\tau} = (\tau_s, \tau_e)^T$ were calculated using inverse dynamics equations (Yamaguchi 2005):

$$\vec{\tau} = M(\vec{\theta}) \cdot \ddot{\vec{\theta}} + B \cdot \dot{\vec{\theta}} + A(\vec{\theta}, \dot{\vec{\theta}}) \qquad [5]$$

where the inertia matrix $M(\vec{\theta}) =$

$$\begin{bmatrix} I_s + I_e + m_s r_s^2 + m_e r_e^2 + I_s^2 m_e + 2 I_s m_e r_e \cos\theta_e & I_e + m_e r_e^2 + I_s m_e r_e \cos\theta_e \\ I_e + m_e r_e^2 + I_s m_e r_e \cos\theta_e & I_e + m_e r_e^2 \end{bmatrix} \qquad [6]$$

the torques with quadratic angular velocity terms $A(\vec{\theta}, \dot{\vec{\theta}}) =$

$$\begin{bmatrix} 0 & -I_s m_e r_e \sin\theta_e & -2 I_s m_e r_e \sin\theta_e \\ I_s m_e r_e \sin\theta_e & 0 & 0 \end{bmatrix} \begin{bmatrix} \dot{\theta}_s^2 \\ \dot{\theta}_e^2 \\ \dot{\theta}_s \dot{\theta}_e \end{bmatrix} \qquad [7]$$

the angular velocity $\dot{\vec{\theta}} = J^{-1} \dot{\vec{P}}$ [8]

and the angular acceleration $\ddot{\vec{\theta}} = J^{-1}(\dot{\vec{P}} - \dot{J}\dot{\vec{\theta}})$ [9]

Here, m_i, r_i, I_i and B represent the mass of arm segment i (= s, e), the distance from the joint to the center of mass of that segment, the inertia moment around the center of mass, and joint viscosity matrix respectively. J represents the Jacobian matrix:

$$J = \frac{d\vec{P}}{d\vec{\theta}} = \frac{\partial(x, y)}{\partial(\theta_s, \theta_e)} = \begin{bmatrix} \frac{\partial x}{\partial \theta_s} & \frac{\partial x}{\partial \theta_e} \\ \frac{\partial y}{\partial \theta_s} & \frac{\partial y}{\partial \theta_e} \end{bmatrix} \qquad [10]$$

where the Jacobian matrix can be calculated based on equation

$$\vec{P} = f(\vec{\theta}) = \begin{bmatrix} l_s \cos\theta_s + l_e \cos(\theta_s + \theta_e) \\ l_s \sin\theta_s + l_e \sin(\theta_s + \theta_e) \end{bmatrix} \qquad [11]$$

3.3.1.4 Inverse Muscle Model

Motor commands were calculated from the joint torques using a simple inverse muscle model (van Beers, Haggard, and Wolpert 2004). In this model, the rotation around each joint was controlled by one second-order linear muscle which could both push and pull and therefore function as a pair of antagonistic muscles. The motor commands $\vec{u} = (u_s, u_e)^T$ of two second-order linear muscles acting independently on the shoulder and elbow joint were estimated via the following equation:

$$\vec{u} = t_e t_a \dddot{\vec{\tau}} + (t_e + t_a)\ddot{\vec{\tau}} + \dot{\vec{\tau}} \qquad [12]$$

where t_e and t_a denote time constants of excitation and activation. In the simulations, t_e was set to 30 ms and t_a was set to 40 ms.

3.3.1.5 Forward Muscle Model

We calculated joint torques from the motor commands by inverting equation A13, (forward muscle model):

$$\ddot{\vec{\tau}} = \frac{1}{t_e t_a}(\vec{u} - \vec{\tau} - (t_e + t_a)\dot{\vec{\tau}}) \qquad [13]$$

The joint torques and their derivatives ($\vec{\tau}, \dot{\vec{\tau}}, \ddot{\vec{\tau}}$) were solved for simultaneously using a fourth order Runge-Kutta method.

3.3.1.6 Forward Dynamics

By rearranging equation A7, we calculated joint angles from the joint torques (forward dynamics):

$$\ddot{\vec{\theta}} = M(\vec{\theta})^{-1}(\vec{\tau} - B \cdot \dot{\vec{\theta}} - A(\vec{\theta}, \dot{\vec{\theta}})) \qquad [14]$$

$\vec{\theta}, \dot{\vec{\theta}}, \ddot{\vec{\theta}}$ in joint coordinates were then solved for simultaneously using a fourth order Runge-Kutta method.

3.3.1.7 Forward Kinematics

Finally, trajectories in endpoint Cartesian coordinates were obtained by transforming the angular motions into hand paths. The hand position $\vec{P} = (x, y)$ was calculated from the angular position $\vec{\theta} = (\theta_s, \theta_e)^T$ of the shoulder joint and elbow joint via forward kinematics:

$$\vec{P} = f(\vec{\theta}) = \begin{bmatrix} l_s \cos\theta_s + l_e \cos(\theta_s + \theta_e) \\ l_s \sin\theta_s + l_e \sin(\theta_s + \theta_e) \end{bmatrix} \quad [15]$$

3.3.2 Parameter Specification

Simulated arm movements were 0.08 m in amplitude and 350 msec in duration, consistent with quick, uncorrected movements. Movements were simulated in 24 directions with respect to the endpoint of the arm. In addition, to assess the generality of the results across the workspace of the reaching arm, movements were simulated using four different initial arm configurations (Table 2).

Representative limb segment lengths, limb masses, moments of inertia and centers of mass were taken from Scheidt et al. (2005) (Table 1). Since joint viscosity may vary with joint angular position, we used joint viscosity matrices that corresponded closely to the different initial arm postures used in this study (Tsuji et al. 1995) (Table 2). For each initial arm posture, we assumed that the joint viscosity matrices remained approximately the same during movement. Although this is not likely the case, the effects of noise in this study were

quantified by analyzing errors in initial movement direction, rather than errors at peak velocity or at the movement endpoint. Since arm postures in the initial portion of the movement did not differ greatly from those at the initial position, we do not believe that violations of this assumption are likely to have strongly affected the results.

Table 1. Anthropometric and mechanical property values. Values are taken from Scheidt et al. (2005). COM = center of mass.

		Upper arm (i=s)	Forearm (i=e)
Length (l_i)	[m]	0.33	0.34
COM (r_i)	[m]	0.165	0.19
Mass (m_i)	[kg]	1.93	1.52
Inertia (I_i)	[kg·m^2]	0.0141	0.0188

Table 2. Joint viscosity matrices corresponding to the four initial arm postures. We used mean values of joint viscosity matrix estimated from subject A in Tsuji et al. (1995).

Initial arm posture	Joint angle (deg)		Joint viscosity matrix B (Nms/rad)	
	θ_s	θ_e		
1	62.708	77.260	0.651 0.236	0.239 0.407
2	41.870	62.578	0.723 0.335	0.313 0.507
3	102.185	59.420	0.708 0.209	0.304 0.454
4	37.301	126.831	0.421 0.126	0.129 0.468

3.3.3 Movement Error Quantification

In this study, noise was introduced into different stages of movement production. The effects of noise were assessed by analyzing errors in initial movement direction (directional errors), rather than errors at peak velocity or at the movement endpoint. Initial movement direction was specified as the direction of the actual trajectory during the initial phase of the movement ($1/3^{rd}$ of total movement time). Directional errors were quantified as the deviation of the initial movement direction from the idealized, straight-line trajectory connecting the starting position to the target (α in Fig. 3). For all these simulations, the variability of directional errors (over all simulation trials) was quantified using the circular standard deviation (CSD) which could be calculated using the following equation (Fisher, 1993):

$$CSD = \sqrt{\frac{\left(\sum \sin(DirErr)\right)^2 + \left(\sum \cos(DirErr)\right)^2}{n^2}} \qquad [16]$$

where n denotes the number of repeated trials for a single movement direction.

Chapter 4

NEURAL MECHANISMS OF LIMB POSITION ESTIMATION

4.1. Abstract

Understanding the neural mechanisms of limb position estimation is important both for comprehending the neural control of goal directed arm movements and for developing neuroprosthetic systems designed to replace lost limb function. Here we examined the role of area 5 of the posterior parietal cortex in estimating limb position based on visual and somatic (proprioceptive, efference copy) signals. Single unit recordings were obtained as monkeys reached to visual targets presented in a semi-immersive virtual reality environment. On half of the trials animals were required to maintain their limb position at these targets while receiving both visual and non-visual feedback of their arm position, while on the other trials visual feedback was withheld. When examined individually, many area 5 neurons were tuned to the position of the limb in the workspace but very few neurons modulated their firing rates based on the presence/absence of visual feedback. At the population level however decoding of limb position was somewhat more accurate when visual feedback was provided. These findings support a role for area 5 in limb position estimation but also suggest that visual signals regarding limb position are only weakly represented in this area, and only at the population level.

4.2. Introduction

Visually-guided reaching movements require the integration of visual and somatic feedback in order to estimate limb position before, during, and after movement. However the mechanisms underlying this integration process, as well as limb position estimation in general, remain poorly understood. In the

sensory domain, integrating information across modalities can reduce uncertainty in estimated position. This is achieved by weighting each modality according to its relative reliability, a process referred to as 'optimal cue integration'. Although a large amount of theoretical and psychophysical work exists in support of optimal cue integration, neurophysiological support is relatively lacking. This is due to the fact that testing the predictions of this theory neurophysiologically can be challenging, particularly in the arm movement system. For example, although visual and auditory cues associated with extrinsic objects do on occasion occur in isolation, visual cues about arm position never occur naturally without concomitant somatic input. This limits the ways in which optimal cue integration can be probed in the arm movement system and also limits the ways in which data obtained from studies of multisensory integration for the arm can be interpreted. As a result of these and other difficulties, studies of the neural mechanisms of multisensory integration for arm movements have not to date explicitly examined whether limb position activity in arm movement related areas is consistent with optimal cue integration.

Although a direct neurophysiological investigation of optimal cue integration for the arm is problematic, it is still possible in this system to assess the role of unimodal and multimodal signals in limb position estimation. This could be accomplished in a number of ways. For example, one could artificially alter the relative reliability of individual unimodal cues and examine the resulting effects on neural responses, as Angelaki and colleagues have done in their studies of self-motion perception in macaque visual cortex (Morgan, DeAngelis, and Angelaki 2008). Alternatively, one could simply examine the responses of neurons to two or more cues presented together or in isolation. Additional

insights into mechanisms of cue integration could be achieved with this approach by also taking advantage of 'natural' variations in the reliability of different unimodal cues. For example, the relative reliability of somatic and visual signals in estimating arm position has been shown to vary as a function of arm configuration (van Beers, Sittig, and van der Gon 1998; van Beers, Wolpert, and Haggard 2002). Thus, by varying limb configurations across the workspace while simultaneously varying the number of available sensory signals, one could obtain substantial insight into the role of these signals in limb position estimation.

Which arm movement related brain areas are best suited for probing the neural mechanisms of limb position estimation? Ideally these areas would contain neurons that respond to both visual and somatic signals. In non-human primates several areas have been implicated in the integration of somatic information with visual information of limb position near the body. These areas include the putamen, ventral/dorsal premotor cortex (PMv/d), and the following parietal areas: 5, 7, the medial intraparietal area (MIP) and the ventral intraparietal area (VIP) (Duhamel et al. 1997; Graziano, Cooke, and Taylor 2000; Graziano and Gross 1993; Graziano, Gross, et al. 2004; Graziano, Yap, and Gross 1994). Any of all of these areas could serve as a target of investigation of the neural correlates of limb position estimation.

Previous studies suggest that area 5, located in the superior parietal lobule (SPL) of the posterior parietal cortex (PPC), would be a particularly good candidate for probing the neural correlates of limb position estimation. For example, in humans, injury to the SPL has been shown to result in profound difficulty in maintaining limb position and grip force in the absence of vision, supporting a role for this structure in integrating sensory and motor information

for the purposes of estimating limb 'state' (Wolpert, Goodbody, and Husain 1998). In addition, in non-human primates, the SPL has been shown to receive both visual and somatosensory inputs (Cavada and Goldman-Rakic 1989; Andersen et al. 1990; Caminiti, Ferraina, and Johnson 1996) as well as an efference copy of ongoing arm movement commands (Rushworth, Nixon, and Passingham 1997). This latter finding is supported by anatomical studies indicating direct projections from PMd and motor cortex to area 5 (Caminiti, Ferraina, and Johnson 1996).

Neurophysiological studies of non-human primates also suggest a role for area 5 in the integration of somatic and visual limb position cues. In an experimental paradigm where a monkey's unseen arm was passively varied between positions that were either congruent or incongruent with the position of a visible, fake monkey arm, Graziano and colleagues (Graziano, Cooke, and Taylor 2000) found that area 5 neurons encoded the position of the unseen arm as well as the position of the seen, fake arm. Variations in discharge due to manipulations of the unseen or 'felt' arm were attributed to somatic signals, while variations due to the fake 'seen' arm were interpreted as being related to visual information about limb position. These findings were interpreted as evidence that area 5 is involved in integrating visual and somatic signals about limb position. However, in this study animals were not required to make a perceptual judgment nor were they required to actively control the position of their limbs. Thus, it is unclear the extent to which the animals perceived the fake arm as being part of their own bodies.

The integration of visual and somatic limb position signals in area 5 has been studied more recently in a task that required animals to maintain their limb

position while actuating pushbuttons on a vertically oriented target array (C. A. Buneo & R. A. Andersen, unpublished observations). These experiments showed that most area 5 neurons encoded the position of the arm in eye-centered rather than body-centered coordinates, even in the absence of visual signals about the arm. This suggests that somatic and visual information about arm position are encoded in the same eye-centered reference frame in area 5, which could arise as the result of somatic signals being transformed from body to eye-centered coordinates. In addition, as in the study by Graziano and colleagues (2000), a subset of neurons was modulated by visual signals about the arm. However, the relatively small percentage of neurons (~15-20%) is not what one would expect of an area that plays a critical role in estimating limb position based on both visual and somatic signals. This could be a consequence of the experimental paradigm, where the combination of tactile, proprioceptive and force feedback experienced by the animals during the button presses likely provided a very reliable estimate of limb position, reducing the importance of visually-based limb position signals. As a result we sought to examine the integration of visual and somatic signals in area 5 under conditions where visual information should be more critical to task performance, i.e. during the maintenance of static limb positions in free (3D) space.

4.3. Methods

4.3.1 Behavioral Paradigms: General Information

Our aim was to explore the role of area 5 of the posterior parietal cortex in estimating limb position based on visual and somatic signals. Cells relevant to this study could encode limb position using both somatic information and visual information. Thus, our behavioral paradigms involved holding the arm at different

positions with or without the aid of vision. Also, an active arm reach paradigm was used instead of the paradigm where arm positions were passively varied by external force sources since the former paradigm reinforced the demand for a more precise estimation of arm position. To minimize postural variation when the hand was held at the same target location for different trials, it would be appropriate that the animal always started reaching from the same position. As a result, a center-out reach paradigm was used. Another important consideration was that animal's eye movements had to be controlled as well since many previous studies research have shown that neurons in area 5 of the posterior parietal cortex encode information of eye position. In order to prevent visual input of target location from confounding neural activities, reach targets were extinguished shortly after target was acquired.

Taking all the above criteria into account, we employed two behavioral paradigms in our study. For both paradigms, the animal was required to start out from the center of a single vertical plane and reach to a virtual target ball presented at one of eight target locations in the periphery. Either of two visual conditions was assigned for each trial: visual input of the endpoint of the arm was either allowed all the time for visual trials or disallowed during a specified period for somatic trials. Each combination of target position and visual condition in a single trial was repeated 5 times for a total number of 80 trials for each recorded cell. Each of the 80 trials was run in pseudo-random order. Based on when vision information of the endpoint was disallowed for somatic trials, two behavioral paradigms could be differentiated. In Paradigm 1 (P1), visual input of the endpoint of the arm was disallowed shortly after target acquire (at the same time when target extinguished). In Paradigm 2 (P2), visual input was disallowed

after the onset of movement toward the peripheral target. The detailed description of experimental paradigms was presented in the following sections. The experimental protocol was approved and monitored by the Arizona State University Institutional Animal Care and Use Committee and conformed to the "Guiding Principles in the Care and Use of Animals" publication of the American Physiological Society.

4.3.1.1 Paradigm 1

A schematic of Paradigm 1 is illustrated in Figure 13. For both visual and somatic trials, at the start of each trial, a green target sphere was presented in the center of the virtual workspace. The animal was required to match this position with a green spherical cursor representing the endpoint of the arm and maintain this position for a set amount of time (500 msec for Monkey X, 300 msec for Monkey B). Once this center position was acquired and maintained, the first target was extinguished and a second green target sphere was presented at one of 8 positions in a vertical plane. The presentation of the second target sphere instructed the animal where to place its arm and also served as a 'go' signal, cueing the animal to move its arm to the target. The animal had no more than 1400 msec to acquire the second target. If for any reason, the animal could not acquire the target within 1400 msec, the whole trial would abort and a new trial would start all over again. Once the second target position was acquired, this target remained illuminated for a very short period of time (300 msec for Monkey X and 400 msec for Monkey B) which helped the animal stabilize the arm. Then the target sphere was extinguished and at approximately the same time a yellow target sphere for eye fixation was presented in the center of the vertical plane. The animal had to continue to hold the arm at the target position

for another 800 ~ 1200 msec while simultaneously maintaining visual fixation at the yellow target sphere. A juice reward was delivered at the end of each successful trial and no juice reward was delivered for failed trials.

During the static arm holding period under gaze control, visual input of the endpoint of the arm based on peripheral vision continued to be allowed on visual trials but was disallowed on somatic trials by blanking the arm cursor. The location of the potential targets with respect to the animal is shown in Figure 13. All potential target locations were arranged in an array. For Monkey X, the distance between rows of the array was 4 cm and the distance between columns was 5 cm. For Monkey B, both row distance and column distance were 5 cm. The window radius for determining target acquire was no larger than half of the distance between adjacent targets. This setting allowed no overlap between target positions. For center target acquires, the window radius was 1.6 cm for Monkey X and 2.4 cm for Monkey B. For peripheral target acquires, the window radius was 2 cm for Monkey X and 2.4 cm for Monkey B. The window radius for fixation was 2.8 cm (about 8° of visual angle)) for both monkeys.

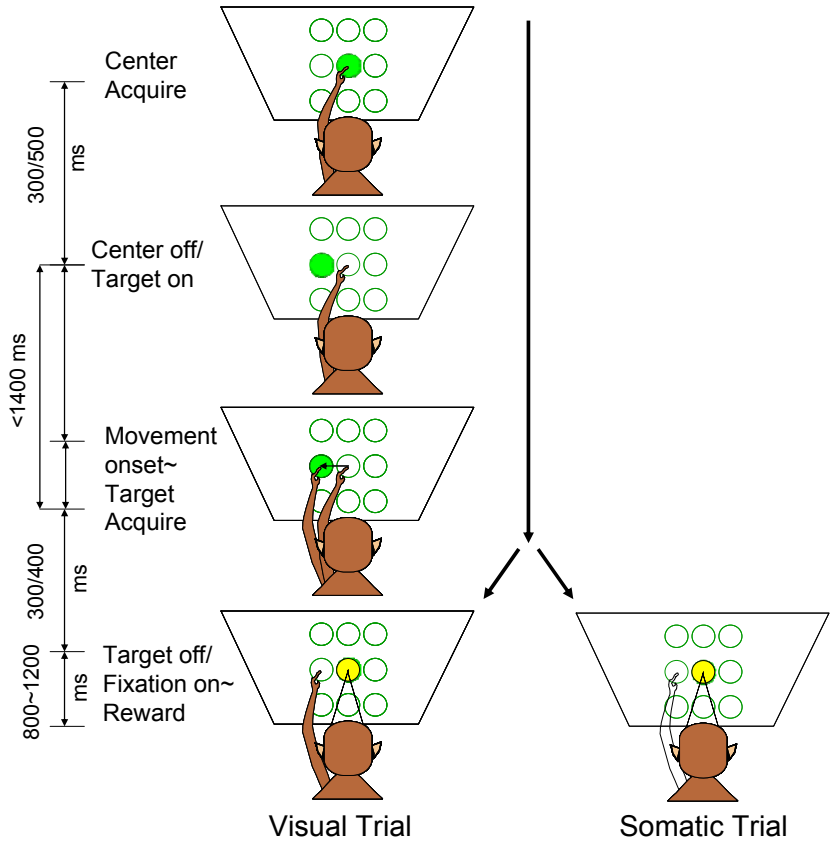

Figure 13. Schematic of behavioral paradigm P1. Sequence of events and timing are illustrated for visual trial and somatic trial. Animal and target display are viewed from behind; targets (circles) are located in a vertical plane surrounding the central starting and fixation position.

4.3.1.2 Paradigm 2

A schematic of Paradigm 2 is illustrated in Figure 14. On visual trials, the sequence of behavioral events with associated timing was the same as that in Paradigm 1. The spherical arm cursor was visible all the time from the beginning toward the end of the trial. On somatic trials, the arm cursor was blanked at movement onset and continued to be blanked till the end of the trial. Compared to Paradigm 1 where on somatic trials the arm cursor was blanked shortly after the acquisition of the second target, Paradigm 2 provided less visual information

in regard to the position of the arm at target location on somatic trials since the arm cursor was blanked before target acquires. Thus, it was more difficult to train animals to do trials in Paradigm 2 than in Paradigm 1. Monkey X was trained and recorded in both Paradigm 1 and Paradigm 2. Monkey B was trained and recorded only in Paradigm 1.

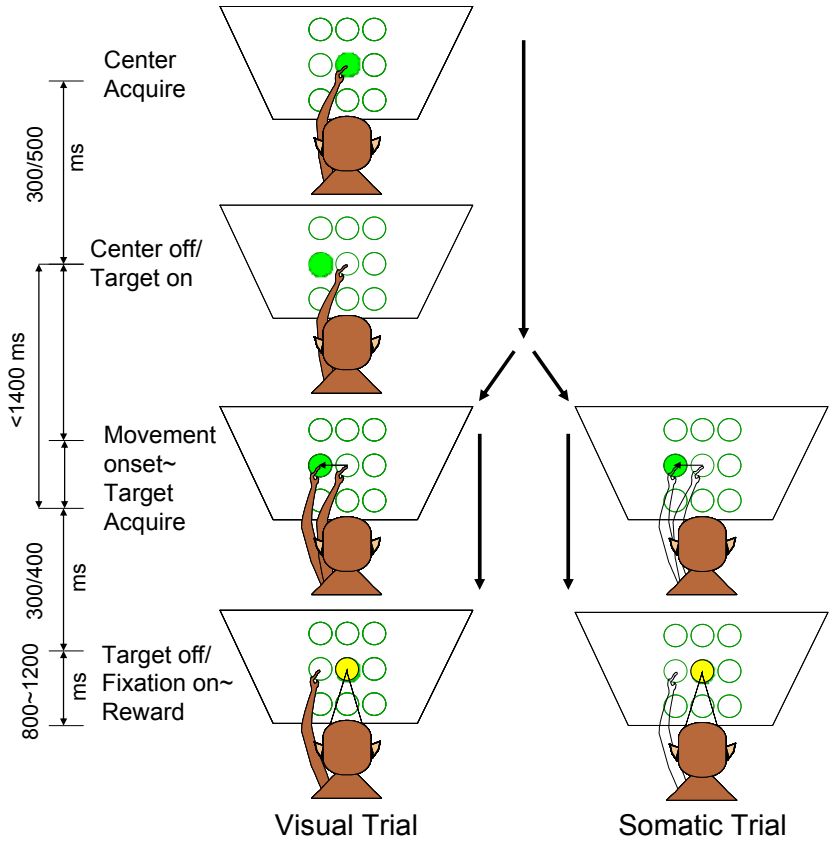

Figure 14. Schematic of behavioral paradigm P2. Sequence of events and timing are illustrated for visual trial and somatic trial. Animal and target display are viewed from behind; targets (circles) are located in a vertical plane surrounding the central starting and fixation position.

4.3.2 Surgical Procedure

The surgical procedures of this study followed federal guidelines and were approved by the Arizona State University Institutional Animal Care and Use

Committee. During the early period of the behavioral training process, three head posts with titanium pedestals were surgically fixed to the skull. The head posts served as anchoring points for holding the head stable when attached to a head holder and a halo. After the animal was well trained, a second surgery was scheduled for implanting a recording chamber over the designated brain area (posterior parietal cortex of the left hemisphere, which was contralateral to the working hand). The animal was initially anesthetized and intubated with administration of an isofluorane-air mixture. Under sterile conditions, a minimum piece of scalp was removed and a craniotomy was performed to expose the dura mater underneath the skull. The exposed dura was surrounded by a circular recording chamber (Crist Instrument Co., Inc.) placed over the remaining skull. Multiple titanium supporting screws were threaded into tapped holes in the skull around the chamber and buried within a dental acrylic head cap which was used to hold and secure the recording chamber. The inner cross-section of the chamber was slightly larger than the exposed dura area and had an inner diameter of about 20 mm. The outside diameter of the chamber was fit for mounting a NaN microdrive (NaN Instruments LTD.) on the chamber. Two male rhesus monkeys (Macaca mulatta) underwent surgery in this study (animals X and B). In monkeys the stereotaxic location of the chamber center was approximately at interaural zero and 10 mm lateral to the midline.

4.3.3 Data Analysis

While animals were performing the tasks of either Paradigm 1 or Paradigm 2, neurophysiological recordings were made in dorsal area 5 of the superior parietal lobule (SPL). Single action potentials (spikes) were recorded extracellularly from a neuron which was isolated from background noise and

other cells by real-time sorting. Arm position and eye position signals were recorded simultaneously with the neural data. Both neural data and behavioral data were stored in the same file for subsequent off-line analysis.

4.3.3.1 Behavior Analysis: Endpoints

We first examined movement endpoint positions on visual and somatic trials for each target location. The endpoint of each movement was determined by averaging the animal's limb position recorded during the time when the animal was holding its arm at a certain target and fixating at the center at the same time. For each target location, we compared the distribution of endpoints between visual trials and somatic trials. For both trial types, we plotted different views of the endpoint distributions and examined differences in endpoint distributions by visual inspection. In order to quantitatively determine if there was a difference in the distributions between the two trial types, a Kruskal-Wallis test was to performed, which is a non-parametric balanced one-way ANOVA for comparing the means of two groups of data. The test statistic was based on calculating the distance between each 3D endpoint position $(\mathrm{x},\mathrm{y},\mathrm{z})$ and the mean position $(\overline{\mathrm{x}},\overline{\mathrm{y}},\overline{\mathrm{z}})$. It performed simultaneously for each x, y, z coordinate and returned the p-value for the null hypothesis that the mean positions of the two groups are equal. In this analysis, one group of data was endpoint position data associated with somatic trials. The other group was endpoint position data associated with visual trials. The significance level for the p-value was 0.05.

4.3.3.2 Neural Responses

The effects of limb position and the visual conditions (vision of the hand ('vision') vs. no hand vision ('no-vision')) on neural responses were assessed

both at the single cell level and at the population level. We focused on cell activities during the time period when the animal was holding the arm on the specified position while maintaining gaze at the center.

4.3.3.2.1 Single Cell Analysis

The first step in neural data analysis involved detailed characterization of the physiological properties of the individual neurons. In this first stage, peri-stimulus time histograms (PSTH) were used to investigate the firing patterns of individual neurons. PSTH measures the average rate of neuronal firing across user-defined time bins. To generate PSTHs in our study, we first calculated average neuronal firing rate in each time bin of 20 ms and then smoothed the data to get instantaneous firing rate via convolution with a Gaussian kernel. The average neuronal firing rate in each time bin was obtained by grouping spike trains of repetitive trials together and counting the spikes in each time bin and dividing the number of spikes by the number of repetitive trials and the bin size. By visually examining individual PSTHs, we could recognize the variation of neuronal firing rate over the time course of the trials. When two PSTHs of different conditions were compared, the effects of different conditions on firing patterns of the recorded neuron could be visually checked.

To quantitatively identify the effects of limb position and visual condition on single cell responses, we ran a 2-factor analysis of variance (ANOVA) of the mean firing rate during the static holding period with gaze control. For neural data recorded from Monkey X, the period examined was specified by a time window of 800 msec which started at 400 msec after target acquire and ended at 1200 msec after target acquire. For Monkey B, this period was defined from 500 msec till 1200 msec after target acquire. We chose this time window to find a

stable period during which the cell activity appeared to be stabilized. The statistical analysis of the average activity during this epoch involved examination of two factors: limb position (P) and visual condition (V). There were 8 levels of factor P (8 limb positions) and 2 levels of factor V (vision of the hand ('vision') vs. no hand vision ('no-vision')). All 16 treatment combinations were repeated for 5 times. A total of 80 trials were run in pseudo-random order for each recorded cell. The ANOVA analysis provided a statistical test of the significance of the main effect of factor P, main effect of factor V and the interaction effect between factor P and factor V. We calculated p-values associated with each effect. The significance level (α) was 0.05. If the p-value was less than 0.05, the effect was considered to be significant.

4.3.3.2.2 Population Analysis

At the population level, cells were classified into sub-populations based on ANOVA's performed on a single cell level. The effects of limb position and visual conditions on single cell activities were statistically tested by the ANOVA analysis. Cells showing a significant main effect of limb position (P), main effect of visual conditions (V), and/or a significant interaction effect (I) between the two main factors were considered task related. For all the task related cells, cells with the same pattern of position and vision dependence were grouped together. To study the proportion of different cell groups in area 5, we counted the number of cells for each group and created statistical pie charts to compare proportions of cells between groups.

We have recently begun using Bayesian decoding techniques to probe the roles of visual and somatic signals in representing limb position in area 5. The location of the limb on a given trial was predicted from activity of different

population of cells recorded independently. The decoding accuracy of a cell population determines how well the activity of cells in this population encodes the limb position. In addition, by comparing decoding accuracy on somatic trials and visual trials, we could see how vision of the endpoint of the limb affects population activity. If visual signals were helping cells encode limb position, we would expect to see an enhanced decoding accuracy for visual trials. In contrast, it would be hard to see any difference in decoding accuracy between visual trials and somatic trials if visual signals did not affect cell population activities.

The Bayesian decoding approach used was similar to that described by Scherberger,and colleagues (Scherberger, Jarvis, and Andersen 2005). We assumed Poisson spike statistics for the spiking activity and statistical independence between different cells. The sequentially recorded cells were treated as if simultaneously recorded. To estimate the limb position on a given trial, we first introduced the vector $a = (a_1,...,a_N)$ which represents the neural activity of the ensemble of all recorded cells. N equals the number of recorded cells, and each a_i represents the spike count of the i^{th} cell during the static holding period. We also defined the scalar $x \in \{1,...,8\}$ to denote the limb position. The estimated limb position $\hat{x}$ on a given trial was chosen to be the one that maximized the posterior probability $P(x|a)$ of the limb position x given population activity a:

$$\hat{x} = \underset{x}{\operatorname{argmax}}(P(x|a)) \qquad [17]$$

According to Bayes' rule, the posterior probability $P(x|a)$ was given by:

$$P(x|a) = \frac{P(a|x) \cdot P(x)}{P(a)} \qquad [18]$$

where $P(a|x)$ is the conditional probability of population activity a given limb position (or the likelihood of limb position x), $P(x)$ is the prior probability which is uniform by design, $P(a)$ is the marginal probability which serves as normalizing denominator so that the sum of $P(x|a)$ for all eight limb positions becomes unity.

Since statistical independence was assumed between different cells, $P(a|x)$ could be calculated using the following equation:

$$P(a|x) = \prod_{i=1}^{N} P(a_i|x) \qquad [19]$$

where $P(a_i|x)$ is the conditional probability of single cell activity a_i given x.

On a given trial, $P(a_i|x)$ followed a Poisson distribution:

$$P(a_i|x) = \frac{1}{a_i!}\lambda^{a_i} \cdot e^{-\lambda} \qquad [20]$$

where $i \in \{1,...,N\}$, λ was estimated from the mean activity of the i^{th} cell during the period when the limb was held at position x.

Based on the law of total probability, $P(a)$ could be represented as

$$P(a) = \sum_{x=1}^{8} P(a|x) \cdot P(x) \qquad [21]$$

Decoding accuracy of the estimation process was examined separately for visual trials and somatic trials. For each visual condition, leave-one-out cross validation was used to assess the decoding performance. One trial was selected from 5 repetitive trials at each limb position and set aside as test data. The parameter λ of the Poisson distribution for calculating $P(a_i|x)$ was estimated from the mean firing activity in the remaining 4 trials for each cell ($i = 1,...,N$). We used bootstrapping techniques to estimate the mean activity since the number of

training trials was limited. $P(x|a)$ was then determined for each limb position x using the test data. The limb position that maximized $P(x|a)$ was selected as the predicted limb position of the test trial. This process was repeated by treating each of the remaining trials as test data. The probability of decoded limb position given population activity $P(x|a)$ was averaged over all test trials. The mean probability was calculated for each actual limb position and for each decoded limb position. The results were graphically represented as confusion matrices.

4.4. Results

4.4.1 Behavioral Analysis: Endpoints

In order to properly investigate the influence of visual and somatic signals on limb position activity in this experiment it was critical that animals exhibited identical endpoint positions on visual trials (with vision) and somatic trials (without vision) for each target location. That is, any difference on the two trial types must reflect the manner in which vision and somatic information are processed in the PPC and cannot be due to the fact that the animal held its arm at slightly different positions in space on the two trial types, a distinct possibility in this type of experiment. To guard against this possibility we examined movement endpoint positions averaged across the time when the animal was holding its arm at a certain target and fixating at the center at the same time. The distribution of endpoints was compared between the two trial types for each of the eight target locations. In the subsequent dissertation sections, the results of behavioral analysis were presented for both single experimental session and a summary of all sessions. Behavioral data presented were collected from Monkey X. (However, Monkey B exhibited similar behavioral pattern.)

4.4.1.1 Single Session

4.4.1.1.1 Paradigm 1

We first examined endpoint position data from a single session of 80 trials. Figure 15 shows endpoint positions obtained from a single session in Paradigm 1. The top three plots and bottom left plot in Figure 15 give the different views (side, front, top and 3D view) of endpoint positions associated with the two visual conditions for each of the eight target locations. At each of the eight target locations, the endpoints of visual trials were blended with those of somatic trials. No apparent difference in the two distributions of endpoints could be recognized by visual inspection. Statistical tests confirmed the results of visual inspection: none of the p-values presented in the bottom right table was less than 0.05. This suggested that at each target location the effect of visual condition on distribution of endpoint positions was not significant. In other words, for this single session, the animal exhibited the same behavior (endpoint positions) on visual and somatic trials.

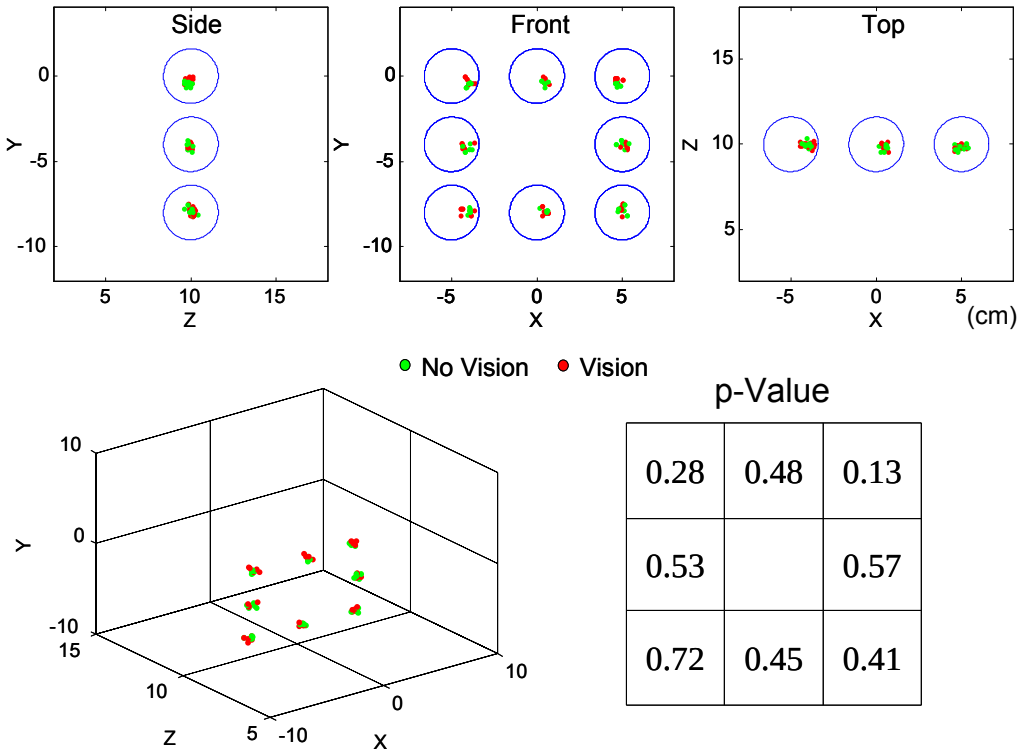

Figure 15. Behavioral data of movement endpoints during a single session in Paradigm 1. Top three plots give the side, front and top view of endpoint distributions for eight positions. Bottom left plot gives the 3D view of endpoint distributions. Endpoints associated with visual or somatic trials are indicated by red ('vision') or green ('no-vision') dots. Blue circle represents the window radius for determining target acquire at each target location. Bottom right table presents p-values for testing endpoint differences between visual trials and somatic trials at each of the eight target locations.

4.4.1.1.2 Paradigm 2

In this section, endpoint position data are presented for a single experimental session in Paradigm 2. Compared to Paradigm 1, where visual input of the endpoint of the arm was disallowed shortly after target acquire for somatic trials, in Paradigm 2 visual input was disallowed after the onset of

movement towards the peripheral target for somatic trials. Just by visual inspection of different views of the endpoint distributions in Figure 16, the endpoints associated with Paradigm 2 appeared to be more scattered for each target location than those associated with Paradigm 1. In this particular experimental session, for some target locations, the green dots representing endpoints of somatic trials appeared to be segregated from the red dots representing endpoints of visual trials. The results of the Kruskal-Wallis test (one-way ANOVA) indicated there was a difference in the endpoint distributions for visual trials and somatic trials for three target locations. That is, p-values presented in the bottom right table of Figure 16 were all greater than 0.05 except those associated with upper left, upper right and middle right target locations. This suggested that for these three target locations, the animal tended to hold its arm at slightly different positions in space on the two trial types. However, for other target locations, the animal did not appear to behave differently on the two trial types.

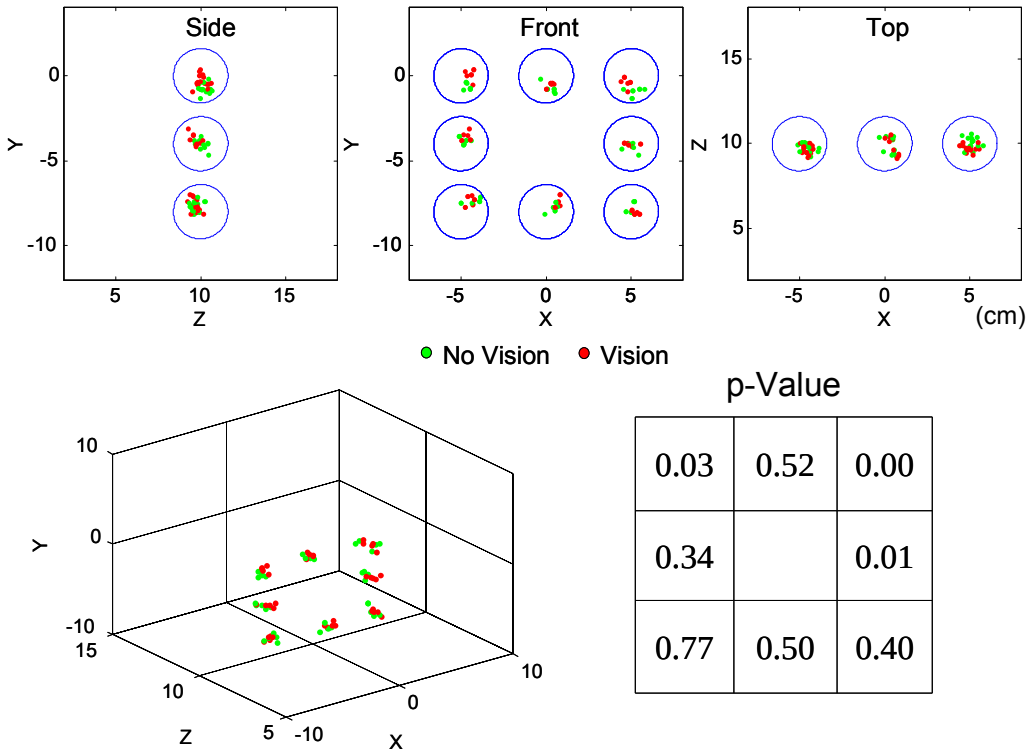

Figure 16. Behavioral data of movement endpoints during a single session in Paradigm 2. Figure conventions are the same as in Figure 15.

4.4.1.2 All Sessions

4.4.1.2.1 Paradigm 1

Here we present the results of statistical analysis of behavioral data over all 191 sessions in Paradigm 1. We tested statistically the difference in endpoint distribution between visual trials and somatic trials at each of the eight target locations for each single session. For each target location, we counted the number of sessions which had a significant difference in endpoint positions for the two trial types at that particular target location and calculated the corresponding percentage. Figure 17 gives a pie chart showing the proportion of sessions having a significant difference in endpoint distribution between visual trials and somatic trials for each of the eight target locations. For each target

location, approximately 10% or less of sessions showed a significant difference in endpoint positions between visual trials and somatic trials. That means, for the vast majority of 191 sessions, the endpoint positions for visual trials were not significantly different from those for somatic trials at each target location. From session to session, no consistent differences in the two distributions of endpoints were observed for each target location. In summary, the endpoint positions at each target location were similar when visual information regarding the arm position was provided or not provided. In other words, the animals exhibited the same behavior on vision and no-vision trials.

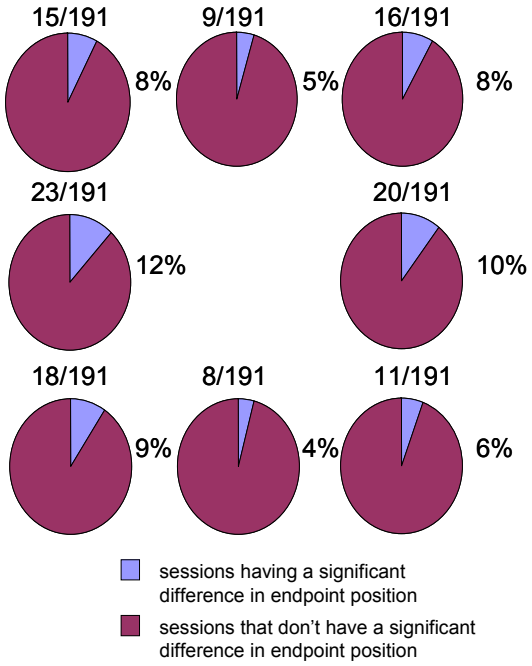

Figure 17. Behavioral data of movement endpoints for all sessions in Paradigm 1. Each pie chart gives the proportion of sessions having a significant difference in endpoint distribution between visual trials and somatic trials for a certain target location. Marked above and to the right of each pie chart are the number and percentage of sessions respectively that were significantly different. The pie charts are placed corresponding to target locations.

4.4.1.2.2 Paradigm 2

Here we present the results of statistical analysis of behavioral data over all 113 sessions in Paradigm 2. Figure 18 shows the proportion of sessions having a significant difference in endpoint distributions between visual trials and somatic trials for each of the eight target locations. We found that in Paradigm 2, for some target locations, more than 50% of sessions showed a significant difference in endpoint positions between visual trials and somatic trials. For other target locations, the percentage of sessions showing a significant difference in endpoint distributions was smaller than 50% but larger than ~20%. However, at any target location, we did not observe a significant difference in endpoint positions between visual trials and somatic trials for all sessions. This means that although differences in movement endpoints were often observed for some target locations these differences were not generally consistent from session to session. When comparing Paradigm 2 with Paradigm 1, we found that for each target location the percentage of sessions in Paradigm 2 was much larger than the corresponding percentage of sessions in Paradigm 1. That suggests more sessions in Paradigm 2 showed the differences in movement endpoints between visual trials and somatic trials.

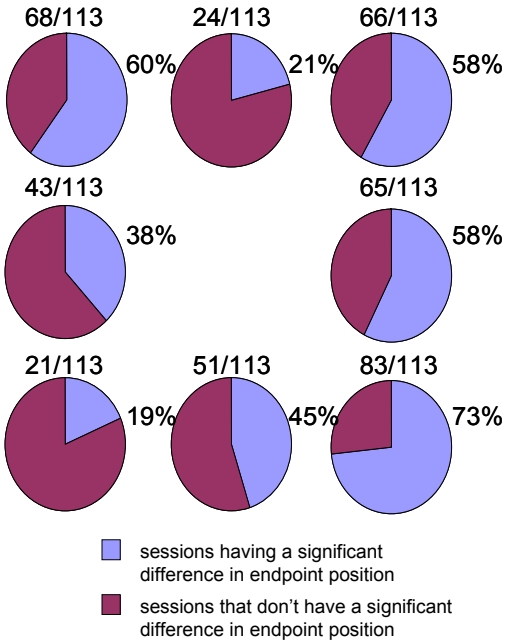

Figure 18. Behavioral data of movement endpoints for all sessions in Paradigm 2. Figure conventions are the same as in Figure 17.

4.4.2 Neurophysiology

When the animal was doing behavioral tasks in Paradigm 1/Paradigm 2, neurophysiological recordings were made in dorsal area 5 of SPL. We examined the effect of limb position and the visual conditions (vision of the hand ('vision') vs. no hand vision ('no-vision')) on neural responses both at the single cell level and at the population level. Neural data presented were collected from Monkey X. (However, Monkey B exhibited similar pattern of neural activities.)

4.4.2.1 Single Cell Responses

4.4.2.1.1 Paradigm 1

Single cell activities associated with Paradigm 1 were analyzed for each neuron recorded in area 5. Figure 19 shows neurophysiological data from two representative cells among all recorded task-related cells. For each cell, peri-

stimulus time histograms (PSTH) of the average firing rate were generated for eight limb positions and for two visual conditions. On top of PSTH is the corresponding raster plot of 5 individual spike trains recorded on 5 repeated trials. Each dot in the raster plot marks the time of occurrence of a single spike. Each panel in Figure 19a and 7b corresponds to a single limb position in the vertical plane. Neural activities during visual trials and somatic trials (or no-vision trials) are indicated by red and green, respectively. Data are aligned to the time of acquisition of the target.

By visual inspection of Figure 19a, several points could be made regarding the responses of Cell A. First of all, this cell exhibited tuned perimovement activity (as evidenced by the burst occurring slightly before time 0) as well as tuned static positional discharge. For both types of visual feedback conditions, discharge was greatest when the animal held its hand at the target located in the lower right position of the display (315°). Second, the activity of this neuron was very similar on vision and no-vision trials. That is, even after the visual stimulus corresponding to the endpoint position was extinguished on no-vision trials (T=0.4 s), the neuron continued to fire in roughly the same manner as on visual trials. ANOVA analysis on the mean firing rate during the static holding period with gaze control indicated a significant main effect of position ($p<0.05$) but no significant main effect of the visual conditions ($p = 0.1$) and no significant position/visual conditions interaction ($p = 0.5$). Thus, this neuron either encoded static limb position using only somatically derived information, or if it did receive visual input it weighted this information minimally in the context of this task.

Figure 19b shows single cell responses from a different cell (Cell B). Again by visual inspection, a couple of points could be made in regard to

activities of Cell B. First, as with Cell A, Cell B also exhibited tuned perimovement activity as well as tuned static positional discharge. However, for both types of visual feedback conditions, discharge of Cell B was greatest when the animal held its hand at the target located in the lower left position of the display (225°), which was different from Cell A. In addition, Cell B fired more frequently for different endpoint positions. For example, the mean firing rate of Cell B during the static holding period for the position to which it was tuned was around 40 Hz while the corresponding firing rate of Cell A was around 20 Hz. Second, unlike the apparent difference of neural activity between endpoint positions, the activity of this neuron appeared to be very similar on vision and no-vision trials. ANOVA analysis on the mean firing rate during the static holding period with gaze control, however, indicated a significant main effect of the visual conditions as well as a significant main effect of position ($p < 0.05$). No significant effect of interaction between those two factors was indicated ($p = 0.24$). Note the p-value associated with the effect of the visual conditions ($p = 0.03$) was close to the significance level ($\alpha = 0.05$) while the p-value associated with the effect of the position was much less ($p<0.00001$).

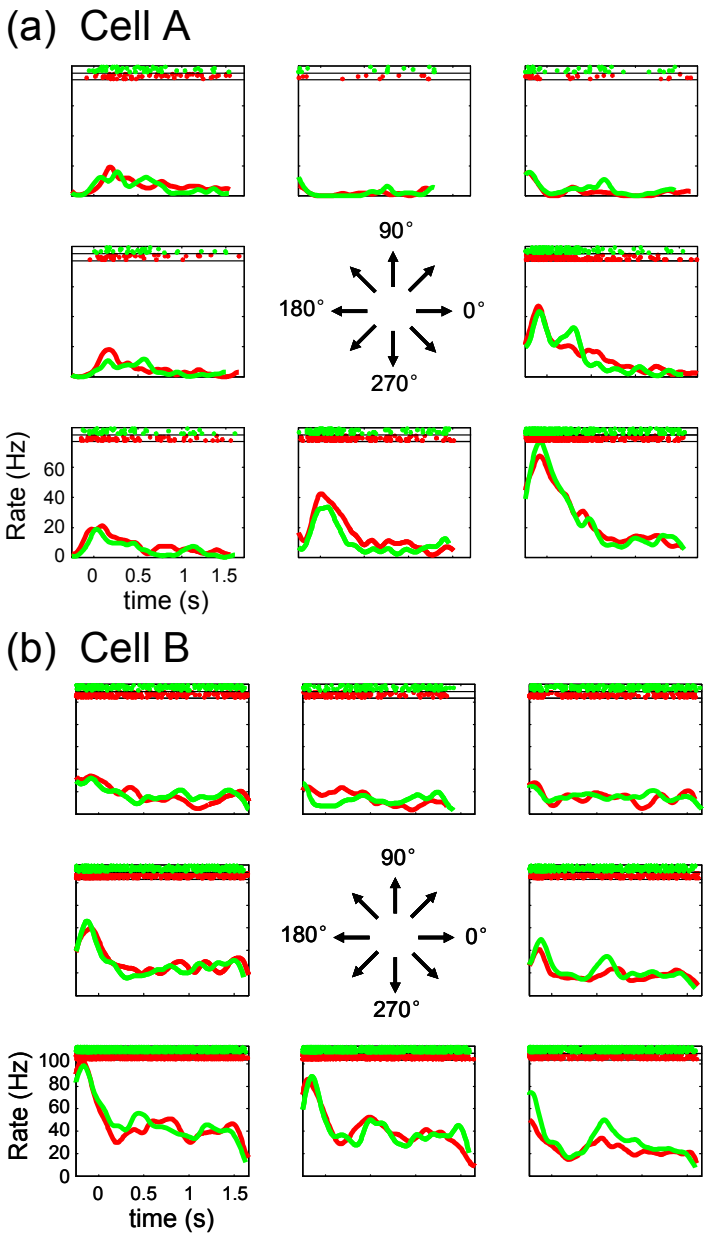

Figure 19. Responses of two area 5 neurons with different tuning properties ((a) and (b)). Neural activities were recorded during a single session of 80 trials in Paradigm 1. Activities for visual trials are marked by red color and those for somatic trials are marked by green color. Each panel in a) and b) corresponds to a single limb/target location in the vertical plane. The arrows in the center point to 8 different movement directions associated with each panel. All data are aligned to target acquire at time 0.

4.4.2.1.2 Paradigm 2

Figure 20 illustrates single cell activities from two task related cells (Cell C and Cell D) which were recorded when the animal was doing tasks in Paradigm 2. By visual inspection, we didn't observe apparent perimovement activity for each cell. Both cells however exhibited static positional discharge. The activity of Cell C was much lower (< 20Hz) and more variable across time. For Cell C, there might be a slight difference in the static positional discharge for different endpoint positions. But it was difficult to identify the endpoint position at which the discharge was greatest since the visual conditions might have had an effect on the activity of this cell. For example, cell activity appeared to be the highest for the upper left endpoint position on vision trials while on no-vision trials cell activity appeared to be the highest for the lower left position. An ANOVA on the mean firing rate during the static holding period with gaze control indicated a significant main effect of position ($p = 0.04 < 0.05$) and a significant position/visual conditions interaction ($p = 0.02 < 0.05$). No significant main effect of the visual conditions ($p = 0.18$) was indicated. This cell might be involved in estimating static limb position using both somatically and visually derived information. For the cell shown in Figure 20b (Cell D), the effect of endpoint position on cell activity was much more easily appreciated than for Cell C in Figure 20a. For both vision trials and no-vision trials, the discharge of Cell D was greatest when the animal held its hand at the target located in the upper left position of the display (135°). And overall the activity of this neuron was very similar for the two trial types. An ANOVA of activity of Cell D indicated a significant main effect of position ($p<0.05$) but no significant main effect of the visual conditions ($p = 0.6$) and no significant position/visual conditions interaction

($p = 0.7$). The activities of the two single cells illustrated in Figure 20 were different from cell activities illustrated in Figure 19: both cells in Figure 20 did not appear to feature a burst of perimovement activity slightly before time 0. Note this difference in cell activity is not related to the different experimental paradigms. For example, in Paradigm 2, we have recorded cells with similar firing patterns as those illustrated in Figure 19. Similarly, cells with similar firing patterns shown in Figure 20 were found in Paradigm 1.

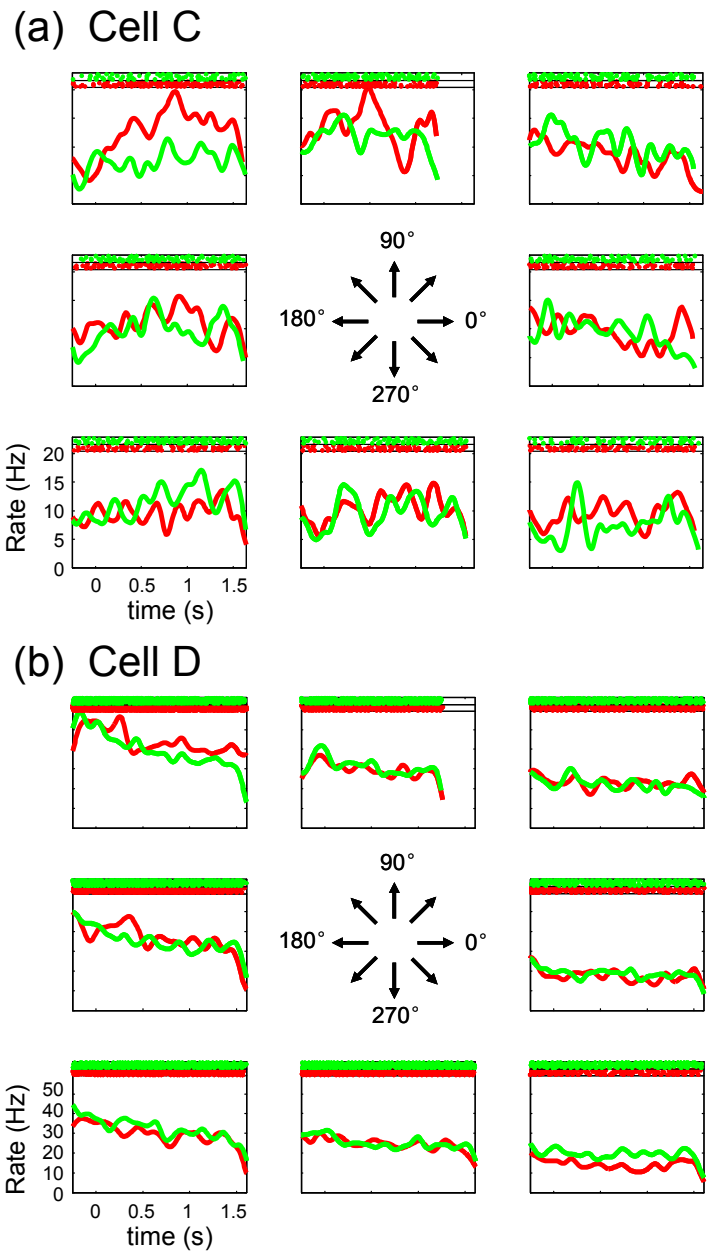

Figure 20. Responses of two area 5 neurons with different tuning properties ((a) and (b)). Neural activities were recorded during a sing session of 80 trials in Paradigm 2. Other figure conventions are the same as in Figure 19.

4.4.2.2 Population Responses

4.4.2.2.1 Paradigm 1

A total of 219 neurons were recorded when the animal was doing tasks in Paradigm 1. For each individual neuron in this population, we tested the effects of endpoint position and visual conditions on neural activity using the two-factor ANOVA described previously. Cells showing the same effects of endpoint position and visual conditions were grouped together as follows. Cells showing at least one significant main effect or a significant interaction effect could be classified into seven non-overlapping sub-populations: P (main effect of position), V (main effect of visual conditions), I (interaction of position and vision), P&V, P&I, V&I, P&V&I. The proportion and relative size of each sub-population are illustrated in the bar chart shown in Figure 21.

We found, first of all, that about 34% of the cells showed only a significant main effect of endpoint position (P). Those cells either encoded static limb position using only somatically derived information, or if they did receive visual input they weighted this information minimally in the context of this task. If we also included cells having a significant interaction effect (I) and cells having various combinations of different effects (P&V, P&I, V&I, P&V&I), about 42% of the cells could be considered having some effects of endpoint position. This proportion is comparable to what have been reported previously. In our study, the proportion might be slightly less, which may be due to the different manner in which cells were recorded: we recorded almost every cell we found at least early in the experiment while other researchers may not record every cell they found unless that cell appears to be position tuned.

We found that few cells (5%) showed only a significant main effect of the visual conditions (V). Those cells may encode the vision of the endpoint of the arm in space, but may not use this visual information to estimate limb position.

We also noticed only ~8% of the cells showed either a significant effect of position/visual conditions interaction (I) or had various combinations of different effects (P&V, P&I, V&I, P&V&I). Those cells are most likely involved in integrating both visual signals and somatic signals for limb position estimation. However, the proportion of those cells potentially involved in this integration mechanism was relatively low.

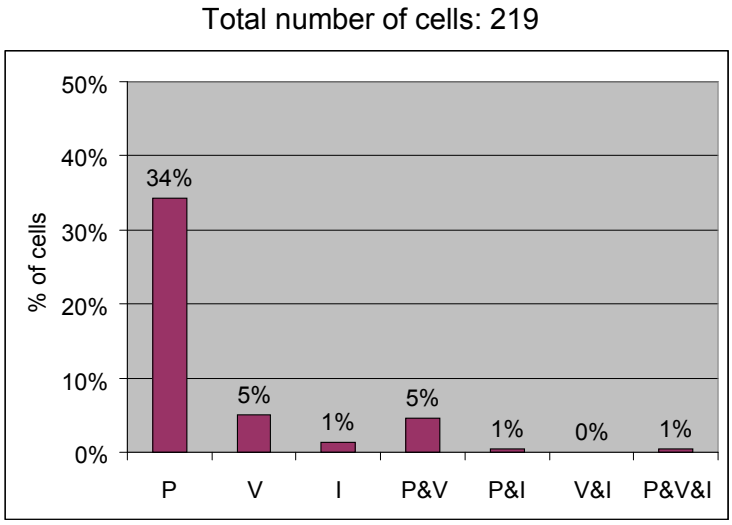

Figure 21. Results of ANOVA for the population of 219 cells studied in P1. P: Cells showing a significant main effect of position. V: Cells showing a significant main effect of visual feedback conditions. I: Cells showing a significant effect of interaction between position and visual feedback conditions.

4.4.2.2.2 Paradigm 2

A total of 114 neurons were recorded when the animal was doing tasks in Paradigm 2. As in Paradigm 1, cells were classified into seven non-overlapping sub-populations: P, V, I, P&V, P&I, V&I, P&V&I (Figure 22). We found that ~39% of the cells showed only a significant main effect of endpoint position (P), ~50% of cells showed some effects of endpoint position (P, P&V, P&I, V&I, P&V&I),

~3% of cells showed only a significant main effect of visual conditions (V), and ~11% of the cells either showed only a significant effect of position/visual conditions interaction (I) or had various combinations of different effects (P&V, P&I, V&I, P&V&I). Despite the behavioral differences described earlier, neural responses were relatively consistent between Paradigm 2 and Paradigm 1, in terms of sensitivity to position and visual feedback condition. For both paradigms, neurons with positional activity were quite common (42% of the population for Paradigm 1; 50% for Paradigm 2). In contrast relatively few cells showed some effects of visual feedback condition (13% for Paradigm 1; 14% for Paradigm 2). Fewer cells showing some effects of both endpoint position and visual feedback condition (8% for Paradigm 1; 11% for Paradigm 2).

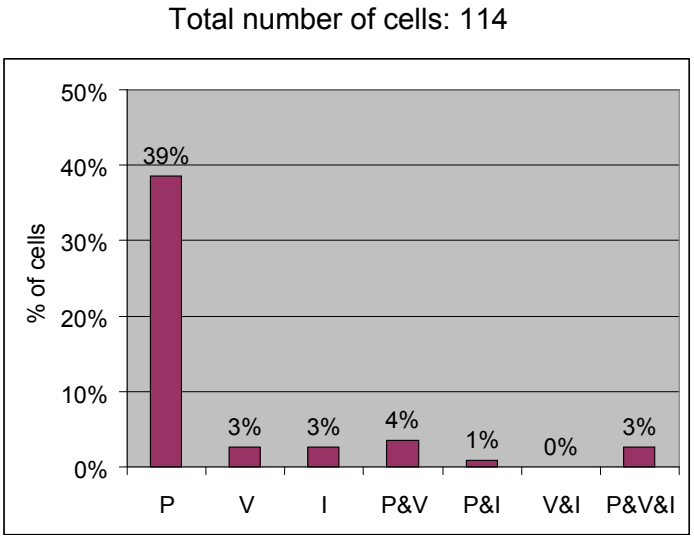

Figure 22. Results of ANOVA for the population of 114 cells studied in P2. Figure conventions are the same as in Figure 21.

4.4.2.3 Bayesian Decoding on Population Responses

4.4.2.3.1 Paradigm 1

In the previous section, based on ANOVA's of single cell activity, cells were classified into seven non-overlapping groups: P, V, I, P&V, P&I, V&I, P&V&I. For simplicity, we used the term "P cells" to refer to cells that showed only a significant main effect of endpoint position (P), used "V cells" to refer to cells that showed only a significant main effect of visual conditions (V), and used "PV cells" to refer to cells that were in the rest of the seven groups (I, P&V, P&I, V&I, P&V&I). PV cells were considered as cells that showed some effect of both endpoint position and vision.

In this section, we present the results of Bayesian population decoding analyses in Paradigm 1. Predictions in regard to the location of the limb were computed for different populations of cells and for different visual conditions. Note the total number of cells used for decoding analyses (147) was different from what is reported in the ANOVA (219). This is because in decoding analyses we excluded the cells with an incomplete experimental session while ANOVA test could accept cells when few trials were missing. Figure 23 shows confusion matrices associated with each cell population under either of the two visual conditions. Each single element of a confusion matrix gives the probability of predicted position given the population activity associated with the actual limb position. We used confusion matrices to provide a sense of how accurately the decoding algorithm could predict the limb position based on cell population activity. Confusion matrices with Perfect decoding accuracy would result in confusion matrices with probabilities of 1 along the diagonal and 0 for the off diagonal matrices.

First we compared confusion matrices under different visual conditions for each population of cells. The most interesting finding was regarding the P cells

which demonstrated effects of position but no effect of the visual feedback conditions according to the ANOVA. Despite the fact that the ANOVAs for this population did not generally show an effect of the visual feedback conditions, decode performance was noticeably different depending on the presence or absence of visual feedback. That is, performance was reasonably accurate in the absence of hand vision but improved when vision of the hand was simultaneously available. This result suggests that the ANOVA lacks the sensitivity required to fully assess the effects of vision in this task. Moreover, this result suggests that visual signals may in fact play a role in representing limb position in this area, though not to the same extent as somatic signals. Not surprisingly, decode performance was slightly improved with vision of the hand for PV cells which were tuned to both position and the visual feedback conditions. Lastly, there was no distinct difference of decode performance between the two visual conditions for V cells which only showed an effect of vision by the ANOVA. In fact, decode performance of V cells was poor for both visual conditions.

We also compared confusion matrices across cell populations. Note we must be careful in comparing confusion matrices across cell populations since decode performance could largely be affected by the population size. That is, the more cells showing some effects of position that are included in the population, the better the decode performance should be. We found decode performance was improved by grouping P cells with PV cells. However, grouping V cells with P cells and PV cells undermined decode performance, though these detrimental effects were not dramatic since very few V cells were used in this study. When we also included all the rest of the cells to predict limb position, we found that decode performance was not improved and if fact appeared to

decrease slightly with respect to performance using only P and PV cells. This meant, unlike P cells and PV cells, which may provide a hint of where the limb was in space, V cells and other cells in the population do not help to improve the accuracy of position decoding and hence may not involved in encoding the limb position in space.

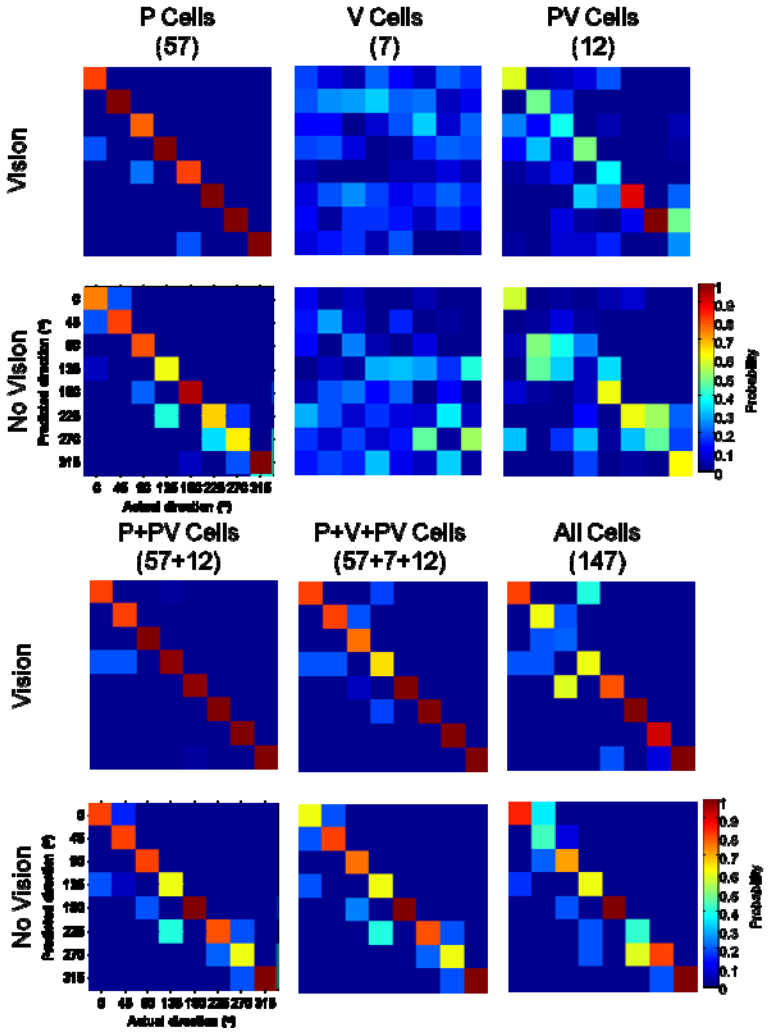

Figure 23. Results of Bayesian population decoding analysis in Paradigm 1. Confusion matrices are shown to give decoding accuracy of limb positions under two visual conditions and for different cell populations. Color code indicates the

probability of decoded position (x coordinate) given population activity associated with actual limb position (y coordinate).

4.4.2.3.2 Paradigm 2

As described in the previous section, we computed confusion matrices based on population activity on visual trials and somatic trials in Paradigm 2. Figure 24 shows the results of this Bayesian population decoding analysis. In general, the results obtained from Paradigm 2 were similar to those from Paradigm 1. Decode performance was slightly better under the “vision” condition than that under the “no-vision” condition for P cells and PV cells but not for V cells. V cells and the rest of the cells did not appear to provide information about the limb position in space. However, compared with Paradigm 1, overall decode performance in Paradigm 2 was poorer and the difference in decode performance between visual conditions was less distinct. The poorer decode performance might be explained by the fact the fewer cells were recorded in Paradigm 2. It is currently unclear why we did not see a much worse decode performance under the “no-vision” conditions in Paradigm 2, where visual information of the hand was disallowed before target acquire under the “no-vision” condition. This might also be related to the relative fewer cells (especially P cells and PV cells) recorded in Paradigm 2.

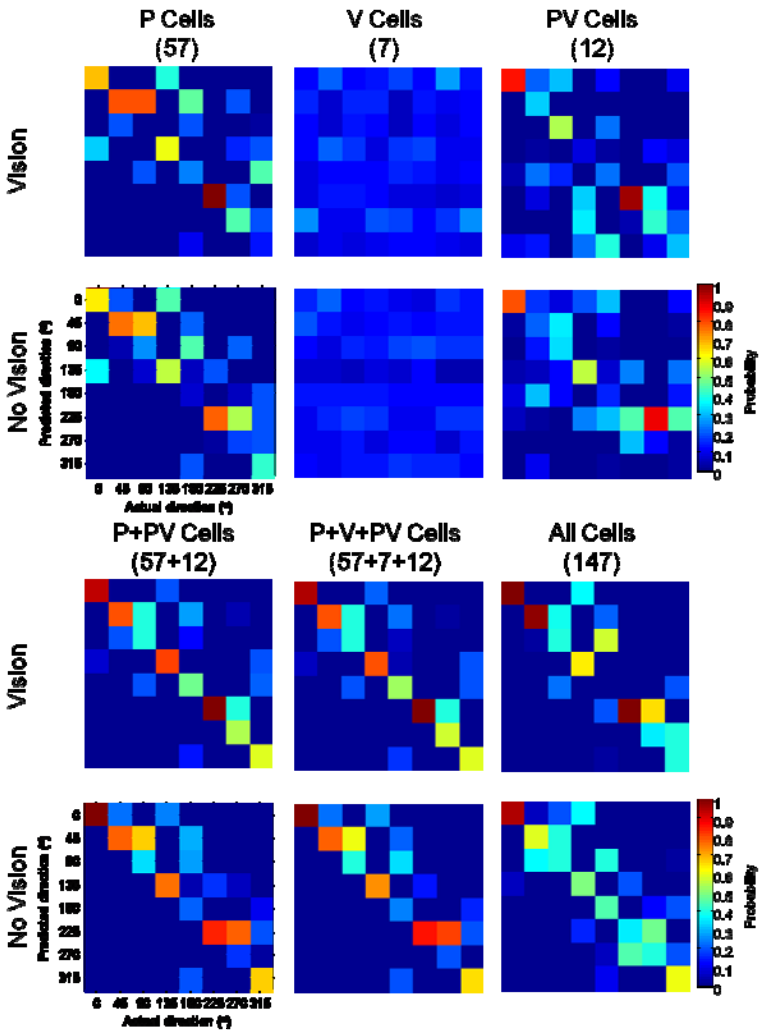

Figure 24. Results of Bayesian population decoding analysis in Paradigm 2. Figure conventions are the same as in Figure 23.

4.4.3 Effects of Window Radius

Based on ANOVA analysis of single cell activity in Paradigms 1 and 2, very few cells were shown to be modulated by the vision of the endpoint of the limb. One possible explanation was that visual signals regarding limb position were not weighted strongly under both the “vision” and “no-vision” condition. This could often be seen in a well practiced task where task performance was not highly contingent on presence of vision. To test this possibility, we varied the 3D

behavioral window associated with the acquisition of each target ("window radius") and examined the effect of this window radius on the animal's behavior as well as on single cell responses. The experiments were done in Paradigm 1 on Monkey X.

4.4.3.1 Behavior

Behavioral performance of the animal was quantified by counting the number of target misses for each single session of trials. A target miss was considered whenever the animal attempted but missed the peripheral target or failed to hold the endpoint of the limb within the peripheral target window for a specified amount of time. For each of the two visual conditions ("vision" VS. "no vision") in a single session, we counted the number of misses until the animal completed 80 successful trials. The mean value and standard deviation of the number of misses were computed across sessions with the same window radius. For this study, we examined 33 behavioral sessions window radius of 0.8 cm, 46 with that of 1.2 cm, 23 with that of 1.6 cm and 26 with that of 2.0 cm. Also note in previous result sections, window radius was 1.6 cm for neurophysiological recordings. Figure 13 shows the effect of window radius on the animal's behavior. We found the number of misses decreased monotonically with increasing window radius. Behavioral performance was more variable for smaller window radius as indicated by the error bar of standard deviation. For all window radii examined, behavioral performance appeared to be better (indicated by the lower mean) and more stable (indicated by the smaller standard deviation) in the presence of vision. In fact, p values presented in

Table 3 indicates there was a significant behavioral difference between the vision and no vision conditions for window radii smaller than 2.0 cm ($p<0.05$).

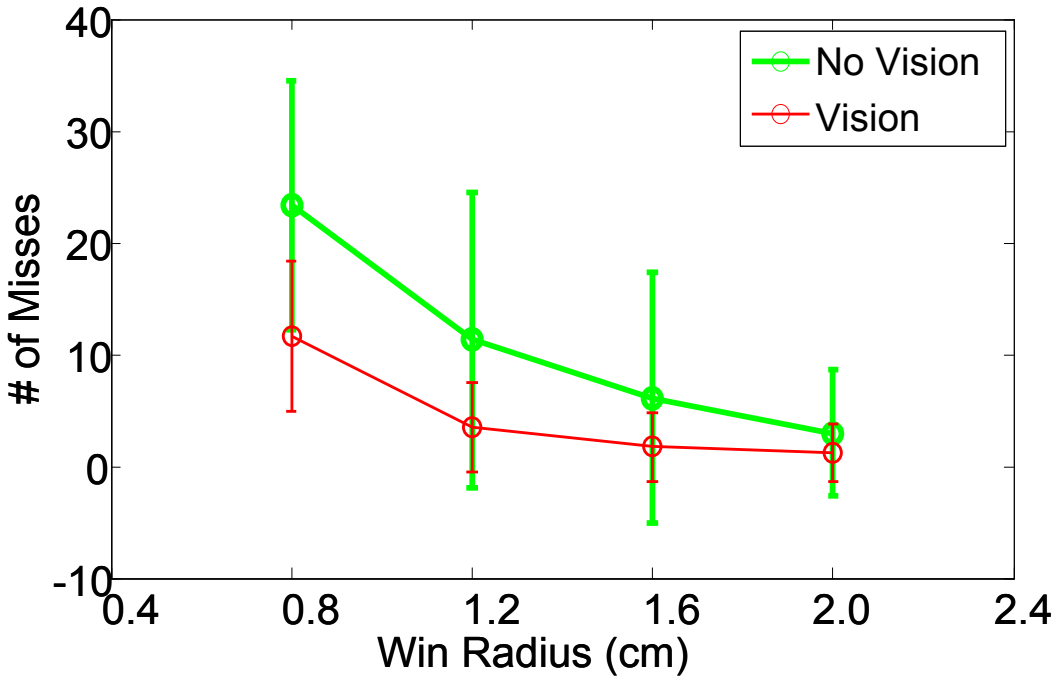

Figure 25. Number of misses in a session of 80 trials under the "vision" and "no-vision" condition for various window radii (0.8, 1.2, 1.6, 2.0 cm). Mean values present the mean across all single sessions. Error bars denote standard deviation of the number of misses.

Table 3. Values of mean and standard deviation of number of misses under the "vision" or "no-vision" condition for various window radii (0.8, 1.2, 1.6, 2.0 cm). Also given in the far left column of the table are p-values for testing the equivalence of the mean of number of misses under the two visual conditions.

	Vision		No Vision		
Win R (cm)	Mean (#)	Standard deviation(#)	Mean (#)	Standard deviation(#)	p-Value
0.8	11.6000	6.7158	23.3200	11.1729	0.0000
1.2	3.5000	3.9862	11.3077	13.2462	0.0000
1.6	1.7188	3.0505	6.1250	11.2558	0.0112
2.0	1.2727	2.5823	2.9545	5.6361	0.0709

4.4.3.2 Neurophysiology

Although the results presented in the previous section indicated that there was a significant behavioral performance difference between the two visual conditions for smaller window radii, analyses of single cell responses did not show corresponding difference in cell activity. Figure 26 illustrates the PSTHs generated from a sample cell for two different window radii. As with Cell A shown in Figure 19, this cell also exhibited tuned perimovement activity as well as tuned static positional discharge. For both window radii (2 cm and 1.2 cm), there was no apparent difference in the activity of the cell between vision and no-vision trials. In fact, shrinking the window radius did not appear to affect the responses of this cell: Figure 14a appears quite similar to Figure 14b. We also performed an ANOVA on the mean firing rates of cell responses associated with each window radius. The results of these ANOVAs further corroborated this finding. For both window radii, there was a significant main effect of position ($p \approx 0 < 0.05$) but no significant main effect of the visual conditions ($p = 0.5$, $p = 0.3$) and no significant position/visual conditions interaction ($p = 0.6$, $p = 0.5$). Examination of other cells also did not show a significant difference in cell responses for different window radii.

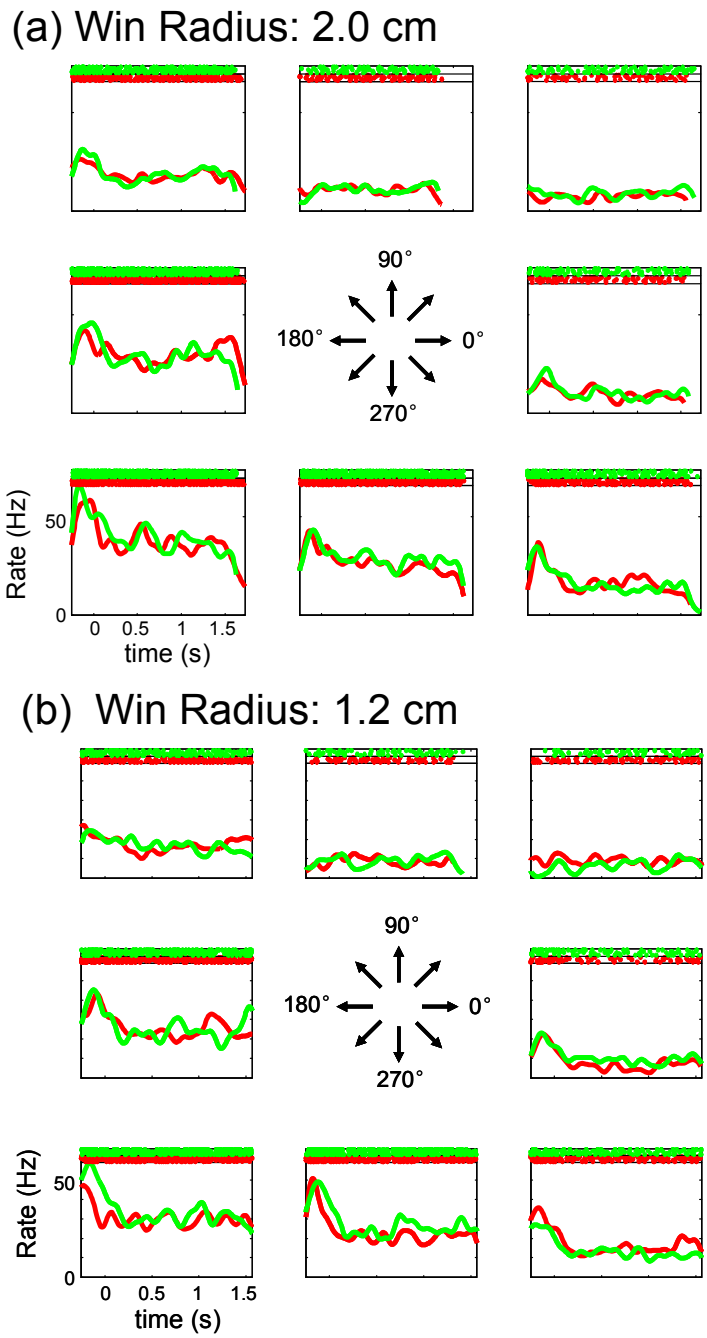

Figure 26. Responses of one area 5 neuron when window radius was 2.0 cm (a) or 1.2 cm (b). Neural activities were recorded during a sing session of 80 trials in Paradigm 1. Other figure conventions are the same as in Figure 19.

4.5. Discussion

In this chapter, we described work aimed at trying to understand how the brain integrates somatic and visual information for limb position estimation. We assessed the activity of neurons in the area 5 of the PPC as the arm was held at various positions with respect to the body. In this experiment, activity was mapped at each position under conditions where visual and somatic input were concurrently available ("somatic + visual") as well as in the absence of visual input ("somatic"), controlled via a virtual-reality system. We did single cell analysis which focused on changes in peak response magnitude induced by viewing the arm. The results showed that, while about half the cells in this region appeared to be modulated by static limb position, only about 10% of the neurons appeared to differentiate between somatic and somatic + visual conditions. Even more surprisingly, very few of these latter cells were also tuned to position and very few cells overall showed a significant interaction between position and sensory conditions. These results indicate that relatively few individual area 5 neurons appear to be modulated by the sight of the limb during static holding. When we enhanced the relevance of vision in this task by shrinking the window radius within which the endpoint of the limb needed to be maintained, cells in this area still did not demonstrate strong effects of the visual conditions. The results also remained largely the same when we used an experimental paradigm (Paradigm 2) where visual information and somatic information about limb position were supposed to be weighted even more unevenly between trial conditions. Thus, analyses of single cell activities suggested very few cells in area 5 appeared to integrate visual information about limb position with somatically-derived signals. However, a decoding analysis at the population

level showed that vision does appear to play a role in representing limb position in this area. The results of these analyses showed that, for the population of neurons that demonstrated effects of position but no effect of the visual feedback conditions (according to ANOVA), the decoding performance in predicting the actual limb position was slightly better when visual input was present. However, the results also suggest that the presence of purely visually modulated cells appears to interfere with the coding of limb position even in populations of purely position-tuned cells. Thus, visual signals may in fact play a role in representing limb position in this area. However, the relatively modest changes that were observed suggest that area 5 may not be the primary site where cue integration of somatically and visually based limb position signals takes place.

4.5.1 Other Possible Neural Substrates of Integration

Given the observations in this chapter, could other arm-movement-related areas be the primary sites of integration for somatically and visually based limb position signals? In exploring other candidate areas, one consideration should be the relative strength with which unimodal inputs are represented within a given area. That is, the densities of anatomical connections from unimodal areas to a given multimodal area are often variable and relatively unequal, which may place limitations on the extent to which these unimodal inputs can be weighted in a given task (Apker, Shi, and Buneo 2009). Dorsal area 5, while reportedly multimodal, appears to be dominated by somatic input while the adjacent MIP appears to represent visual and somatic signals more equally (Caminiti, Ferraina, and Johnson 1996; Colby and Duhamel 1991). The relatively strong visual responsiveness of neurons in this MIP and its reported involvement in eye-centered coding of spatial information suggests MIP would likely be a good site

to find cells with activities showing strong effects of limb vision. More experiments are needed in this area since most of the recordings performed in the superior parietal lobule of PPC have focused on surface cortex (area 5) with smaller numbers of neurons being recorded in MIP.

Other possibilities include areas thought to be functionally downstream of the PPC. Premotor areas receive inputs from PPC and appear to interact with the PPC in the computation of motor plans requiring information about the current location of limb. In addition it has been reported that premotor areas integrate somatic input with visual input near the body (Graziano, Hu, and Gross 1997; Graziano, Yap, and Gross 1994; Graziano 1999). Thus premotor areas could possibly play an important role in the integration of somatic and visual signals for limb position estimation. Regarding the different premotor areas, PMv certainly appears to be more visually driven than PMd or area 5, but the results of Hoshi and Tanji suggest that PMv neurons do not strongly encode information on the particular arm (left or right) that will be used to make a given movement (Hoshi and Tanji 2002) but instead reflect the visual motion of the hand in a limb-independent manner (Ochiai, Mushiake, and Tanji 2005). Thus, although PMv neurons may represent both visual and somatic information about the hand to be moved, this information may not be integrated in this area. Clearly more experiments are needed. On the other hand, cells in PMd exhibit responses that could point to a role in visuosomatic integration for the limb position estimation. PMd neurons encode information about both the static position and configuration of the limb (Pesaran, Nelson, and Andersen 2006; Scott, Sergio, and Kalaska 1997) and the area is known to receive visual input via the parietal lobe (Caminiti, Ferraina, and Johnson 1996). In addition, and in contrast to PMv, PMd strongly

encodes information on the arm that will be used to make a given movement (Hoshi and Tanji 2000). Given aforementioned reasons, all these other areas could be involved in integrating visual and somatic signals for limb position estimation. However, we also have to point it out that it does not necessarily mean that stronger visual input about limb position could be found in these areas as well. That is, cue integration for limb position estimation could be a collaborative result of two or more brain areas and it still is not entirely clear now whether vision is strongly required for the task in this study. The details of explanations are presented below and in the last part of the discussion section.

Note that cue integration for limb position estimation could arise from the operations of the distributed network containing two or more areas. The previously described predictions presume that cue integration will manifest neurally as changes in the mean firing rates of neurons in a given area. The results are consistent with the idea that multisensory cue integration is achieved via the convergence of input from largely unimodal areas onto higher order multisensory areas, which may subsequently be fed back to lower level unisensory areas (Bauer 2008). However, neural correlates of cue integration could also manifest as a synchronous activation of two or more areas that are largely devoted to either visual or somatic processing. It has been suggested that some aspects of cue integration could also be achieved via lateral interactions between unimodal areas (Bauer 2008). A recent study has provided evidence for such a mechanism by showing increased interareal synchrony between sites in the auditory cortex and the STS when auditory and visual looming signals (i.e., signals indicating the rapid approach of potentially harmful objects) are presented together (Maier, Chandrasekaran, and Ghazanfar 2008).

Presentation of combined auditory and visual looming signals was also previously shown to result in enhanced perception of looming signals (Maier et al. 2004). Taken together, these results suggest that interareal synchronization might prove to be a useful probe for some aspects of cue integration, particularly if such synchrony can be shown to covary with behavioral measures of integration (Bauer 2008).

4.5.2 Role of Visual Input in Area 5

Thus far, studies of area 5 suggest that visual information about arm position is not strongly represented in this area. In the study by Graziano and colleagues (Graziano, Cooke, and Taylor 2000), only a small percentage of neurons (~15-20%) were modulated by visual signals about the passively placed static arm. In a more "active" paradigm where arm movement was required (Buneo et al. 2003), only 10% of the neurons were modulated by visual information about the hand at the starting position. The present results also suggest that visual information regarding arm position is not strongly represented in area 5. This is true even under conditions where visual input is expected to have a strong effect, that is, during the maintenance of static positions in free 3D space. Note that the finding that a code for hand position in eye-centered coordinates exists in area 5 is not incongruent with this idea. That is, such a coding scheme is still possible via coordinate transformations of somatic signals. Note also that the aforementioned findings do not mean that cells in this area are not visually responsive. An anatomical basis exists for visual information to flow into both the superior and inferior parietal lobules (Caminiti et al., 1996) and moderate to strong responses to visual stimuli have been well documented in these areas (Andersen & Buneo, 2002, 2003; Buneo & Andersen, 2006). The

relatively weak evidence for multisensory integration of visual and somatic arm-position information is therefore surprising, given the history of recordings in the PPC (Andersen, Snyder, Bradley, & Xing, 1997). Visual input to area 5 may have more to do with specifying the locations of extrinsic objects, rather than the positions of parts of the body.

4.5.3 How Much is Visual Input Weighted In this Task?

It is much easier to probe the neural mechanisms of cue integration if visual and somatic signals are perceptually equivalent during the task. However, if visual signals are relatively unreliable and consequently not weighted very strongly in the task, only small differences would be found between the "vision" and "no vision" conditions. In previous studies, animals were passively varying arm positions (Graziano, Cooke, and Taylor 2000) or under conditions where the animals were receiving strong haptic input on visual trials (Buneo and Andersen 2003). Thus visual information may be weighted minimally in the context of these tasks. The present study employed an experimental paradigm where visual input would be expected to have stronger influence, i.e. under conditions where the arm was held statically in free space. However, few area 5 cells were found modulated by visual cues about arm position. Although the experimental paradigm in the present task is expected to have a stronger effect of vision compared with other aforementioned tasks, it is still possible that CNS does not weight visual information strongly if it doesn't require a lot of visual information in order to hold arm stable in space.

How is it possible that visual input about limb position could be minimally required when holding the arm statically in free space? First, let us consider this question: What maintains limb stability? Shadmehr has proposed that generally

there are three mechanisms helping to maintain the hand at a reach target (Shadmehr and Wise 2005). One mechanism concerns the antagonist architecture and intrinsic muscle properties. We know that pairs of muscles that act against each other create antagonist architecture. The antagonist architecture produces a balance of forces or an equilibrium point which helps stabilize the limb. The passive, springlike properties of muscle create intrinsic muscle stiffness which also promotes limb stability. This mechanism responds with almost no delay and provides the first line of defense against perturbations. The second mechanism concerns involuntary short-loop spinal reflexes such as stretch reflexes. This mechanism takes longer and also contributes to limb stability. The third mechanism concerns the long-loop feedback pathways mediated by the brain. These feedback pathways provide a mechanism by which the limb position can be cognitively monitored and controlled. However, it takes even longer since the sensory signals have to reach the brain where they are transformed into motor signals which are transferred back to the periphery. All these mechanisms could help to maintain limb stability in free space. Thus, visual information about limb position may not be that necessary in holding arm statically in free space.

Another reason vision might not have been important in maintaining limb stability in the present tasks could be related with motor learning. In the initial stages of learning to reach to a target, reaching movements could be much more variable since motor plans selected and the corresponding motor commands generated have not been optimized. At this time, vision may play a more important role in successfully reaching a target. However, after a certain amount of practice, an optimal sequence of motor commands that accomplishes the goal

can be formed and consolidated. At this point, visual information may be less required. In our study, it is possible that animals (especially Monkey X) are over trained and visual information about hand position may not be weighted strongly in the movements. Although there may be some reasons why visual information about limb position may not be weighted strongly in the task of this study, it is still possible that visual information about limb position will be more evident when it is needed for online control of limb movements rather than simply during the maintenance of static arm position.

Chapter 5

MOVEMENT VARIABILITY RESULTING FROM VARIOUS NOISE SOURCES

5.1. Abstract

Limb movements are highly variable due in part to noise occurring at different stages of movement production, from sensing the position of the limb to the issuing of motor commands. The independent contributions of noise at each stage to overall movement variability are difficult to determine experimentally and are therefore not well understood. Here we used a simulation approach to predict the effects of noise associated with 1) sensing the position of the limb ('position sensing noise') and 2) planning an appropriate movement vector ('trajectory planning noise'), as well as the combined effects of these factors, on arm movement variability across the workspace. Results were compared to those predicted by a previous model of the noise associated with movement execution ('execution noise'). We found that the effects of sensing and planning related noise on movement variability were dependent upon both the planned movement direction and the initial configuration of the arm and were different in many respects from the effects of execution noise. The effects of trajectory planning noise alone were substantially greater than those due to position sensing noise and the interaction between sensing noise and planning noise was highly complex across movement directions. Variability due to execution noise was also shown to be arm configuration dependent and was more direction-dependent than that due to position sensing noise, trajectory planning noise or their combined effects. These results provide important insights into the relative roles of sensing, planning and execution noise in movement variability that

should prove to be useful for neurophysiological investigations seeking to relate variability at the neural level to variability at the behavioral level.

5.2. Introduction

The term ‘noise’ refers to random fluctuations in a signal. Noise is present not only in signals carried by electronic components but also in signals carried by the nervous system and has been shown to have both negative and positive effects on information processing (Faisal, Selen, and Wolpert 2008). In general, however, neurally-derived noise is thought to be problematic for the brain. For example, noise associated with sensing the position of the limbs as well as noise occurring during the planning and execution of motor acts results in movement variability, a hallmark of human motor performance. In many neurological diseases this variability can be magnified (Contreras-Vidal and Buch 2003; Hermsdorfer and Goldenberg 2002; Longstaff and Heath 2006; Thies et al. 2009), which can affect the performance of even simple motor acts. Thus, understanding the consequences of noise occurring at different stages of movement production can lead not only to a better understanding of neural processing but may also lead to better treatment approaches for some neurological disorders.

In the arm movement system, noise in the sensory systems responsible for estimating limb and/or target position (i.e. proprioception and vision) has been shown to contribute to arm movement variability (Buneo et al. 1995; McIntyre, Stratta, and Lacquaniti 1998; Apker, Darling, and Buneo 2010; Rossetti, Desmurget, and Prablanc 1995; Sober and Sabes 2003). The effects of this noise manifests somewhat differently in the visual and somatosensory systems, due to the unique properties of their corresponding sensors. For example,

localization of the hand by proprioception is more precise when the hand is closer to the body and is more precise in depth than in azimuth, which appears to be due in part to posture-dependent changes in the arrangement of the proprioceptors in the arm (van Beers, Sittig, and van der Gon 1998). Vision is also more precise for positions closer to the eyes/body but is more precise in azimuth than in depth, which is likely due to the limitations of visual depth perception (van Beers, Wolpert, and Haggard 2002). These differences in precision across the workspace mean that the joint probability distribution describing the static position of the hand in the horizontal plane can appear to be isotropic or anisotropic in shape, depending on which sensors are used and where the hand is positioned in the workspace (van Beers, Sittig, and van der Gon 1998, 1999). The consequences of this sensing noise on movement production are not well understood however.

Noise can also arise during the movement planning process. For example, it has been argued that the spatial distributions of movement endpoints following arm movements performed in the horizontal plane result from noise associated with the independent planning of the direction and amplitude of required reach vectors (Gordon, Ghilardi, and Ghez 1994). For movements in 3D space, patterns of movement variability are even more complex and appear to be dominated by noise associated with planning movements in depth (Apker, Darling, and Buneo 2010; McIntyre, Stratta, and Lacquaniti 1997). These complex patterns of movement variability may also be related to distortions associated with transforming reach-related variables from visual to motor coordinates (McIntyre et al. 2000). Such distortions affect patterns of endpoint variability as errors are passed from one coordinate frame to the next.

Noise generated during movement execution can also profoundly affect movements. Buneo et al. (1995) examined the effects of random fluctuations in the magnitude of joint torques at the shoulder and elbow and found that the resulting movement variability was direction dependent and fundamentally different in nature than the direction-dependent variability that results from sensor noise introduced at the elbow joint. More recently, van Beers and colleagues (2004) explored the effects of noise introduced directly into the motor commands (rather than to the torques that result from these commands). These investigators also found that simulated endpoint variability was direction dependent and, moreover, was very similar to the patterns of movement variability that were produced by neurologically intact human subjects when sensing and planning noise were minimized. In other words, when other sources of noise were reduced in magnitude, patterns of arm movement variability appeared to be largely determined by execution-related noise.

Overall, the relative contributions of sensing, planning, and execution-related noise on movement production across the workspace are not well known. In addition, while these noise sources have traditionally been evaluated independently, they naturally interact during the production of movement and the consequences of this interaction are only beginning to be investigated. For example, Wolpert and colleagues (2009) have argued that planning and execution-related noise combine near-optimally in the temporal domain (Faisal and Wolpert 2009). In addition, patterns of arm endpoint variability in 3D space have recently been shown to arise from differences in the relative levels and spatial distributions of planning and execution-related noise (Apker, Darling, and Buneo 2010). However, despite recent progress in this area, the manner in

which noise occurring at different levels interacts to influence movement variability remains poorly understood. Here we used a simulation approach to characterize the effects of position sensing noise and trajectory planning noise, as well as their combined effects, on arm movement variability across the workspace and compared the resulting movement variability to that predicted by execution noise. The results provide important insights into the consequences of noise occurring at different stages of movement production. In addition, the results may ultimately prove useful for developing strategies to reduce the exaggerated movement variability that arises in patient populations and for the interpretation of neurophysiological investigations designed to relate variability at the neural level to variability at the behavioral level.

5.3. Methods

5.3.1 Noise Simulation I: Errors in Sensing Initial Conditions

Simulation I (SI) evaluated the effects of noise in the sensing of initial conditions on errors in movement direction. This was simulated by introducing random perturbations into the initial hand position/arm configuration and assuming that the motor system was unaware of these perturbations and thus failed to compensate for them. Two random perturbation distributions were independently assessed (Figure 27). The isotropic (circular) perturbation distribution was chosen as a general approximation of the joint visual-somatic probability distribution describing hand position estimation in the horizontal plane (van Beers, Sittig, and van der Gon 1999). Perturbations were drawn from a Gaussian distribution and had a standard deviation of 0.02828 m along any given axis. The anisotropic (elliptical) distribution had a standard deviation of 0.02 m along its minor axis and 0.04 m along its major axis and was thus equal in area

to the isotropic distribution. For the anisotropic distribution, the minor axis was collinear with a vector pointing from the shoulder to the hand, an approximation to the anisotropy in somatically based hand localization reported by van Beers and colleagues (van Beers, Sittig, and van der Gon 1998). Note that the level of position sensing noise (i.e. the size of the ellipses illustrated in Figure 27) was arbitrarily determined as the focus of these simulations was not on the overall magnitude of movement variability but on its direction dependence (distribution in space) and arm configuration dependence.

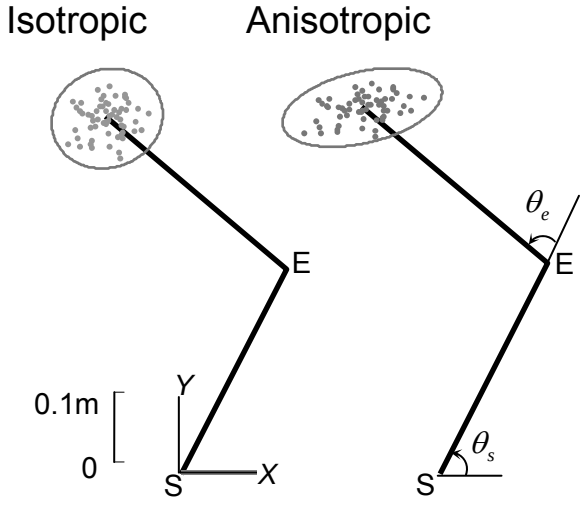

Figure 27. Illustration of the arm endpoint perturbations used in SI and SII for one arm posture. Two random error distributions were used (isotropic and anisotropic). The isotropic error distribution was chosen as an approximation to the joint visual-somatic probability distribution describing hand position estimation in the horizontal plane (van Beers, Sittig, and van der Gon 1999). The anisotropic distribution was chosen as an approximation to the anisotropy in somatically based hand localization (van Beers, Sittig, and van der Gon 1998). S: shoulder. E: elbow. θ_s: shoulder angle. θ_e: elbow angle.

Figure 28a illustrates the effect of a single perturbation trial in SI. In this simulation, movement directions were defined with respect to the initial hand position only and were not directed to particular locations in the workspace. As a result, planned movement vectors under perturbed conditions were simply translated versions of vectors that would have been planned under unperturbed conditions. Despite this fact, errors in movement direction were generated in the perturbed condition as a result of a failure to compensate for differing initial conditions. That is, perturbations introduced a discrepancy between the 'sensed' and 'actual' initial conditions. Since the joint torques associated with a given movement direction depend on the initial conditions, failure to recognize this discrepancy resulted in the wrong torques being 'selected' for the required movement. This resulted in deviations of the actual trajectory from the required trajectory through the conducting chain of forward transformations.

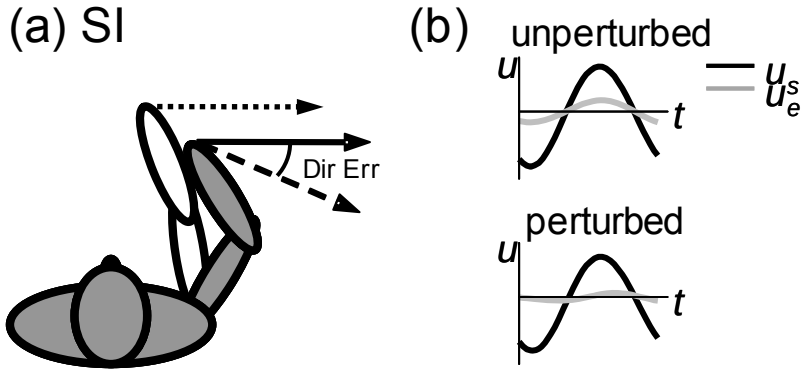

Figure 28. (a) Schematic illustration of the movement errors (Dir Err) generated on single perturbation trials in Noise Simulation I (SI): Errors in sensing initial conditions. Filled (gray) arm shows the arm configuration under unperturbed conditions while the unfilled (white) arm represents the perturbed conditions. Solid black vector: movement planned under unperturbed conditions. Dotted vector: Movement planned under perturbed conditions. In this simulation,

movements were not planned to a fixed spatial location, thus perturbation of the arm simply caused a translation of the planned movement vector. As a result, the movement error (dashed vector) resulted solely from a misestimation of initial arm configuration. (b) Schematic of the motor commands at the shoulder (u_s) and elbow (u_e) under unperturbed and perturbed conditions in SI.

5.3.2 Noise Simulation II: Errors in Sensing Initial Conditions + Errors in Trajectory Planning

Simulation II also involved the introduction of random perturbations (isotropic and anisotropic) into the initial hand position/arm configuration and quantification of the resulting movement errors. In contrast to SI however, planned movement directions in SII were defined by vectors connecting the perturbed initial hand positions to fixed spatial targets (Figure 29a), which is more like what a human subject might encounter in real life. In this situation, movement vectors planned from the perturbed hand locations were not the same as those that would be planned under unperturbed conditions but differed from these in both direction and extent. As a result, directional errors in this simulation can be attributed to two sources: 1) a failure to compensate for changing initial conditions (as in SI) and 2) errors in trajectory planning.

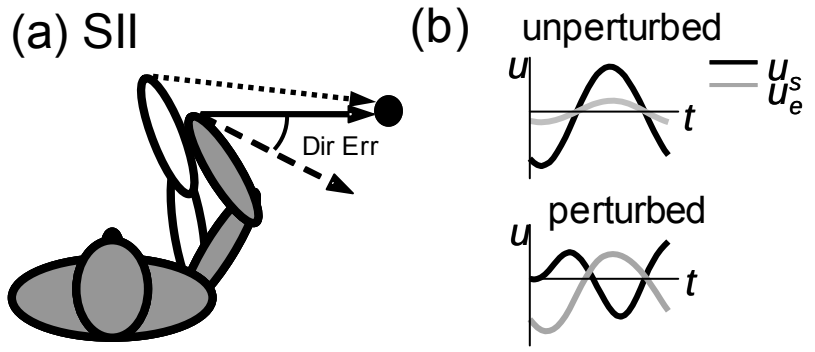

Figure 29. (a) Schematic illustration of the movement errors (Dir Err) generated on single perturbation trials in Noise Simulation II (SII): Errors in sensing initial conditions + errors in trajectory planning. Since movements were planned to a fixed spatial location (filled circle), perturbation of the arm resulted in a translation and rotation of the planned movement vector. The movement error resulted from a misestimation of the initial conditions and a misestimation of required movement vectors. (b) Schematic of the motor commands under unperturbed and perturbed conditions in SII. Other figure conventions are the same as in Figure 28.

5.3.3 Noise Simulation III: Errors in Movement Execution

In this simulation, rather than introducing noise into the estimated position of the limb we instead introduced noise into the elbow and shoulder motor commands responsible for generating the simulated movements (Figure 30). The noise in motor commands arises during the execution stage of movement production. In our simulation, this 'execution noise' was generated using a model proposed by Van Beers and colleagues (2004). Based on this model, execution noise was composed of three components: signal-dependent noise (SDN), signal-independent noise or constant noise (CN), and temporal noise (TN). SDN

was first proposed by Harris and Wolpert (1998) as noise whose variance increases with the size of the neural control signal. SDN was modeled as Gaussian white noise in the magnitude of the signal with zero mean and a standard deviation (σ_{SDN}) proportional to the absolute value of the motor command. Stated mathematically, σ_{SDN} was defined as $\sigma_{SDN} = k_{SDN} \cdot u$, where u is the motor command and k_{SDN} defines the level of the noise. CN was proposed by Van Beers and colleagues to result from the background activity of neurons and was modeled as a constant level of noise that was independent of the neural control signal. CN was modeled in a similar way as SDN, but with a standard deviation (σ_{CN}) that was independent of the motor command: $\sigma_{CN} = k_{CN}$. CN and SDN were assumed to be independent, with the total amount of noise having a standard deviation of $\sqrt{\sigma_{SDN}^2 + \sigma_{CN}^2}$. Lastly, TN accounts for variability in movement duration and as a result was added to the motor commands after the inverse transformations. The level of TN was defined by the coefficient of variation k_{TN}. For a single simulated movement, the duration of the motor commands was scaled by a factor c that was randomly sampled from a normal distribution with mean of one and standard deviation of k_{TN}. Since movements with a longer duration tend to have a lower peak velocity, the magnitude of the motor command was scaled by a factor of $1/c^2$ when movement time was scaled by a factor of c (van Beers, Haggard, and Wolpert 2004).

The values of the parameters k_{SDN}, k_{CN}, k_{TN} were previously estimated by van Beers and colleagues (2004) by fitting the noise model to experimental data so as to optimize the log likelihood of observed movement endpoints. The best fitting parameters were $k_{SDN} = 0.103$, $k_{CN} = 0.185$, and $k_{TN} = 0.083$. Noise levels were assumed to be the same for both the shoulder and elbow motor commands

and were added to the two joint motor commands simultaneously and independently. Figure 30b illustrates the shoulder and elbow motor commands determined for rightward (0˚) movements under normal (uncorrupted) conditions (upper plot), as well as when these commands are corrupted by noise (lower plot).

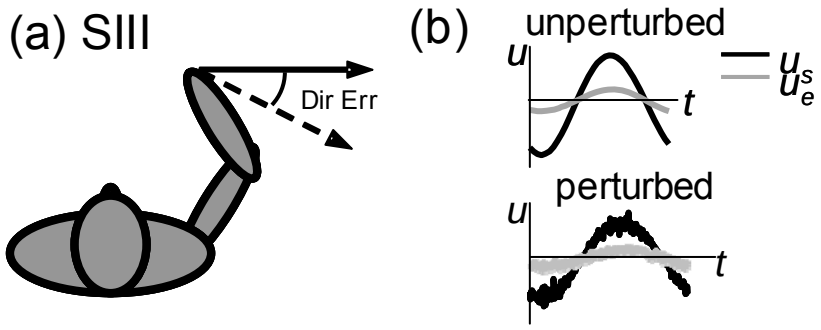

Figure 30. (a) Schematic illustration of the movement errors (Dir Err) generated on single perturbation trials in Noise Simulation III (SIII): Errors in movement execution. No perturbations of the initial arm configuration were introduced. Movement error results from noise introduced into the motor commands. (b) Schematic of the motor commands in SIII. Figure conventions are the same as in Figure 28 and Figure 29.

5.4. Results

5.4.1 Noise Simulation I: Errors in Sensing Initial Conditions

5.4.1.1 Simulation Results for One Initial Arm Posture

In this simulation, random perturbations were introduced into the initial hand position to simulate imprecise limb position estimation and the resulting effects on movement variability were quantified. Results are shown in Figure 31 for one initial arm posture (initial arm posture 1 in Table 2) and both perturbation

conditions (isotropic and anisotropic). Figure 31a shows simulated hand paths associated with 4 movement directions. For both perturbation distributions, the average handpath generally aligned with the planned movement direction: mean directional error was generally between ±1° for any single simulated movement direction. The handpaths generated for any given planned direction were variable however, with the extent of this variability differing somewhat for different movement directions. This can be best appreciated in Figure 31b which plots the circular standard deviation (CSD) of the directional errors resulting from isotropically and anisotropically distributed sensing noise. For both perturbation distributions, these plots were elliptical in shape, indicating that the variability introduced by sensing errors was direction dependent. In addition, for both perturbation distributions, variability was largest along an axis that was aligned approximately with the forearm (i.e. the 135°/315° axis in Figure 31b). The variability associated with the two perturbation distributions did differ in some respects however. For example, variability associated with isotropic perturbations was generally smaller and more elongated or more direction-dependent than the variability associated with anisotropic perturbations, even though the two perturbation distributions were equal in area.

In summary, in SI, the distribution used to simulate imprecise limb position sense in the workspace appeared to have consequences for both the magnitude and direction-dependence of resulting patterns of movement variability but did not appear to influence the movement direction associated with maximal variability.

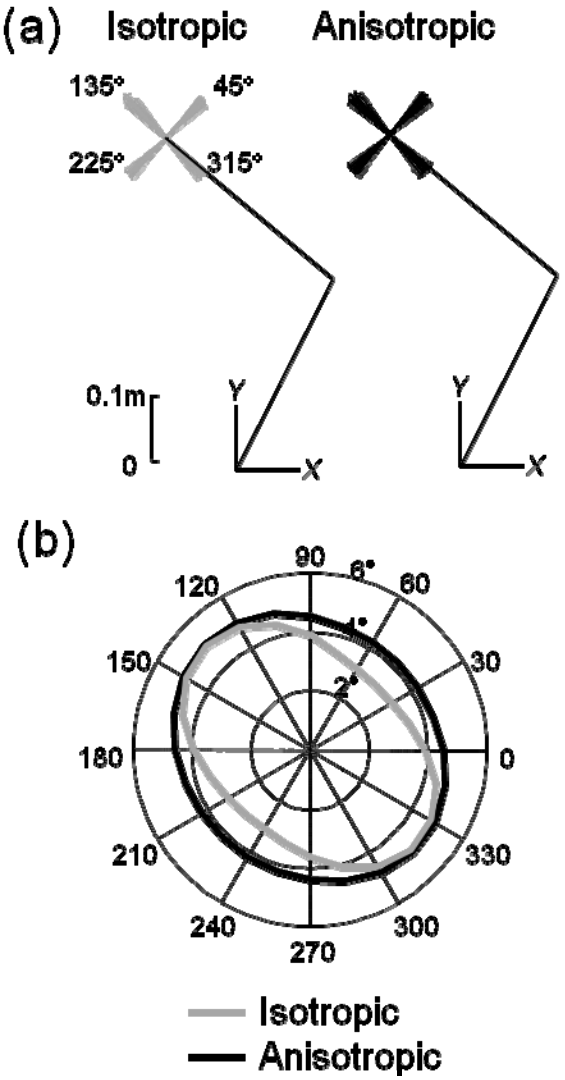

Figure 31. Results obtained from SI for one arm posture. (a) Simulated hand paths for four movement directions in the presence of isotropically and anisotropically distributed endpoint noise. (b) Polar plots of the circular standard deviation (CSD) of the directional errors associated with 24 movement directions.

5.4.1.2 Simulation Results for Multiple Initial Arm Postures

To examine the relationship between movement variability and initial arm configuration, we repeated the analysis shown in Figure 31 for three additional arm configurations (Figure 32). The shoulder and elbow angles corresponding to

these postures can be found in Table 2. For simplicity of presentation, only results associated with isotropic position sensing noise are shown in Figure 32. This figure shows that for the more extended arm positions, direction-dependent aspects of movement variability were not fixed in space, but rotated as the arm posture changed, maintaining a roughly constant spatial relationship with respect to the forearm. In fact, for all three of these arm positions, the axes of maximum variability were aligned with the long axis of the forearm. The magnitude of variability however did not change appreciably with arm posture for these more extended positions, which can be appreciated from the relative the sizes of the CSD plots. However when arm posture changed such that the endpoint was positioned closer to the body, movement variability became noticeably larger and also less direction-dependent. This increased variability can be attributed to the larger changes in joint angles that accompany displacements of the endpoint at this position. This larger change in joint angles results in larger difference in the torques required to move in a given direction (compared to more extended arm postures), thus the effect of a given perturbation is larger at this position.

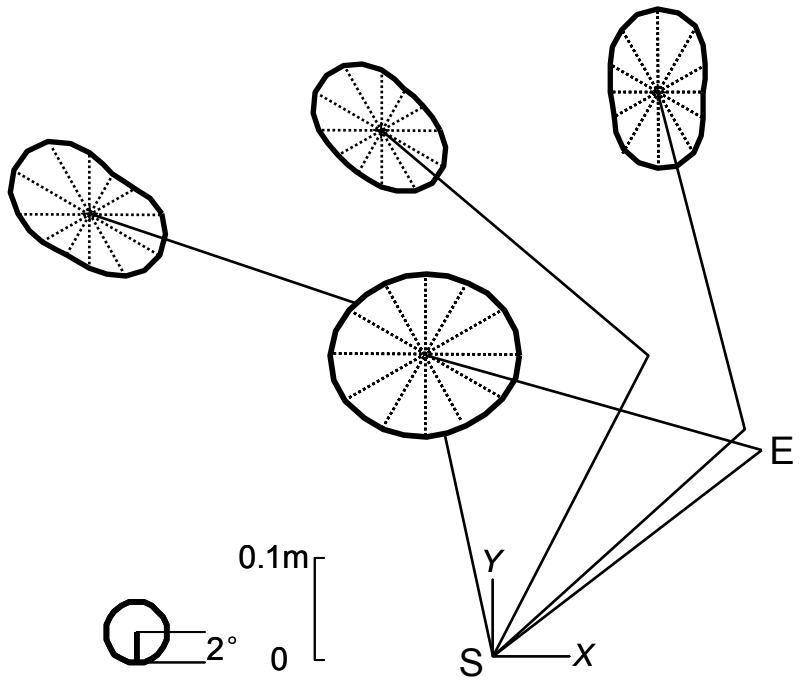

Figure 32. Results from SI for four arm postures. Polar plots of the CSD of the directional errors associated with 24 movement directions are shown for each arm posture. S: shoulder. E: elbow.

5.4.1.3 Sensitivity Analysis of Sensing Noise

Since SI employed random perturbations of the arm endpoint that varied therefore in both magnitude and direction it was difficult to independently assess the effects of the direction and amplitude of these perturbations on observed patterns of movement variability. As a result we also separately characterized the effects of perturbation amplitude (ρ) and perturbation direction (β) on errors in initial movement direction.

5.4.1.3.1 Sensitivity Analysis: Amplitude

For the sensitivity analysis of perturbation amplitude, three different amplitudes were used (0.005, 0.01, 0.02m) and for each amplitude simulations

were conducted for 24 perturbation directions spaced 15° apart. Figure 33 shows the results of these analyses for one initial arm posture (similar results were obtained for the other initial arm postures). Figure 33a shows simulated handpaths associated with three movement directions (0°, 120° and 240°) when perturbations of amplitudes 0.005, 0.01, and 0.02m were applied in each of 24 directions. Variability of the handpaths increased slightly with the progressively larger perturbation amplitudes. This can be appreciated more clearly in Figure 33b where movement direction errors associated with three movement directions (indicated by the different line styles) are plotted as a function of perturbation direction (abscissa) and perturbation amplitude (indicated by line color). Figure 33b shows that for a given planned movement direction, progressively larger amplitude perturbations in a given perturbation direction produced larger errors. In fact, directional error appeared to be roughly proportional to perturbation amplitude. This approximately linear relationship is illustrated in the inset of Figure 33b using one movement direction (0°) and one perturbation direction (50°). The inset plotted the linear polynomial fitting curve based on three data points. The associative R^2 (coefficient of determination) is very close to one and SSE (residual sum of squares) is very close to zero, which indicates the linear regression line almost perfectly fits the data. The linear relationship between directional error (α) and perturbation amplitude (ρ) can be summarized mathematically as:

$$\alpha \approx k \cdot \rho \qquad [22]$$

where k is a scalar denoting the slope.

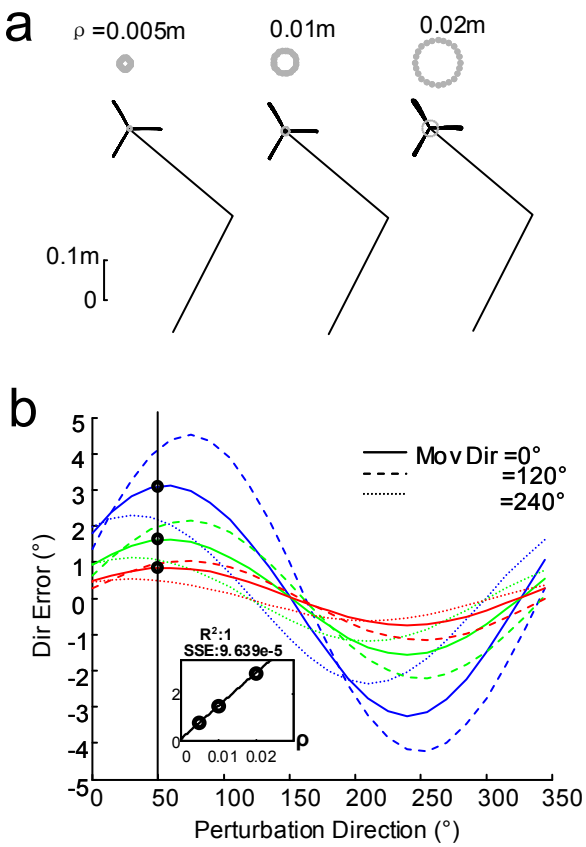

Figure 33. Sensitivity analysis of perturbation amplitude (ρ) for one initial arm posture in SI. (a) Simulated handpaths for 3 movement directions (0°, 120° and 240°) under equal perturbation amplitude of 0.005m (left), 0.01m (middle) or 0.02m (right). Grey circles on top of the three plots illustrate the relative sizes of three equal amplitude perturbations applied in 24 directions. Also shown is the two link system representing the upper and lower arm in each of the three plots. (b) Directional error plotted as a function of perturbation direction for each of three movement directions (0°, 120° and 240°) and three perturbation amplitudes (0.005 (red), 0.01 (green), and 0.02m (blue). The inset shows the linear polynomial fitting curve for three data points (Directional error (α) Vs. Perturbation Amplitude (ρ)) when perturbation direction was fixed at 50° and movement direction was 0°.

5.4.1.3.2 Sensitivity Analysis: Direction

For the sensitivity analysis of direction, perturbation amplitude was fixed at 0.01m and directional errors were evaluated for each of 24 perturbation directions spaced 15°apart. The effects of perturbation direction were found to be more complex than those due to perturbation amplitude. The complex relation between directional error and perturbation direction is illustrated in Figure 34. Here variations in directional error as a function of perturbation direction are shown for all 24 movement directions, given one perturbation amplitude (0.01 m). For each planned movement direction, errors varied roughly sinusoidally with perturbation direction, with a period of about 2π. In addition, these sinusoidal 'waveforms' were not identical but varied in amplitude and phase for different movement directions. As a result, for a given perturbation (with fixed amplitude and direction), directional errors varied across movement directions. This variation in errors could be quite large for some perturbation directions (e.g. ~75° and ~255°), while for some other perturbation directions (i.e. ~15° and ~195°), the variation could be rather small and errors were nearly identical for different movement directions.

The sensitivity to perturbations applied in a single direction is shown in a different format in the lower panel of Figure 34. Here the directional errors associated with each of four perturbation directions (45°, 135°, 225°, 315°) are plotted in polar form. Clockwise directional errors are plotted using solid lines, while counterclockwise errors are plotted using dashed lines. Each of the plots represents a 'slice' through the sinuosoidal curves shown in the upper panel. The variation in directional errors across movement directions can be better appreciated from these plots. These plots show that even fixed amplitude

perturbations applied in a single perturbation direction are expected to result in direction-dependent patterns of errors, though the extent of this anisotropy clearly differed between perturbation directions (e.g. 45° and 135°). These plots also show that for oppositely directed perturbation directions (e.g. 45° and 225°), directional errors are expected to be approximately equal in magnitude but opposite in sign.

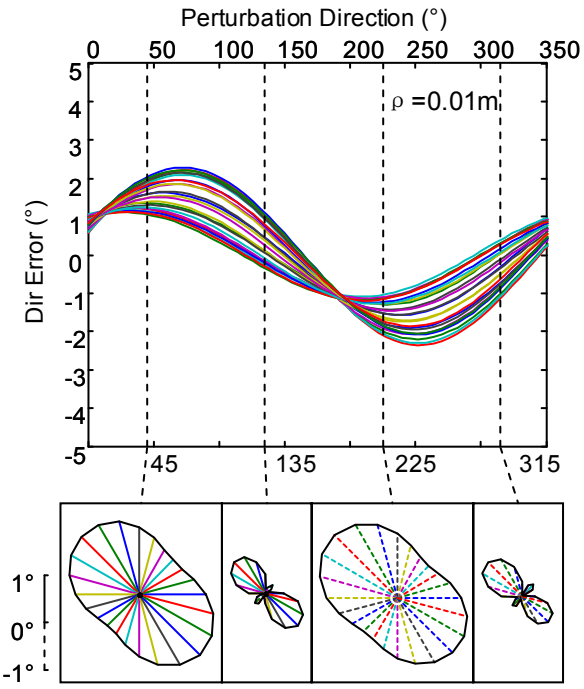

Figure 34. Sensitivity analysis of perturbation direction (β) for one initial arm posture in SI. Data associated with one perturbation amplitude (0.01m) are shown. Upper panel: Directional error as a function of perturbation direction for 24 movement directions (colors). Lower panel: Polar form of directional errors for four perturbation directions (45°, 135°, 225°, 315°). In the polar plots, the orientation of each vector corresponds to a particular movement direction and the magnitude of each vector corresponds to the magnitude of the directional error

(solid lines = clockwise (positive) errors; dotted lines = counterclockwise (negative) errors).

5.4.1.3.3 Discussion and Conclusion

Sensitivity analysis of perturbation amplitude appeared to suggest a simple linear relationship between directional error (α) and perturbation amplitude (ρ). However, sensitivity analysis of perturbation direction indicated that the relation between directional error (α) and perturbation direction (β) was more complex. Directional errors appeared to vary sinusoidally with perturbation direction. These sinusoidal 'waveforms' were not identical but varied in amplitude and phase for different movement directions (Figure 34). These variations, even for constant amplitude perturbations, likely explain why even the relatively simple isotropic perturbation distribution used in SI resulted in a complex pattern of errors across movement directions. Meanwhile, the combined effect of seemingly linear relationship between α and ρ and sinusoidal relationship between α and β may explain why anisotropic perturbations resulted in directional error variability which was less direction-dependent than the variability associated with isotropic perturbations. That is, those perturbations with large/small amplitude were probably associated with a direction resulting in smaller/larger directional error according to the sinusoidal relationship between directional error and perturbation direction. Thus the effect of perturbation amplitude was probably cancelled by the effect of perturbation direction, which resulted in relatively isotropic or less direction-dependent directional error variability. On the hand, if the anisotropic perturbations were oriented in a way that the effect of perturbation amplitude was not cancelled but added to the effect

of perturbation direction, the resulted directional error variability would be much more anisotropic or direction-dependent. Thus, the orientation of anisotropic perturbation distribution may have an effect on pattern of directional errors across movement directions as well.

Directional errors varied across movement directions even for the same perturbation amplitude and direction. The pattern of directional errors across movement directions was quite complex and varied for different perturbation directions (lower panel of Figure 34). To further examine the relation between directional error and movement direction, directional error was plotted as a function of movement direction in Figure 35. Each trace gives directional error as a function of movement direction for one perturbation direction. Directional error appeared to be a sinusoidal function of movement direction with a period of π. Since variation of perturbation direction (β) could move the sinusoidal trace up or down and change its peak to peak amplitude, it appeared that this sinusoidal function was also dependent on perturbation directions (β). For a pair of oppositely directed perturbation directions (with a difference of 180°), directional error traces were symmetrical with respect to horizontal 0 axis, which is consistent to what was suggested by lower panel of Figure 34.

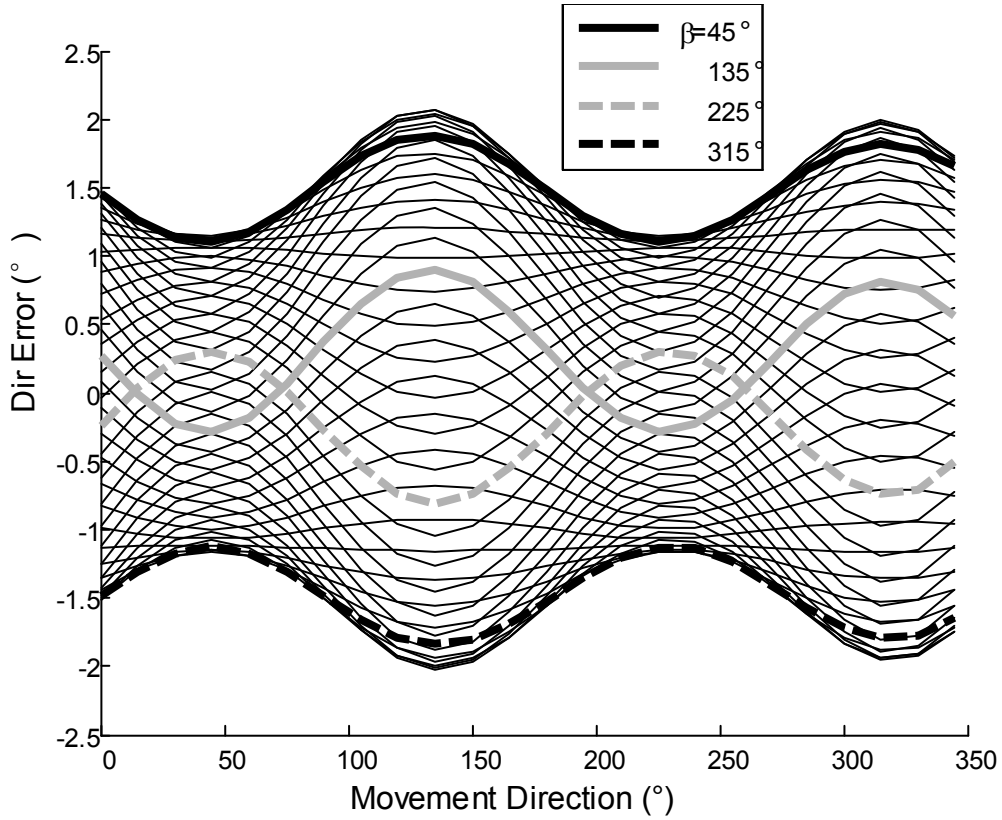

Figure 35. Directional error as a function of movement direction for 48 perturbation directions and one perturbation amplitude (ρ=0.01m). Thick grey lines represent directional error as a function of movement direction when perturbation directions (β) were 135° (solid) and 315° (dashed). Thick black lines are associated with perturbation directions of 45° (solid) and 225° (dashed).

Given what was shown in Figure 33-Figure 35, directional error appeared to be a function of perturbation amplitude, perturbation direction and movement direction. Further examination showed that directional errors could be best approximated by the following mathematical function:

$$\alpha \approx \rho(k_1(\sin((2\gamma + \delta_1) + (\beta + \delta_2)) + \sin((2r + \delta_1) - (\beta + \delta_2))) + k_2 \sin(\beta + \delta_3))$$

[23]

where α denotes directional error, ρ and β represent perturbation amplitude and direction, γ denotes movement direction, and δ_1, δ_2, δ_3, k_1, and k_2 are some constants. However, according to this function, variation of k_1 and k_2 could affect the magnitude of directional error (α); variation of δ_1, δ_2 and δ_3 could have an effect on the phase shift of the directional error waveforms shown in Figure 34. Since previous analyses associated with multiple initial arm postures suggested directional errors were also posture dependent, δ_1, δ_2, δ_3, k_1, k_2 may vary with initial arm posture.

In summary, the sensitivity analyses suggested that perturbation amplitude and perturbation direction did not contribute in the same manner to the direction-dependent and posture-dependent patterns of movement variability observed in Simulation I. For a given arm posture, perturbation direction appeared to be the largest contributor to the direction-dependent aspects of movement variability. In contrast, perturbation amplitude appeared to simply magnify the effects of perturbations applied along a given direction.

5.4.2 Noise Simulation II: Errors in Sensing Initial Conditions + Errors in Trajectory Planning

5.4.2.1 Simulation Results for One Initial Arm Posture

In this simulation (SII), random perturbations were again introduced into the initial hand position to simulate imprecise limb position estimation. The results of SII are summarized in Figure 36 for one initial arm posture (initial arm posture 1 in Table 2) and both perturbation distributions (isotropic and anisotropic). Figure 36a shows simulated hand paths associated with 4 movement directions. For both perturbation distributions, the average handpath

generally aligned with the planned movement direction. The handpaths generated for any given planned direction were quite variable however and the directional variability of handpaths was somewhat different for different movement directions. For example, the directional error variability appeared to be larger for the 135° movement direction rather than for the 315° movement direction. We also found that the extent of this variability also differed for different perturbation conditions: the directional error variability was slightly smaller for the isotropic perturbation distribution than for the anisotropic perturbation distribution. This can be best appreciated in Figure 36b which plots the circular standard deviation (CSD) of the directional errors resulting from isotropically and anisotropically distributed sensing noise. For all 24 movement directions, the CSD resulting from isotropic perturbations was smaller than that resulting from anisotropic perturbations. For both perturbation distributions, variability in directional error was direction dependent. This dependence on movement direction could be indicated by the asymmetry of the variability about the center of the CSD plots illustrated in Figure 36b. The variability pattern resulting from anisotropically distributed sensing noise appeared to be shifted from center along approximately the 120° movement direction while the variability pattern resulting from isotropically distributed sensing noise appeared to be shifted along approximately the135° movement direction. As a result, for both perturbation distributions, the largest variability was found along one movement direction and the smallest along the opposite movement direction. For errors resulting from anisotropically distributed sensing noise, the largest/smallest variability was approximately along the 120°/300° axis, while it was along the 135°/315° axis for largest/smallest variability resulting from isotropically

distributed sensing noise. Lastly, the CSD plots also show that variability associated with isotropic perturbations was generally smaller than the variability associated with anisotropic perturbations.

In summary, SII showed that the movement variability arising from both arm position sensing and trajectory planning noise was movement direction-dependent and generally much larger than the variability due to sensing noise alone. As in SI, variability also depended on the particular distribution used to simulate the estimation of limb position, with more anisotropic perturbation distributions generally resulting in greater movement variability.

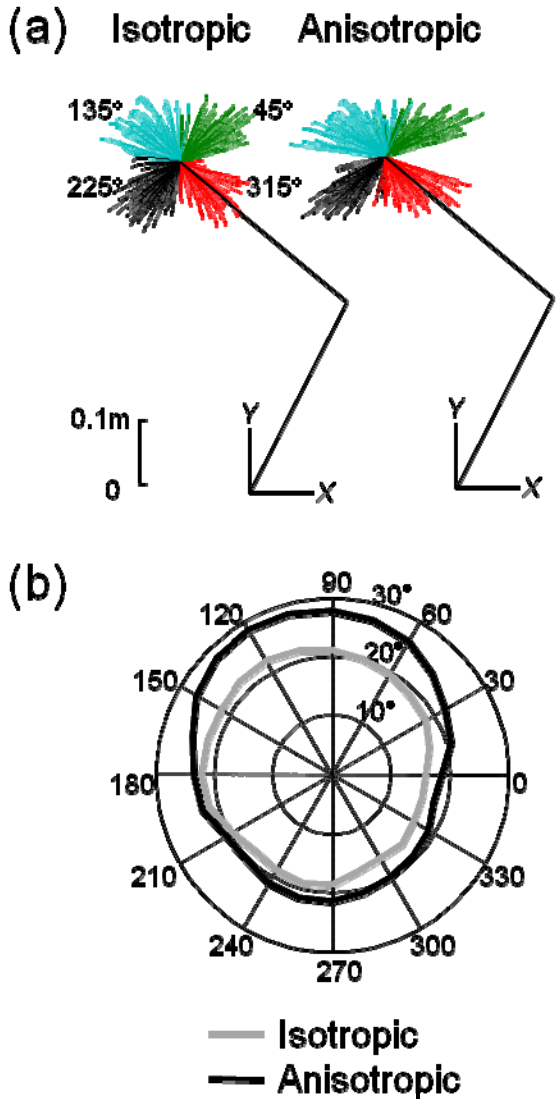

Figure 36. Results obtained from SII for one arm posture. (a) Simulated hand paths for four movement directions in the presence of isotropically and anisotropically distributed endpoint noise. (b) Polar plots of the circular standard deviation (CSD) of the directional errors associated with 24 movement directions.

5.4.2.2 Simulation Results for Multiple Initial Arm Postures

As for SI we also examined the relationship between movement variability and initial arm configuration in SII by repeating the analysis for three additional

arm configurations (Table 2). Figure 37 shows polar plots of the movement variability resulting from combined sensing and trajectory planning noise for four arm postures. For simplicity of presentation, only results for the isotropic position sensing noise distribution are shown. In general, the shapes and sizes of these CSD plots were very similar for the four arm postures. The magnitude of variability did not change appreciably with arm posture. On the other hand, direction-dependent aspects of movement variability were not fixed in space, but rotated as the arm posture changed, maintaining a roughly constant spatial relationship with respect to the forearm.

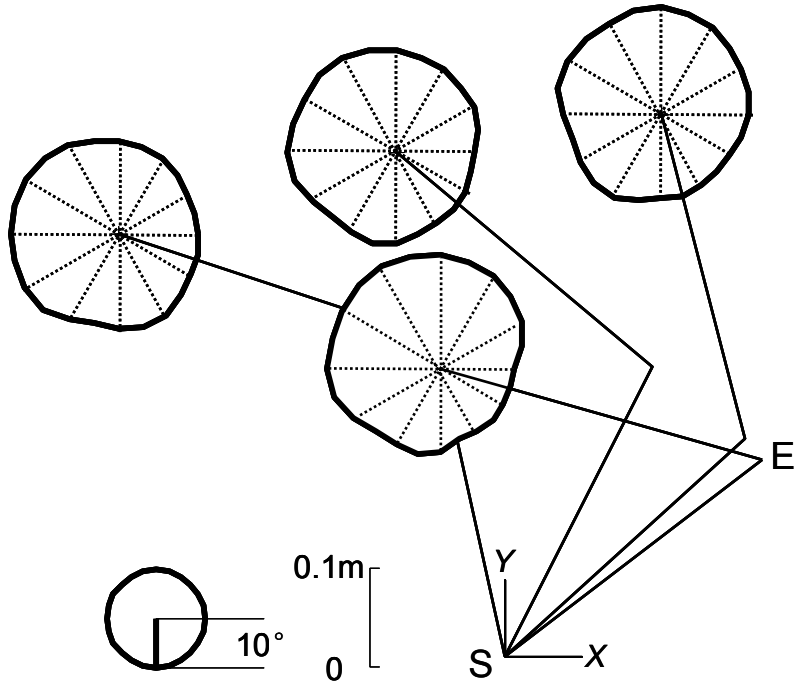

Figure 37. Results from SII for four arm postures. Polar plots of the CSD of the directional errors associated with 24 movement directions are shown for each arm posture. S: shoulder. E: elbow.

5.4.2.3 Interaction Analysis Between Sensing noise and Planning noise

Directional errors in SII can be attributed to two sources: 1) a failure to compensate for changing initial conditions (as in SI) and 2) errors in trajectory planning. To examine how these two sources combined to contribute to errors in movement direction, we studied the effects of planning and sensing noise separately and compared the resulting movement variability to that arising from their combined effects. Since the directional errors resulting from errors in sensing initial conditions were already analyzed in SI, we calculated the directional errors that would be expected to result from trajectory planning errors alone. This was done by translating the planned movement vectors following perturbation to the unperturbed arm endpoint and conducting the simulations as in unperturbed conditions. In this way we removed errors in sensing the initial conditions from the simulations.

Figure 38 shows polar plots of the directional error variability associated with position sensing noise, trajectory planning noise as well as a combination of both noise sources. The figure illustrates that the variability resulting from trajectory planning noise alone was movement direction dependent when this noise was due to anisotropic (elliptical) perturbations. The corresponding CSD plot was elliptical with the major axis (i.e. the axis associated with maximal variability) being orthogonal to the major axis of the anisotropic perturbations. In contrast, the CSD plot resulting from trajectory planning noise alone was circular for isotropic (circular) perturbations, suggesting directional error variability does not depend on movement direction. All of these findings suggested that direction-dependent errors resulting from trajectory planning noise alone were closely related to the pattern of sensing error distributions. This is because

actual movement direction in part reflects planned direction which is determined by sensed positions of the hand and the target. In our simulations, sensed target positions were always the same and noise in planned direction directly resulted from noise in sensing hand location.

Figure 38 also illustrates that the asymmetric pattern of variability in the presence of both position sensing noise and trajectory planning sources arises from a complex interaction between these two noise sources for movements in different directions. Variability associated with trajectory planning noise alone was generally symmetric about the center of the CSD plot and accounted for most of the variability observed when both noise sources were present. However, the manner in which this variability interacted with variability due to position sensing noise was highly direction-dependent. For a range of movement directions, e.g. 30°-210°, the directional errors induced by each noise source tended to be equal in sign. As a result, for these movement directions the effects of position sensing noise and trajectory planning summed together and were therefore greater than the noise due to either source alone. For other movement directions the effects of each noise source were opposite in sign leading to a partial cancellation of their effects. That is, for these directions the movement errors induced by position sensing noise appeared to subtract from those due to trajectory planning noise. Thus, CSD plots were not symmetric about the center but shifted along the direction which appeared associated with the direction of maximum variability due to sensing noise alone. This was true for both the isotropic and anisotropic perturbation distributions. The complex interaction between sensing noise and trajectory planning noise across movement directions

resulted in the asymmetric pattern of variability shown here and in Figure 36 as well.

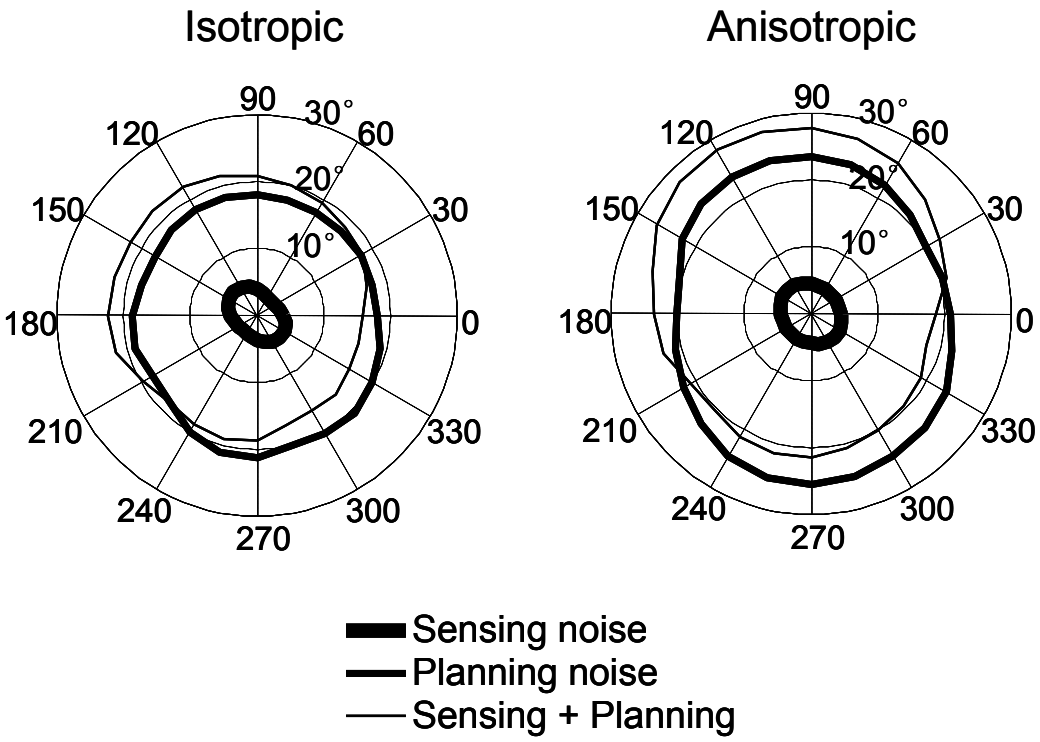

Figure 38. Polar plots of the circular standard deviation (CSD) of the directional errors associated with position sensing noise, trajectory planning noise, and a combination of sensing and trajectory planning noise. Left plot gives CSD associated with isotropically distributed sensing noise. Right plot gives CSD associated with anisotropically distributed sensing noise.

5.4.3 Noise Simulation III: Errors in Movement Execution

5.4.3.1 Simulation Results for One Initial Arm Posture

In this simulation, we examined the effects of noise in execution on movement variability. Figure 39 shows the results of these simulations for one initial arm posture (initial arm posture 1 in Table 2). As in Figure 31 and Figure

36, hand paths for 4 movement directions are illustrated in panel (a) while the CSD of the directional errors associated with 24 movement directions are plotted in panel (b). In our simulations, the average handpath generally aligned with the planned movement direction. The variability of errors due to execution noise was fairly small (< 3°). For different movement directions, variability due to execution noise was highly anisotropic however. For example, Figure 39b shows that variability along the 75˚/225˚ axis was predicted to be only about 1/3rd of that along the orthogonal 165˚/315˚ axis.

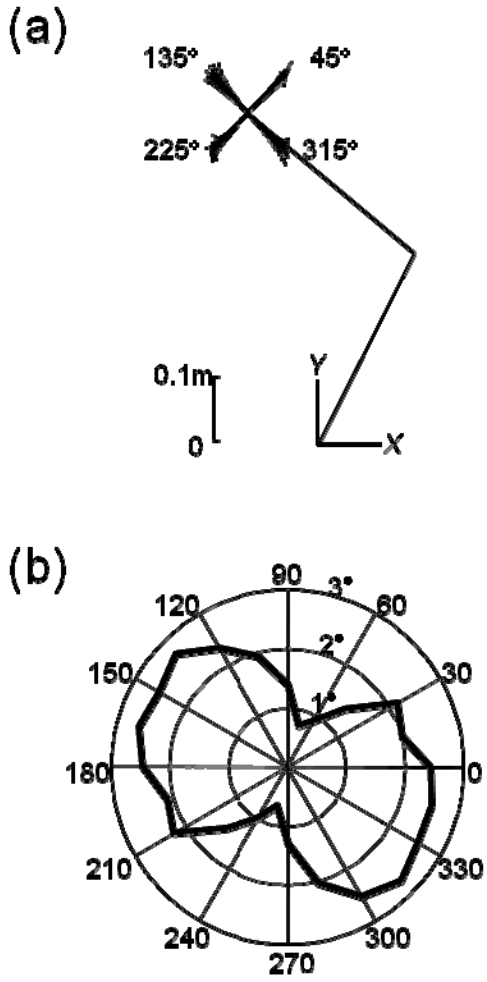

Figure 39. Results obtained from SIII for one arm posture. (a) Simulated hand paths for four movement directions in the presence of execution noise. (b) Polar plots of the circular standard deviation (CSD) of the directional errors associated with 24 movement directions.

5.4.3.2 Simulation Results for Multiple Initial Arm Postures

In SIII, we also examined the relationship between movement variability and initial arm configuration by repeating the analysis for three additional arm configurations (Table 2) as in SI and SII. Figure 40 shows polar plots of the movement variability resulting from execution noise for four arm postures. We

found execution noise resulted not only in direction-dependent patterns of movement variability but posture dependent ones as well. In general, the pattern of variability across directions was not fixed in space but remained roughly aligned with the long axis of the forearm as arm posture changed. On the other hand, the magnitude of execution-related variability was predicted to be quite similar across arm postures. The shapes and sizes of these CSD plots did not change appreciably with arm posture.

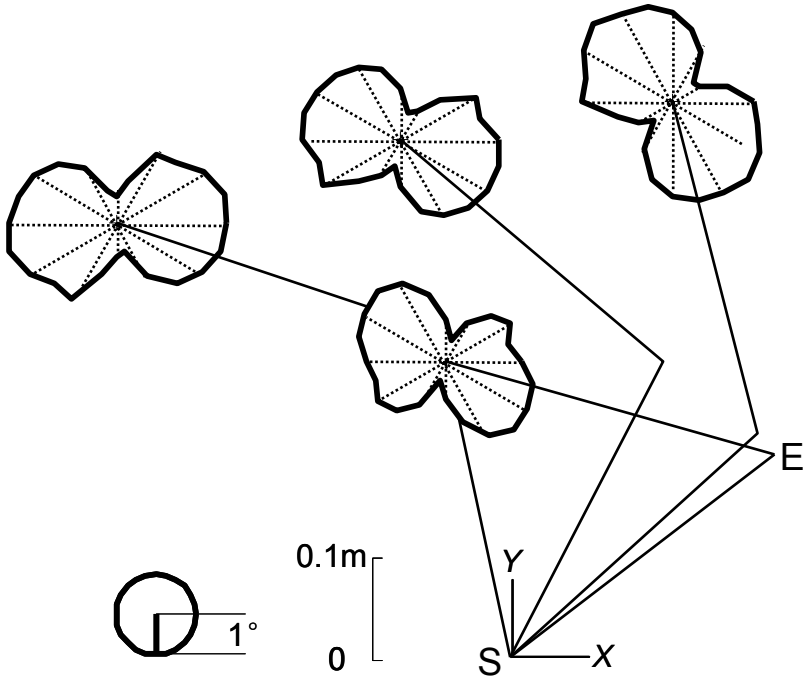

Figure 40. Results from SIII for four arm postures. Polar plots of the CSD of the directional errors associated with 24 movement directions are shown for each arm posture. S: shoulder. E: elbow.

5.4.3.3 Simulation Method Verification

Here we tried to verify the execution noise model proposed by van Beers and colleagues (2004) could be applied in SIII. Note the parameters associated with the noise model (k_{SDN}, k_{CN}, and k_{TN}) were taken from previously estimated

values based on experimental data (van Beers, Haggard, and Wolpert 2004). In particular, these parameters were derived in an investigation using a single arm posture which also had different movement specifications and anthropometric physical parameter values from our simulations. Thus, in order to verify the same noise model could be applied in our simulations, we compared the variability resulting from our simulation method with the observed and predicted variability from the experiment and model simulation of van Beers and colleagues (2004). This was done by adapting the movement conditions in SIII to those used in this previous investigation and calculated the resulting variability. The anthropometric and mechanical property values for the verification simulation are listed in Table 4. The viscosity coefficient of both joints was set to 0.8 kg m^2/s (Nakano et al. 1999). Movement amplitude was 0.096 m and movement duration was a constant of 0.35s. Although the initial arm posture could differ across subjects in previous investigation, we chose the closest initial arm posture ((θs, θe) =(69°, 77°)) to verify our simulation method in SIII.

Table 4. Anthropometric and mechanical property values. Values are taken from Kawato (1995) and are similar to those used by Van Beer et al. (2004). COM = center of mass.

		Upper arm (i=s)	Forearm (i=e)
Length (l_i)	[m]	0.25	0.35
COM (r_i)	[m]	0.12	0.15
Mass (m_i)	[kg]	0.9	1.1
Inertia (I_i)	[kg·m^2]	0.0071	0.0206

The results of this comparison are illustrated in Figure 41. Since in the previous investigation, variability was quantified as the reciprocal of the circular standard deviation (1/CSD) rather than simply the CSD, we compared 1/CSD of current verification simulation with that of previous experimental observation and model prediction. Figure 41 shows the polar plots of 1/CSD from the previous investigation (Figure 41a) and the current investigation (Figure 41b). We found that movement variability in the current verification simulation was quite similar to that reported by van Beers and colleagues (2004). Note in the latter investigation variability was highly anisotropic (Figure 41a). Variability due to execution noise in the current investigation was also highly anisotropic (Figure 41b). Moreover, the shape and orientation of this anisotropy were also quite similar, resembling a spindle with the axis associated with the minimum variability (or maximum 1/CSD) aligned approximately with the 68°/242° axis.

It is also shown in Figure 41 that the magnitude of 1/CSD in the current investigation was bigger, meaning the variability was smaller. This difference could be due to the differences in the simulation method. Although we modified the movement specifications and parameter values to closely approximate the movement conditions in previous research, there were some limitations we could not overcome. First of all, in the study by van Beers and colleagues (2004), motor commands were estimated from mean trajectories. As a result, in contrast to the straight idealized trajectories used in the present study, the mean trajectories could be curved. In the previous study, movement amplitude and duration were not fixed across movement directions. Although the target distance was 0.096 m, subjects tended to overshoot or undershoot for particular directions. Thus, the motor commands calculated from the trajectories were likely different

from our investigation. In addition, the results of simulations can be sensitive to the choice of the anthropometric and physical parameters. The values of parameters in van Beers (2004) were not exactly like those from Kawato (1995): the arm lengths were measured from each subject and other parameters were scaled accordingly based on Kawato's data. Lastly, the previous investigation did not specify the number of time-steps used in the simulations. Since signal dependent noise and constant noise were added to the motor command at each time-step in the simulations, the movement variability was predicted to be smaller if more time steps were involved. It is likely we applied more time steps in our simulations.

Overall, it is appropriate to apply the previously proposed execution noise model in our simulations. Although the magnitude of variability in the verification simulations was different from previous experimental data, the direction dependent pattern of variability due to execution noise generated by the model was quite similar. This is important as the focus of these simulations was not on the overall magnitude of movement variability but on its direction dependence and arm configuration dependence which we compared cross different simulations (SI, SII, and SIII). On the other hand, it should be also noted that the model parameters could vary for different arm postures in SIII. The execution noise model therefore may need to be refined if applied to a range of arm postures.

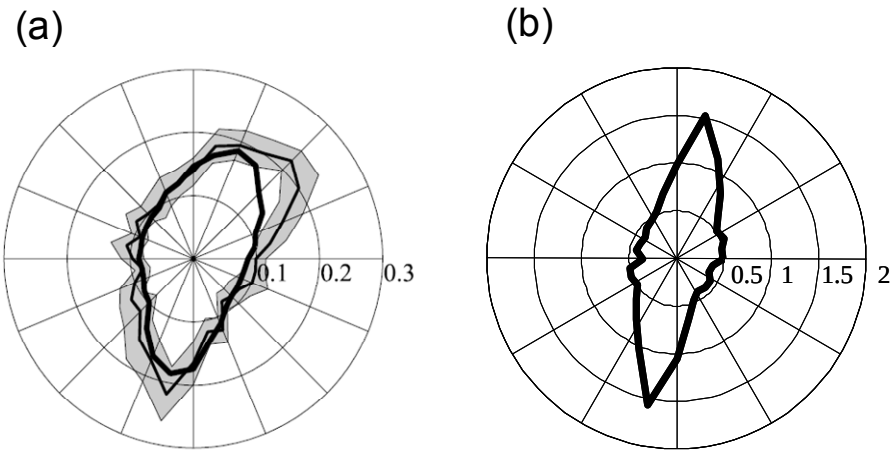

Figure 41. Polar plots of the reciprocal of circular standard deviation (1/CSD) associated with 24 movement directions. (a) Experimental results and model prediction by Van Beers et al (2004). The black curve shows the mean of all subjects in the experiment and the grey area around it represents intersubject variability. The thick black line represents the model prediction. (b) Model prediction using the simulation method in SIII.

5.4.4 Comparison Across Three Simulation Conditions

In this section, we compared the effects of noise on movement variability across three simulation conditions: errors in sensing initial conditions (SI), errors in sensing initial conditions + errors in trajectory planning (SII), and errors in movement execution (SIII). We examined the differences and similarities in variability across the three simulations, focusing on three aspects: overall magnitude of variability, direction dependent pattern of variability and posture dependent pattern of variability.

5.4.4.1 Overall Magnitude of Variability

For all three simulation conditions, the average handpath generally aligned with the planned movement direction. The overall magnitude of

variability in the initial direction of handpaths, however, was different for different simulation conditions. Compared to SI, the most striking observation in SII was the very large increase in variability of initial movement direction for both the isotropic and anisotropic distributions. This larger degree of variability can be explained by the additional directional errors that were introduced in the early stages of movement planning, as illustrated schematically in Figure 29. In contrast to SI, planned movement directions in SII were defined by vectors connecting the initial hand position with fixed spatial targets (see Figure 29). Thus, in this situation, misestimation of the initial conditions (position sensing errors) was compounded by errors in planning the appropriate movement vectors (trajectory planning errors). That is, in SII not only was the initial starting position altered but the planned movement trajectory as well and these effects combined to generally produce larger movement errors. In SIII, note that variability due to execution noise in our simulations was fairly small; this is due to the fact that the noise parameters k_{SDN}, k_{CN}, and k_{TN} used in SIII were derived from movements performed by neurologically-intact human subjects (van Beers et al., 2004). The noise level in SI and SII, however, was arbitrarily determined as the focus of these simulations was not on the overall magnitude of movement variability but on its direction dependence (distribution in space) and arm configuration dependence. Thus, the relatively small variability in SIII is not critical for the current investigation.

We also found that, for both SI and SII, directional error variability was slightly smaller for the isotropic perturbation distribution than for the anisotropic distribution. The smaller variability for the isotropic perturbation distribution in SII is likely a consequence of position sensing errors since variability resulting from

trajectory planning errors alone was not always smaller for the isotropic perturbation distribution as suggested by interaction analysis between position sensing errors and trajectory planning errors.

5.4.4.2 Direction Dependence of Variability

We found, for all three simulation conditions, variability in directional error varied across movement directions. This direction dependent pattern of movement variability manifested differently however for different simulation conditions. First of all, variability in directional error was asymmetrical with respect to the center in SII but was symmetrical in SI and SIII. The asymmetric pattern of variability in SII was likely a consequence of the complex interaction between sensing noise and trajectory planning noise across movement directions. On the other hand, variability due to execution noise in SIII was highly anisotropic, much more so than the variability due to position sensing noise (SI), trajectory planning noise (SII), or their combined effects (SII). For example, the maximum variability was predicted to be about three times of the minimum variability. In contrast, the maximum and the minimum variability were generally much closer in SI and SII. Interestingly, the direction along which execution-related variability was greatest was similar to that due to position sensing noise.

5.4.4.3 Posture Dependence of Variability

We also focused on comparing the pattern of movement variability across three simulation conditions when the initial arm posture was changed. We found, for all three simulation conditions, the pattern of movement variability was not only direction dependent but also posture dependent as well. Generally, the pattern of variability across directions was not fixed in space but rotated with the

long axis of the forearm as arm posture changed. In SI, although the direction-dependent pattern of variability remained roughly aligned with the forearm as arm posture changed, the variability for more flexed arm postures was noticeably larger and less direction-dependent than for the more extended posture. This differs somewhat from the results in SII and SIII, where the shapes and sizes of polar plots of movement variability were generally very similar for the four arm postures (Figure 37 and Figure 40). This difference between SI and SII is very likely due to the fact that variability in SII was dominated by trajectory planning noise; thus differences in variability across arm postures due to sensing noise alone was simply not as apparent in this simulation. Likewise, although direction-dependent aspects of movement variability also appeared to rotate somewhat with changes in arm posture in SII, these changes were also not as noticeable as in SI, likely for the same reasons as mentioned above.

5.5. Discussion

In the present study we examined the effects of misestimating the position of the arm on movement variability across the workspace and compared this to the effects of noise associated with movement execution. We reasoned that incorrectly estimating limb position would present at least two distinct problems for the motor system. First, even for the same planned movement vector, misestimating limb position would lead to a difference in the sensed vs. actual initial conditions (position sensing noise), resulting in the wrong motor commands and/or torques being selected for the required movement. Second, for movements directed to particular locations in space, misestimating limb position would be expected to result in additional noise in movement planning (trajectory planning noise), specifically the planning of required movement

vectors. We found that position sensing noise and trajectory planning noise are predicted to result in distinct direction-dependent and posture-dependent patterns of movement variability that differed in many respects from the patterns of movement variability expected to result from noise in execution.

5.5.1 Model Parameters

In this investigation, we used previously published anthropomorphic and mechanical parameters for our biomechanical model (Scheidt et al. 2005). Although the results of our simulations can clearly be sensitive to the choice of these parameters, we used the same biomechanical model for SI, SII and SIII and simply introduced noise into different stages of this model. That is, our focus was on the observed differences across the different simulations. One long term goal of this effort is the prediction of patterns of movement variability that result from neuromotor disorders. Such an effort will ultimately require an in-depth sensitivity analysis of the various biomechanical model parameters used in this study. This effort will also certainly require a refinement of the very simple muscle model used in the execution noise simulations, as well as the noise parameters used in this simulation. In particular, we used the same model parameters for signal dependent noise, constant noise and temporal noise for all arm postures. However, these parameters were derived for a single arm posture in the investigation by van Beers and colleagues (2004) and may therefore need to be refined if applied to a range of arm postures.

5.5.2 Direction and Posture Dependence

A consistent finding across the different simulations was the direction-dependent variability arising from both sensing and execution noise. It is not

immediately clear whether the nervous system needs to accounts for such effects during movement production and if so how this is accomplished. Although the degree of direction-dependence varied in SI, SII and SIII, the directions along which variability is predicted to be greatest appeared to be very similar across the different simulations. That is, the direction of maximum variability generally rotated to in a counterclockwise fashion as hand position was varied from right to left in the workspace. This suggests that the effects of noise on movement variability are at least partially fixed to the arm, and are greatest along directions requiring the highest degree of control, i.e. those directions requiring substantial movement of both the shoulder and elbow (vs. primarily the elbow). Interestingly, the impedance properties of the limb (specifically stiffness) exhibit a similar pattern of posture dependence. Patterns of endpoint stiffness have been shown to rotate in a counterclockwise fashion as hand position is varied from right to left in the workspace (Mussa-Ivaldi, Hogan, and Bizzi 1985) with the direction of maximum stiffness appearing to be roughly aligned with the direction of maximum variability as demonstrated here. This may act to reduce the effects of noise along the same directions, which could in principle simplify any neural based mechanisms that exist to compensate for direction-dependent variations in movement variability.

In some ways the finding that patterns of movement variability rotated with changes in arm configuration was not surprising. That is, the equations of motion of a two-link arm do not contain terms for shoulder position. Thus, when the elbow angle is kept constant, joint torques can be thought of as being defined in an arm-fixed rather than spatial frame of reference. Direction dependent patterns of movement variability therefore would also be expected to be arm-

fixed as well, rotating in space with changes in shoulder angle. However, in the present simulations we varied the position of the endpoint of the limb in the workspace in such a way that both shoulder and elbow angle were varying, the effects of which could not be predicted a priori. We found that, at least for the range of arm postures examined in this study, direction-dependent patterns of movement variability were still best described as being largely fixed to the limb, rather than being fixed in space. Thus, for the motor system, mechanisms for predicting and compensating for the consequences of noise on movements in space must rely strongly on information related to arm configuration. This information could be provided by proprioception, vision and/or efference copy.

5.5.3 Dependence on Hand Position Estimation

The results of SI and SII suggest that the precision of hand position sense has important implications for the neural systems involved in movement production. Even small errors in estimating hand position (~2 cm) resulted in large directional errors, particularly along certain movement directions. Thus, maintaining an accurate and precise estimate of the position of the hand in space would appear to be of paramount importance to the motor system. Our simulation showed that the particular form of the distribution describing position sense (istotropic or anisotropic) has some implications for movement production. Generally speaking, an isotropic distribution led to more anisotropic errors and vice-versa. Although these differences were small relative to the differences across simulations, they still suggest that the form of these distributions, which arise from properties of the various sensors and their interactions across the workspace, is a factor that the brain must take into account during movement production. In that vein it is interesting to note the relatively larger directional

errors that were generated for positions closer to the body in SI. The enhanced precision of endpoint estimation observed in human subjects for hand positions close to the body (van Beers, Sittig, and van der Gon 1998) may partially compensate for the relatively larger effects of perturbations at these positions.

5.5.4 Relevance to Motor Learning

Several studies have demonstrated that training cannot only improve the accuracy of movements but decrease their variability as well (Cohen and Sternad 2009; Deutsch and Newell 2004; Gribble et al. 2003; Mosier et al. 2005; Ranganathan and Newell 2010). It is unclear however if training can specifically address variability arising from different noise sources, e.g. sensing noise vs. execution noise. Characterizing the relative contributions of sensing noise and execution noise to overall movement variability, as was performed here, is an important first step toward answering this question. Interestingly, it has recently been demonstrated that reduction of movement variability can be optimized by strategically reweighting sensory inputs to take advantage of differences in their relative reliabilities (Guo and Raymond 2010). This begs the question as to whether sensory inputs can also be optimized to compensate, at least in part, for noise arising during movement execution. Answering this question will require in depth knowledge from behavioral studies regarding the manner in which sensory and motor noise interact in both the temporal and spatial domains (Faisal and Wolpert 2009; Apker, Darling, and Buneo 2010). Extending the present simulations to study the interaction of sensory and motor noise under more realistic conditions, including during simulated movements performed in three dimensions, will also contribute substantially to this effort..

5.5.5 Neural Correlates of Movement Variability

Understanding the consequences of noise at different stages of movement production could aid in understanding the roles of different brain areas in movement production and movement variability. There is a growing interest in understanding the role of noise in neural processing and movement production, in particular how variability in neural firing patterns might manifest in behavioral variability. For example, Shenoy and colleagues examined the role of variability in activity in the premotor cortex and its relation to motor behavior (Churchland, Afshar, and Shenoy 2006). These investigators found that variability in neural activity in the premotor cortex before movement onset can account for nearly one half of the variability in movement speed. This was a landmark study in the sense of being the first to demonstrate a link between neural variability and behavioral variability. It is currently unclear whether the remaining variability can be accounted for by variability in the firing at subsequent stages, e.g. in motor cortex. In addition, the study by Churchland et al. (2006) examined the relation between neural variability and movement speed. It would be of interest to know whether variability in neural firing in this or any area can account for variability in spatial aspects of variability, such as movement direction and amplitude. The results of the present study, which characterized some of these effects across a large portion of the workspace of the reaching arm, could prove to be particularly useful in this regard.

Chapter 6

CONCLUSION

6.1. Summary

The ultimate goal of this dissertation was to characterize the neural mechanisms of integration of somatic and visually-based limb position signals and the consequences of misestimating limb position on movement production. While information about limb position is crucial to performing accurate reaching, little is known about how the brain combines various sources of information to provide a single estimate of limb position. Little is also known about how errors in sensing limb position can influence overall movement variability. Thus, in this dissertation we presented two specific aims, each one focused on solving one specific problem. Specific Aim 1 was to characterize the mechanisms of integration of somatic and visually-based limb position signals in area 5 of posterior parietal cortex. Among other brain areas, area 5 has been considered as a very good candidate for probing the neural mechanisms of limb position estimation. Anatomical and lesion studies all seem to support a role for area 5 in integrating sensory and motor information for limb position estimation. In Chapter 4 which is dedicated to Specific Aim1, we provided a novel experimental design for the neurophysiological studies. While overcoming limitations of other studies, this design also took into account the theory of optimal cue integration. This theory is supported by a large amount of theoretical and psychophysical works and should therefore have a neural correlate somewhere in the brain. The study for Specific Aim 1 in the dissertation was trying to seek neurophysiological support for this theory while confirming the role of area 5 at the same time. The other specific aim, Specific Aim 2, addressed the other half of the goal by

characterizing, via biomechanical modeling and simulation techniques, movement variability resulting from various noise sources. Limb movements are highly variable due in part to noise occurring at different stages of movement production such as sensing, planning or execution. The relative contributions of noise at each stage to overall movement variability are difficult to determine experimentally and are therefore not well understood. The study for Specific Aim 2, which was detailed in Chapter 5, provided a simulation approach to predict the effects of various noise sources on movement production. We not only assessed the independent contributions from individual noise sources but also studied the effect of natural interaction between some of the noise sources.

6.2. Specific Aim 1

6.2.1 Conclusion

Previous results have suggested that neurons in area 5 respond to both visual and somatic signals (Cavada and Goldman-Rakic 1989; Andersen et al. 1990; Caminiti, Ferraina, and Johnson 1996). However, although many area 5 neurons were modulated by somatically-derived signals in these studies, visual information regarding arm position was not strongly represented. Note that these results were obtained in tasks where animals were either not reaching to objects in their environment or under conditions where the animals were receiving strong haptic input on both visual and non-visual trials, which could have influenced the weighting of visual input in this area. The present results extended these investigations to conditions where visual input would be expected to have the greatest influence, i.e. under conditions where the arm is held statically in free space. Thus far we have found that even under these conditions relatively few individual area 5 neurons appear to be modulated by the sight of the limb during

static holding. The result remained approximately the same when we tried to either extend the hold time of the limb and when we reduced the window radius within which the endpoint of the limb was held (in order to enhance the relevance of vision in this task). In an experimental paradigm (Paradigm 2) where the relative weighting of individual inputs is expected to differ much more between visual and non-visual trials, we still did not find more cells tuned to visual conditions. All these results appear to imply that area 5 does not receive strong input from areas devoted to the visual processing of body parts and is therefore not likely to be the primary site of integrating visual information about limb position with somatically-derived signals. However, a decoding analysis showed that vision does appear to play a role in representing limb position in this area at the population level. These relatively modest effects suggest that the primary site of integration of visual and somatic limb position information is likely downstream of area 5, presumably PMd or MIP. In addition, the present results suggest that role of visual input in area 5 may have more to do with specifying the locations of extrinsic objects, rather than the positions of parts of the body.

6.2.2 Future Studies

Given the relatively weak evidence for area 5 involvement in integrating visual signals about limb position with somatically-derived signals, future studies could target neural responses in other cortical areas. The adjacent MIP area would likely be a good candidate due to the relatively stronger visual responsiveness of neurons in this area and its reported involvement in eye-centered coding of spatial information (Caminiti, Ferraina, and Johnson 1996; Colby and Duhamel 1991). Another consideration could be PMd in premotor cortex. Previous studies suggest PMd neurons encode information about both

the static position and configuration of the limb (Pesaran, Nelson, and Andersen 2006; Scott, Sergio, and Kalaska 1997). PMd is also known to receive visual input via the parietal lobe (Caminiti, Ferraina, and Johnson 1996). Thus, it is very likely that cells encoding visual information about limb position will be found in PMd.

Future studies could also address other aspects of neural coding. The present neurophysiological study focused on neural correlates of cue integration for limb position estimation, with an emphasis on changes in mean firing rates under the "vision" versus "no vision" condition. In addition to mean firing rate of spiking activity, analysis of local field potentials (LFPs) may prove to be useful for studying cue integration for limb position estimation in the brain. In contrast to action potentials, which are thought to arise largely from the soma or axon hillock of pyramidal or stellate cells (Humphrey and Schmidt 1990) and reflect the output of a cortical column (Mitzdorf 1985), LFPs are a summation signal of excitatory and inhibitory potentials generated near the dendrites and may reflect the input and local processing in a cortical column (Chandrasekaran and Ghazanfar 2009; Gray et al. 1989; Lakatos et al. 2005; Liu and Newsome 2006). LFPs can be relatively easily recorded and it has been proposed that LFPs provide a critical link between spikes and behavior (Buzsaki and Draguhn 2004). Some recent literature supported modulation of LFPs during visual-auditory cue integration in the auditory cortex and STS (Ghazanfar et al. 2005; Maier, Chandrasekaran, and Ghazanfar 2008; Lakatos et al. 2007). Analysis of LFPs may provide insights into the neural mechanisms of cue integration that are not attainable through analysis of mean firing rates alone. This approach will likely be useful not only

for studying higher order sensory areas but also for the study of areas involved in transforming such sensory information into plans for movement.

By manipulating the availability of visual information about limb position, this study was a first attempt at seeking neurophysiological support for the theory of optimal cue integration. It could be a precursor to an experiment which tests some other predictions of optimal cue integration in arm-movement-related areas of the brain. The work of van Beers and colleagues suggested the precision of somatic and visual sense of limb position varies as a function of arm configuration, with the somatic sense being more precise for hand locations closer to the body (van Beers, Sittig, and van der Gon 1998; van Beers, Wolpert, and Haggard 2002). Since cells in most arm-movement-related areas of the brain exhibit static positional discharge that is spatially tuned in two or three dimensions (Georgopoulos, Caminiti, and Kalaska 1984; Kettner, Schwartz, and Georgopoulos 1988), according to van Beer's work cells with preferred limb positions located farther from the body should be modulated more by concurrent visual input of the limb than cells with preferred positions located closer to the body, reflecting the decreased precision of somatic information at more extended arm positions. A further study of cell responses to changes in limb position in depth will help to test this prediction of optimal cue integration.

6.3. Specific Aim 2

6.3.1 Conclusion

For this specific aim, a simulation approach was employed to predict the effects of noise associated with 1) sensing the position of the limb ('position sensing noise') and 2) planning an appropriate movement vector ('trajectory planning noise'). Results were also compared to those predicted by a previous

model of the noise associated with movement execution ('execution noise'). We found that the effects of limb position sensing noise on movement variability were dependent upon both the planned movement direction and the initial configuration of the arm. The effects on movement variability also depended on the particular pattern of sensing noise used to simulate the estimation of limb position, with more anisotropic sensing noise leading to less direction-dependent (more isotropic) patterns of movement variability.

In our simulations, the effects of trajectory planning noise were closely related to patterns of sensing noise. Since trajectory planning was dependent on defining a vector which connects the hand position with target position, sensing noise would be expected to result in additional trajectory planning noise for movements directed to particular locations in space. In this situation, movement directional errors could be attributed to both sensing errors and errors in trajectory planning. Movement directional error variability due to trajectory planning noise alone would reflect some nature of sensing noise.

The combined effect of sensing noise and trajectory planning noise resulted in much larger movement variability than that from sensing noise alone and the variability in large part was dominated by the effects of trajectory planning noise. The asymmetric pattern of movement variability resulting from both noise sources also suggested that the interaction between sensing noise and planning noise was highly complex across movement directions.

In this study, variability due to execution noise was also shown to be arm configuration dependent and was more direction-dependent than that due to position sensing noise, trajectory planning noise or their combined effects. Overall, these results provide important insights into the relative roles of sensing,

planning and execution noise in movement variability that should prove to be useful for neurophysiological investigations seeking to relate variability at the neural level to variability at the behavioral level.

6.3.2 Future Studies

Future studies could involve refinement of the two-link biomechanical arm model. First, the various biomechanical model parameters used in this study may need to be reconsidered more carefully. In this investigation, we used a biomechanical model with same parameters for SI, SII and SIII since our focus was on the observed differences across the different simulations. However, the results of individual simulations can clearly be sensitive to the choice of these parameters. As a result, in-depth sensitivity analyses of the various biomechanical model parameters may be ultimately required. Second, the refinement will require an improvement of the very simple muscle model used for the execution noise simulations. The muscle model in the study simply used two second-order linear muscles each of which controlled the rotation around one joint (shoulder or elbow). The motor commands of two muscles also acted independently on the shoulder and elbow joint. However, real muscles can produce forces only by contraction and at least a pair of antagonistic muscles is needed for controlling rotation around one joint. In reality, even more muscles could be involved due to the existence of muscles that cross more than one joint. In addition, synergism found in muscle activation also indicates motor commands of two muscles could be correlated (Torres-Oviedo, Macpherson, and Ting 2006). Third, the biomechanical arm model could be improved to simulate movements in three-dimensional space. In this study, the arm model was only developed to simulate movements in the horizontal plane. However, under more realistic

conditions, arm movements are often executed in 3D space. For this more complicated situation, an arm model with 2 degrees of freedom in this study is not suitable.

Lastly, a model of execution noise will need to be validated across the workspace of the arm. In this investigation, we used the same model parameters for execution noise for all arm postures. These parameters were derived for a single arm posture in the investigation by van Beers and colleagues (van Beers, Haggard, and Wolpert 2004) and may not apply to other arm postures. Therefore, behavioral experiments may be necessary to validate the predictions of execution noise model. We will compare patterns of movement variability observed in normal human subjects with those derived from execution noise simulations. Optimization techniques will be used to find the best values for model parameters associated with different arm postures across the workspace based on behavioral experiments.

Behavioral experiments will also be required if we want to have in depth knowledge regarding interactions between sensing noise and execution noise. In the present study, effects of sensing noise and execution noise on movement variability were independently assessed via simulation methods. However, in reality, they may interact in a complex manner, which could affect the observed movement variability. Previous behavioral studies also suggested sensory and motor noise interact in both the temporal and spatial domains (Faisal and Wolpert 2009; Apker, Darling, and Buneo 2010). It has recently been demonstrated that reduction of movement variability can be optimized by strategically reweighting sensory inputs to take advantage of differences in their relative reliabilities (Guo and Raymond 2010). Thus it would be interesting to

know whether sensory noise can interact with execution noise in an optimal manner in order to reduced movement variability. Extending the present simulations to study the interaction of sensory and motor noise under more realistic conditions, including during simulated movements performed in three dimensions, will contribute substantially to our understanding of this issue.

REFERENCES

Andersen, R. A., C. Asanuma, C. Essick, and R. M. Siegel. 1990. Corticocortical connections of anatomically and physiologically defined subdivisions within the inferior parietal lobe. *J Comp Neurol* 296:65-113.

Apker, G. A., T. K. Darling, and C. A. Buneo. 2010. Interacting Noise Sources Shape Patterns of Arm Movement Variability in Three-Dimensional Space. *Journal of Neurophysiology* 104 (5):2654-2666.

Apker, G.A., Y. Shi, and C.A. Buneo. 2009. The role of visual and somatic signals in the decoding of limb position in area 5. Paper read at Program No. 355.25. Neuroscience 2009 Abstracts, at Washington D.C.

Bauer, M. 2008. Multisensory integration: A functional role for inter-area synchronization? *Curr Biol* 18 (16):R709-R710.

Beck, J. M., W. J. Ma, R. Kiani, T. Hanks, A. K. Churchland, J. Roitman, M. N. Shadlen, P. E. Latham, and A. Pouget. 2008. Probabilistic Population Codes for Bayesian Decision Making. *Neuron* 60 (6):1142-1152.

Bock, O. 1986. Contribution of Retinal Versus Extraretinal Signals Towards Visual Localization in Goal-Directed Movements. *Exp Brain Res* 64 (3):476-482.

Buneo, C. A., and R. A. Andersen. 2003. The role of area 5 somatosensory input in visuomotor transformations for reaching. Paper read at Program No. 14.1. Neuroscience 2003 Abstracts, at Washington D.C.

Buneo, C. A., J. Boline, J. F. Soechting, and R. E. Poppele. 1995. On the form of the internal model for reaching. *Exp Brain Res* 104 (3):467-479.

Buneo, C. A., M. R. Jarvis, A. P. Batista, and R. A. Andersen. 2002. Direct visuomotor transformations for reaching. *Nature* 416 (6881):632-636.

Buneo, C. A., M. R. Jarvis, A. P. Batista, and R. A. Andersen. 2003. Properties of spike train spectra in two parietal reach areas. *Exp Brain Res* 153 (2):134-139.

Buzsaki, G., and A. Draguhn. 2004. Neuronal oscillations in cortical networks. *Science* 304 (5679):1926-1929.

Caminiti, R. , S. Ferraina, and P. B. Johnson. 1996. The sources of visual information to the primate frontal lobe: a novel role for the superior parietal lobule. *Cereb Cortex* 6:319-328.

Cavada, C., and P. S. Goldman-Rakic. 1989. Posterior parietal cortex in rhesus monkey: II. Evidence for segregated corticocortical networks linking sensory and limbic areas with the frontal lobe. *J Comp Neurol* 287 (4):422-45.

Chandrasekaran, C., and A. A. Ghazanfar. 2009. Different Neural Frequency Bands Integrate Faces and Voices Differently in the Superior Temporal Sulcus. *J Neurophysiol* 101 (2):773-788.

Churchland, M. M., A. Afshar, and K. V. Shenoy. 2006. A central source of movement variability. *Neuron* 52 (6):1085-1096.

Cohen, R. G., and D. Sternad. 2009. Variability in motor learning: relocating, channeling and reducing noise. *Experimental Brain Research* 193 (1):69-83.

Colby, C. L., and J. R. Duhamel. 1991. Heterogeneity of extrastriate visual areas and multiple parietal areas in the macaque monkey. *Neuropsychologia* 29 (6):517-37.

Contreras-Vidal, J. L., and E. R. Buch. 2003. Effects of Parkinson's disease on visuomotor adaptation. *Exp Brain Res* 150 (1):25-32.

Deutsch, K. M., and K. M. Newell. 2004. Changes in the structure of children's isometric force variability with practice. *Journal of Experimental Child Psychology* 88 (4):319-333.

Duhamel, J. R., F. Bremmer, S. Ben Hamed, and W. Grof. 1997. Spatial invariance of visual receptive fields in parietal cortex neurons. *Nature* 389:845-848.

Duhamel, J. R., C. L. Colby, and M. E. Goldberg. 1998. Ventral intraparietal area of the macaque: Congruent visual and somatic response properties. *J Neurophysiol* 79 (1):126-136.

Faisal, A. A., L. P. J. Selen, and D. M. Wolpert. 2008. Noise in the nervous system. *Nat Rev Neurosci* 9 (4):292-303.

Faisal, A. A., and D. M. Wolpert. 2009. Near Optimal Combination of Sensory and Motor Uncertainty in Time During a Naturalistic Perception-Action Task. *J Neurophysiol* 101 (4):1901-1912.

Fisher, N. I. 1993. *Statistical Analysis of Circular Data*. New York: Cambridge.

Flanagan, J. R., and A. K. Rao. 1995. Trajectory Adaptation to a Nonlinear Visuomotor Transformation - Evidence of Motion Planning in Visually Perceived Space. *J Neurophysiol* 74 (5):2174-2178.

Flanders, M., S. I. Helms-Tillery, and J. F. Soechting. 1992. Early stages in a sensorimotor transformation. *Behav Brain Sci* 15:309-362.

Georgopoulos, A. P., R. Caminiti, and J. F. Kalaska. 1984. Static spatial effects in motor cortex and area 5: quantitative relations in a two-dimensional space. *Exp Brain Res* 54 (3):446-54.

Ghazanfar, A. A., J. X. Maier, K. L. Hoffman, and N. K. Logothetis. 2005. Multisensory integration of dynamic faces and voices in rhesus monkey auditory cortex. *J Neurosci* 25 (20):5004-5012.

Gordon, J., M. F. Ghilardi, and C. Ghez. 1994. Accuracy of Planar Reaching Movements .1. Independence of Direction and Extent Variability. *Exp Brain Res* 99 (1):97-111.

Gray, C. M., P. Konig, A. K. Engel, and W. Singer. 1989. Oscillatory responses in cat visual cortex exhibit inter-columnar synchronization which reflects global stimulus properties. *Nature* 338 (6213):334-7.

Graziano, M. S. A. 1999. Where is my arm? The relative role of vision and proprioception in the neuronal representation of limb position. *P Natl Acad Sci USA* 96 (18):10418-10421.

Graziano, M. S. A., D. F. Cooke, C. S. R. Taylor, and T. Moore. 2004. Distribution of hand location in monkeys during spontaneous behavior. *Exp Brain Res* 155 (1):30-36.

Graziano, M. S. A., and C. G. Gross. 1993. A Bimodal Map of Space - Somatosensory Receptive-Fields in the Macaque Putamen with Corresponding Visual Receptive-Fields. *Exp Brain Res* 97 (1):96-109.

Graziano, M. S. A., C. G. Gross, C. S. R. Taylor, and T. Moore. 2004. Multisensory neurons for the control of defensive movements. In *The Handbook of Multisensory Processes*, edited by G. Calvert, C. Spence and B. E. Stein. Cambridge: MIT Press.

Graziano, M. S., D. F. Cooke, and C. S. Taylor. 2000. Coding the location of the arm by sight. *Science* 290 (5497):1782-6.

Graziano, M. S., X. T. Hu, and C. G. Gross. 1997. Visuospatial properties of ventral premotor cortex. *J Neurophysiol* 77 (5):2268-92.

Graziano, M. S., G. S. Yap, and C. G. Gross. 1994. Coding of visual space by premotor neurons. *Science* 266 (5187):1054-7.

Gribble, P. L., L. I. Mullin, N. Cothros, and A. Mattar. 2003. Role of cocontraction in arm movement accuracy. *Journal of Neurophysiology* 89 (5):2396-2405.

Gu, Y., D. E. Angelaki, and G. C. DeAngelis. 2008. Neural correlates of multisensory cue integration in macaque MSTd. *Nat Neurosci* 11 (10):1201-1210.

Guo, C. C., and J. L. Raymond. 2010. Motor learning reduces eye movement variability through reweighting of sensory inputs. *J Neuroscience* 30 (48):16241-16248.

Harris, C. M., and D. M. Wolpert. 1998. Signal-dependent noise determines motor planning. *Nature* 394 (6695):780-784.

Hermsdorfer, J., and G. Goldenberg. 2002. Ipsilesional deficits during fast diadochokinetic hand movements following unilateral brain damage. *Neuropsychologia* 40 (12):2100-2115.

Hogan, N., and T. Flash. 1987. Moving Gracefully - Quantitative Theories of Motor Coordination. *Trends Neurosci* 10 (4):170-174.

Hollerbach, JM, and T Flash. 1982. Dynamics interactions between limb segments during planar arm movement. *Biol Cybern* 44:67-77.

Hoshi, E., and J. Tanji. 2000. Integration of target and body-part information in the premotor cortex when planning action. *Nature* 408 (6811):466-470.

Hoshi, E., and J. Tanji. 2002. Contrasting neuronal activity in the dorsal and ventral premotor areas during preparation to reach. *J Neurophysiol* 87 (2):1123-1128.

Humphrey, D.R., and E.M. Schmidt. 1990. Extracellular single-unit recording methods. In *Neurophysiological techniques: applications to neural systems*, edited by A. A. Boulton, G. B. Baker and C. H. Vanderwolf. Clifton, NJ: Humana Press.

Kettner, R. E., A. B. Schwartz, and A. P. Georgopoulos. 1988. Primate Motor Cortex and Free Arm Movements to Visual Targets in 3-Dimensional Space .3. Positional Gradients and Population Coding of Movement Direction from Various Movement Origins. *J Neurosci* 8 (8):2938-2947.

Kording, K. P., and D. M. Wolpert. 2004. Bayesian integration in sensorimotor learning. *Nature* 427 (6971):244-247.

Lakatos, P., C. M. Chen, M. N. O'Connell, A. Mills, and C. E. Schroeder. 2007. Neuronal oscillations and multisensory interaction in primary auditory cortex. *Neuron* 53 (2):279-292.

Lakatos, P., A. S. Shah, K. H. Knuth, I. Ulbert, G. Karmos, and C. E. Schroeder. 2005. An oscillatory hierarchy controlling neuronal excitability and stimulus processing in the auditory cortex. *J Neurophysiol* 94 (3):1904-1911.

Liu, J., and W. T. Newsome. 2006. Local field potential in cortical area MT: Stimulus tuning and behavioral correlations. *Journal of Neuroscience* 26 (30):7779-7790.

Longstaff, M. G., and R. A. Heath. 2006. Spiral drawing performance as an indicator of fine motor function in people with multiple sclerosis. *Hum Movement Sci* 25 (4-5):474-491.

Ma, W. J., and A. Pouget. 2008. Linking neurons to behavior in multisensory perception: A computational review. *Brain Research* 1242:4-12.

Maier, J. X., C. Chandrasekaran, and A. A. Ghazanfar. 2008. Integration of bimodal looming signals through neuronal coherence in the temporal lobe. *Curr Biol* 18 (13):963-968.

Maier, J. X., J. G. Neuhoff, N. K. Logothetis, and A. A. Ghazanfar. 2004. Multisensory integration of looming signals by Rhesus monkeys. *Neuron* 43 (2):177-181.

McIntyre, J., F. Stratta, J. Droulez, and F. Lacquaniti. 2000. Analysis of pointing errors reveals properties of data representations and coordinate transformations within the central nervous system. *Neural Computation* 12 (12):2823-2855.

McIntyre, J., F. Stratta, and F. Lacquaniti. 1997. Viewer-centered frame of reference for pointing to memorized targets in three-dimensional space. *J Neurophysiol* 78 (3):1601-18.

McIntyre, J., F. Stratta, and F. Lacquaniti. 1998. Short-term memory for reaching to visual targets: psychophysical evidence for body-centered reference frames. *J Neurosci* 18 (20):8423-8435.

Mitzdorf, U. 1985. Current source-density method and application in cat Cereb Cortex: Investigation of evoked potentials and EEG phenomena. *Physiol Rev* 65:37-100.

Morasso, P. 1981. Spatial control of arm movements *Exp Brain Res* 42 (2):223-227.

Morgan, M. L., G. C. DeAngelis, and D. E. Angelaki. 2008. Multisensory integration in macaque visual cortex depends on cue reliability. *Neuron* 59 (4):662-673.

Mosier, K. M., R. A. Scheidt, S. Acosta, and F. A. Mussa-Ivaldi. 2005. Remapping hand movements in a novel geometrical environment. *Journal of Neurophysiology* 94 (6):4362-4372.

Mussa-Ivaldi, F. A., N. Hogan, and E. Bizzi. 1985. Neural, mechanical, and geometric factors subserving arm posture in humans. *J Neurosci* 5 (10):2732-2743.

Nakano, E., H. Imamizu, R. Osu, Y. Uno, H. Gomi, T. Yoshioka, and M. Kawato. 1999. Quantitative examinations of internal representations for arm trajectory planning: minimum commanded torque change model. *J Neurophysiology* 81:2140-2155.

Norris, S.A., B.E. Greger, T.A. Martin, and W.T. Thach. 2001. Prism adaptation of reaching is dependent on the type of visual feedback of hand and target position. *Brain Res* 905:207-219.

Ochiai, T., H. Mushiake, and J. Tanji. 2005. Involvement of the ventral premotor cortex in controlling image motion of the hand during performance of a target-capturing task. *Cereb Cortex* 15 (7):929-937.

Pesaran, B., M. J. Nelson, and R. A. Andersen. 2006. Dorsal premotor neurons encode the relative position of the hand, eye, and goal during reach planning. *Neuron* 51 (1):125-134.

Pouget, A., S. Deneve, and J. R. Duhamel. 2002. A computational perspective on the neural basis of multisensory spatial representations. *Nat Rev Neurosci* 3 (9):741-747.

Ranganathan, R., and K. M. Newell. 2010. Influence of motor learning on utilizing path redundancy. *Neuroscience Letters* 469 (3):416-420.

Rossetti, Y., M. Desmurget, and C. Prablanc. 1995. Vectorial coding of movement - vision, proprioception, or both? *J Neurophysiol* 74 (1):457-463.

Rushworth, M. F. S., P. D. Nixon, and R. E. Passingham. 1997. Parietal cortex and movement .1. Movement selection and reaching. *Exp Brain Res* 117 (2):292-310.

Scheidt, R. A., M. A. Conditt, E. L. Secco, and F. A. Mussa-Ivaldi. 2005. Interaction of visual and proprioceptive feedback during adaptation of human reaching movements. *J Neurophysiol* 93 (6):3200-3213.

Scherberger, H., M. R. Jarvis, and R. A. Andersen. 2005. Cortical local field potential encodes movement intentions in the posterior parietal cortex. *Neuron* 46 (2):347-354.

Scott, S. H., L. E. Sergio, and J. F. Kalaska. 1997. Reaching movements with similar hand paths but different arm orientations .2. Activity of individual cells in dorsal premotor cortex and parietal area 5. *J Neurophysiol* 78 (5):2413-2426.

Sekiyama, K., S. Miyauchi, and T. Imaruoka. 2000. Body image as a visuomotor transformation device revealed in adaptation to reversed vision. *Nature* 407:374-377.

Shadmehr, R., and S.P. Wise. 2005. *The computational neurobiology of reaching and pointing*. Cambridge, Massachusetts: The MIT Press.

Sober, S. J., and P. N. Sabes. 2003. Multisensory integration during motor planning. *J Neurosci* 23 (18):6982-6992.

Soechting, J. F., C. A. Buneo, U. Herrmann, and M. Flanders. 1995. Moving effortlessly in 3-dimensions: Does Donders law apply to arm movement. *J Neurosci* 15 (9):6271-6280.

Soechting, J. F., and F. Lacquaniti. 1981. Invariant characteristics of a pointing movement in man *J Neurosci* 1 (7):710-720.

Stanford, T. R., S. Quessy, and B. E. Stein. 2005. Evaluating the operations underlying multisensory integration in the cat superior colliculus. *J Neurosci* 25 (28):6499-6508.

Stanford, T. R., and B. E. Stein. 2007. Superadditivity in multisensory integration: putting the computation in context. *Neuroreport* 18 (8):787-792.

Stein, B. E., and T. R. Stanford. 2008. Multisensory integration: current issues from the perspective of the single neuron. *Nat Rev Neurosci* 9 (4):255-266.

Taylor, D. M., S. I. H. Tillery, and A. B. Schwartz. 2002. Direct cortical control of 3D neuroprosthetic devices. *Science* 296 (5574):1829-1832.

Thies, S. B., P. A. Tresadern, L. P. Kenney, J. Smith, D. Howard, J. Y. Goulermas, C. Smith, and J. Rigby. 2009. Movement variability in stroke patients and controls performing two upper limb functional tasks: a new assessment methodology. *J Neuroeng Rehabil* 6.

Torres-Oviedo, G., J.M. Macpherson, and L.H. Ting. 2006. Muscle synergy organization is robust across a variety of postural perturbations. . *J Neurophysiology* 96 (3):1530-1546.

Tsuji, T., P. G. Morasso, K. Goto, and K. Ito. 1995. Human hand impedance characteristics during maintained posture. *Biol Cybern* 72 (6):475-485.

Uno, Y., M. Kawato, and R. Suzuki. 1989. Formation and Control of Optimal Trajectory in Human Multijoint Arm Movement - Minimum Torque-Change Model. *Biol Cybern* 61 (2):89-101.

van Beers, R. J., P. Baraduc, and D. M. Wolpert. 2002. Role of uncertainty in sensorimotor control. *Philos T Roy Soc B* 357 (1424):1137-1145.

van Beers, R. J., P. Haggard, and D. M. Wolpert. 2004. The role of execution noise in movement variability. *J Neurophysiol* 91 (2):1050-1063.

van Beers, R. J., A. C. Sittig, and J. J. D. van der Gon. 1998. The precision of proprioceptive position sense. *Exp Brain Res* 122 (4):367-377.

van Beers, R. J., A. C. Sittig, and J. J. D. van der Gon. 1999. Integration of proprioceptive and visual position-information: An experimentally supported model. *J Neurophysiol* 81 (3):1355-1364.

van Beers, R. J., D. M. Wolpert, and P. Haggard. 2002. When feeling is more important than seeing in sensorimotor adaptation. *Curr Biol* 12 (10):834-837.

Vetter, P., and D. M. Wolpert. 2000. Context estimation for sensorimotor control. *J Neurophysiol* 84 (2):1026-1034.

Vindras, P., and P. Viviani. 1998. Frames of reference and control parameters in visuomanual pointing. *J Exp Psychol Human* 24 (2):569-591.

Wolpert, D. M., Z. Ghahramani, and M. I. Jordan. 1995. Are arm trajectories planned in kinematic or dynamic coordinates? An adaptation study. *Exp Brain Res* 103 (3):460-70.

Wolpert, D. M., Z. Ghahramani, and M. I. Jordan. 1995. An internal model for sensorimotor integration. *Science* 269 (5232):1880-1882.

Wolpert, D. M., S. J. Goodbody, and M. Husain. 1998. Maintaining internal representations the role of the human superior parietal lobe. *Nat Neurosci* 1 (6):529-533.

Yamaguchi, Gary T., ed. 2005. *Dynamic Modeling of Musculoskeletal Motion: A Vectorized Approach for Biomechanical Analysis in Three Dimensions*: Springer.

Zucker, S. W., L. Iverson, and R. A. Hummel. 1990. Coherent compound motion: corners and nongrid configurations. *Neural Comput* 2:44-57.